TRANSPORT PROPERTIES OF GASES IN POLYETHYLENE/CLAY NANOCOMPOSITES

BY

JIMOH KAYODE ADEWOLE

A Thesis Presented to the

DEANSHIP OF GRADUATE STUDIES

KING FAHD UNIVERSITY OF PETROLEUM & MINERALS

DHAHRAN, SAUDI ARABIA

In Partial Fulfillment of the
Requirements for the Degree of

MASTER OF SCIENCE

In

CHEMICAL ENGINEERING

March, 2011

KING FAHD UNIVERSITY OF PETROLEUM & MINERALS

DHAHRAN 31261, SAUDI ARABIA

DEANSHIP OF GRADUATES STUDIES

This thesis, written by

JIMOH KAYODE ADEWOLE

under the direction of his thesis advisor and approved by his thesis committee, has been presented to and accepted by the Dean of Graduate Studies, in partial fulfillment of the requirements for the degree of

MASTER OF SCIENCE IN CHEMICAL ENGINEERING.

Thesis Committee

Dr. Usamah A. Al-Mubaiyedh
(Thesis Advisor)

Prof. Ibnelwaleed A. Hussein
(Member)

Dr. Usamah A. Al-Mubaiyedh
(Department Chairman)

Dr. Abdulhadi A. Al-Juhani
(Member)

Dr. Salam A. Zummo
(Dean of Graduate Studies)

Date 20/6/11

DEDICATION

TO MY BELOVED PARENTS –

MR. TIJANI ADEWOLE

&

LATE MRS FADHILAT ADEWOLE (MAY ALLAH BE PLEASED WITH HER),

WIFE & CHILDREN

ACKNOWLEDGMENTS

All Praises and Thanks are for Allah (Subhanau-wa-Talla), the Lord of the entire creation. May his peace and Blessings be upon all His Messengers, Prophets, their Companions and all Muslims (alive or dead)- Ameen. I am extremely grateful to Almighty Allah who alone has made this achievement possible. “Glory to You, we have no knowledge except what you have taught us. Verily, it is You, the All-Knower, All-Wise. (Q2:32)”

I am especially indebted to my Parents for all they have done to support me from birth to date. I submit that all my successes and achievements, by the Will of Allah, is a result of their patient, blessings, encouragements and support.

With deep sense of gratitude and appreciation, I would like to express my sincere thanks to my thesis advisor, Dr. Usamah A. Al-Mubaiyedh for his inspiring guidance, help and excellent cooperation in supervising this research work. Thanks to Prof Ibnelwaleed A. Hussein for his academic elucidation, skillful and meticulous review of manuscripts produced from this research. I am also very grateful Dr Abdulhadi A. Al-Juhani for his invaluable suggestions and comments during the experimental design, continuous encouragement, and support.

I will like to give special thanks to King Abdullaziz City Science and Technology (KACST) and King Fahd University of Petroleum & Minerals (KFUPM) for providing the support for this research. This research project was supported by the National Science, Technology and Innovation Program (NSTIP) of KACST. Furthermore, I am highly indebted to the Kingdom of Saudi Arabian government for providing me with a scholarship to pursue an MS program in KFUPM.

My special thanks to Dr. Anwar Ul-Hamid of the Research Institute, KFUPM (for his help in nanoindentation experiment), Prof. N. von Solms and L. Jensen of the Technical University, Denmark for their supports in the permeability experiment. My appreciation also goes to all faculty and staff members for their kind and cheerful cooperation. I also appreciate Mr. Muhammad Saheed of Pyhsics Department, KFUPM for his assistance in XRD test; Adesina A. Ayub for suggestions and training on DSC; Mofizul Islam (of the Polymer Research Laboratory); Abdallah Al-Khalaf, Abu Maher (Taher), Shaji ThaniyuLlah, and Jefrey Comedia for their assistances in administrative matters; Mr Kamal (ME Workshop) for fabricating the mould used for mechanical tests; Dr. Abbasi for training on the use of Instron machine and Parvex for on the use of DMA.

I will like to appreciate the untiring support of my wife and children for their patience and understanding during the seemingly unending hours spent both in the laboratory and in preparing this report. Also, I would like to thank the following individuals for their role in making my MS program a success:- my brother Agbajelola Abdus salam Abdurrauf for his moral and financial supports right from the beginning of my higher education pursuit, 'Wasiu Oluomo, Halimat Sadiat, Lukman, Dr. A. S. Osunleke, Dr. E. A. Taiwo, Dr J. Sonibare, Dr Y. Balarabe, Mr. Bamimore, and Mr Adefemi for their encouragements, supports and prayers. This acknowledgement will be incomplete without expressing special gratitude to the entire Nigerian community of KFUPM. It is one of the most wonderful communities I have ever found myself.

Finally and humbly, I extend my deepest heartfelt appreciation to all that have been involved in making this research a success.

TABLE OF CONTENTS

KING FAHD UNIVERSITY OF PETROLEUM & MINERALS ..... **ii**
Dedication ..... **iii**
ACKNOWLEDGMENTS ..... **iv**
Table of Contents ..... **vi**
LIST OF TABLES ..... **viii**
LIST OF FIGURES ..... **ix**
THESIS ABSTRACT ..... **xi**
CHAPTER 1 ..... **1**
INTRODUCTION **1**
1.1 Nanocomposite Materials 1
1.2 Nano Indentation 4
1.3 Objectives 5
CHAPTER 2 ..... **7**
LITERATURE REVIEW **7**
2.1 Transport Parameters 7
2.1.1 Permeability Coefficient (P) 7
2.1.2 The Solubility Coefficient (S) 8
2.1.3 The Diffusion Coefficient (D) 8
2.2 Laws of Transport Phenomena 8
2.3 Mechanism of Gas Transport Processes in Polymeric Materials 10
2.4 Gas Permeation in Rubbery Polymers 12
2.4.1 Molecular Models 12
2.4.2 Free Volume Theory 14
2.4.3 Gas Permeation in Semicrystalline Polymers 15
2.4.4 Influence of Temperature on Transport Coefficients 16
2.4.5 Influence of Concentration on Transport Coefficients 21
2.4.6 Influence of Pressure on Transport Coefficient 22
2.4.7 Influence of Crystallinity on Transport Coefficient 25
2.4.8 Influence of Polymer Structure on Transport Coefficient 27
2.5 Overview of Gas Barrier Properties in Polymer\Clay Nanocomposites 28
2.6 Mechanical and Physical Properties of Polymer/Clay Nanocomposite 37
CHAPTER 3 ..... **43**
EXPERIMENTAL **43**
3.1 Materials 43
3.2 Sample Preparation 43
3.3 Morphology Characterization 44
3.4 Mechanical Testing 45
3.5 Differential Scanning Calorimetry (DSC) 45
3.6 Dynamic Mechanical Analysis 46
3.7 Surface Mechanical Properties 46
3.8 Measurement of gas permeability 46
CHAPTER 4 ..... **50**
RESULTS AND DISCUSSION: MORPHOLOGY, MECHANICAL, THERMAL AND TRANSPORT PROPERTIES **50**

4.1 X-ray Diffraction Analysis 50
4.2 SEM Analysis 53
4.3 Mechanical Testing 55
4.4 DSC Analysis 60
4.5 Dynamic Mechanical Analysis (DMA) 61
4.5.1 Effect of temperature 61
4.5.2 Effect of frequency 63
4.5.3 Cole–Cole plot 67
4.6 Surface Mechanical Properties 72
4.7 Creep Compliance at End-Use Conditions 79
4.8 Permeability Measurement 84
4.8.1 Influence of temperature 84
4.8.2 Influence of Pressure 85
4.8.3 Influence of Compatibilizer 93
4.8.4 Influence of Nanoclay 93
CHAPTER 5 99
MATHEMATICAL MODELLING OF PERMEABILITY 99
5.1 Introduction 99
5.2 Model Development 102
5.3 Results and Discussion: Permeability Modeling 109
CHAPTER 6 125
6.0 CONCLUSION AND RECOMMENDATIONS FOR FUTURE WORK 125
Reference 131
VITAE 146

LIST OF TABLES

Table 2.1 Molecular size of CH_4 and CO_2 19

Table 4.1 : Tensile Mechanical Properties of the HDPE and Nanocomposites 56

Table 4.2 Thermal Properties of Nanocomposites for various clay contents 59

Table 4.3 Storage modulus of Pure HDPE and HDPE/Clay Nanocomposites as a function of Temperature 64

Table 4.4 Loss modulus of Pure HDPE and HDPE/Clay Nanocomposites as a function of 65

Table 4.5 Tan δ of Pure HDPE and HDPE/Clay Nanocomposites as a function of Temperature 66

Table 4.6 Surface mechanical properties obtained from different HDPE composite materials 78

Table 4.7 Permeability Coefficients obtained for Pure HDPE Samples 86

Table 4.8 Permeability Coefficients obtained for BHDPE 89

Table 4.9 Permeability Coefficient obtained for BHDPE + 1wt% C15A 90

Table 4.10 Permeability Coefficient obtained for BHDPE + 2.5wt% C15A 91

Table 4.11 Permeability Coefficient obtained for BHDPE + 5wt% N1.44P 92

Table 5.1 Characteristics of the permeation experiment 110

Table 5.2 Permeability of Pure HDPE Samples 111

Table 5.3 Permeability of HDPE/1wt% C15A nanocomposite 114

Table 5.4 Model parameters 116

Table 5.5 Activation energy of permeation, E_p, and pre-exponential factor, P_{eo}, of penetrant in polyethylene and its nanocomposites 124

LIST OF FIGURES

Figure 3.1: Schematic of the 2-D permeation cell, with pressure and temperature monitoring and control and data acquisition. 49

Figure 4.1a : XRD patterns for clay and polyethylene/clay nanocomposite for BHDPE+C15A 51

Figure 4.1b: XRD patterns for clay and polyethylene/clay nanocomposite BHDPE+N1.44P 52

Figure 4.2: SEM micrographs of polyethylene/clay nanocomposites (a) BHDPE+C15A-2.5wt% (b) BHDPE+C15A-5wt% (c) BHDPE+N1.44P-2.5wt% (d) BHDPE+N1.44P-5wt%.. 54

Figure 4.3a. Cole – Cole plot of the HDPE and BHDPE+C15A nanocomposites as a function of frequency (at constant temperature of 30^{o}C) 698

Figure 4.3b. Cole – Cole plot of the HDPE and BHDPE+N1.44P nanocomposites as a function of frequency (at constant temperature of 30^{o}C) 69

Figure 4.3c. Cole – Cole plot of the HDPE and BHDPE+C15A nanocomposites as a function of temperature (at constant frequency of 1Hz)..... 70

Figure 4.3d. Cole – Cole plot of the HDPE and BHDPE+N1.44P nanocomposites as a function of temperature (at constant frequency of 1Hz)..... 71

Figure 4.4a. Typical indent obtained from pure HDPE at a maximum load of 20mN..... 74

Figure 4.4b : Force-displacement curves obtained from nanoindentation of pure HDPE at a maximum load of 20 mN. (Normal force (mN) and penetration depth are plotted against time (s) of indentation) 75

Figure 4.4c: Force-displacement curves obtained from nanoindentation of pure HDPE at a maximum load of 20 mN. (Normal force is plotted against depth of penetration). Flat region at the top of the curve indicates deformation at a constant force indicating creep. Modulus of elasticity is obtained from the slope of the unloading curve..... 76

Figure 4.5: Comparison of Results of Micro and Macro Creep as a Function of %Loading 80

Figure 4.6: Comparison of Results of Micro and Macro Moduli 81

Figure 4.7: Variation of Indentation Hardness with %Loading of Nanoclay..... 82

Figure 4.8: Creep Compliance measured at field conditions of 7.5MPa and 50^{o}C 83

Figure 4.9a : Evolution of transport properties of Pure CH_4 as a function of nanoclay type and loadings 100bar 94

Figure 4.9b : Evolution of transport properties of mixed CH_4/CO_2 as a function of nanoclay type and loadings at 100bar 95

Figure 4.9c : Evolution of transport properties of mixed CH_4/CO_2 as a function of nanoclay type and loadings at 50bar 96

Figure 5.1 : Experimental permeability data and fit using eq. (16) for pure CH4 in Pure HDPE..... 118

Figure 5.2 : Experimental permeability data and fit using eq. (17) for mixed gas in Pure HDPE..... 119

Figure 5.3 : Experimental permeability data and fit using eq. (16) for pure CH4 HDPE/clay nanocomposite (1wt% Cloisite 15A)..... 1210

Figure 5.4 : Experimental permeability data and fit using eq. (17) for mixed gas in HDPE/clay nanocomposite (1wt% Cloisite 15A)..... 121

THESIS ABSTRACT

Name: JIMOH KAYODE ADEWOLE

Title: TRANSPORT PROPERTIES OF GASES IN POLYETHYLENE/CLAY NANOCOMPOSITES

Degree: MASTER OF SCIENCE

Major Field: CHEMICAL ENGINEERING

Date of Degree: MARCH 2011

In this work, effects of various types of nanoclays and their concentrations on morphological, transport, thermal, creep, surface and bulk mechanical properties of nanocomposites were investigated for liner application in oil and gas pipeline. Surface mechanical properties were measured using a nanoindentation technique. Permeability test was done for CO_2 and CO_2/CH_4 gas mixture at pressures ranging from 50 to 106 bar and temperatures between 30 and 70^oC. A mathematical model was also developed for predicting permeability of gases in polymer nanocomposites.

Analysis of the results obtained revealed that properties of the nanocomposites are enhanced by addition of nanoclay. Gas permeability was found to decrease by 46.5% and 11.9% by adding 5wt% N1.44P and 1wt% C15A respectively. A recoverable creep of about 93% was achieved using 5wt% N1.44P. Results obtained from nanoindentation tests for surface mechanical properties showed similar trend to that of bulk measurements. For the first time, a permeability model that takes into account the effects of pressure, temperature, crystallinity and nanoparticle loading was developed. The model fit showed good agreement with experimental data. Generally, enhanced properties were observed for C15A based nanocomposites at 2.5wt% clay loading while the enhancement was at 5wt% for N1.44P based nanocomposite. Base on these results a nanoclay additive for a liner grade HDPE/nanocomposite was selected.

خلاصة الرسالة

الاســم: أدىوولـى جيمـوه كـــايودي

العنـــوان:خصائص نقل الغازات في NANOCOMPOSITES البولي ايثيلين الطين
الدرجة العلمية : ماجستير العلوم
مجال التخصص : هندسة كيميائية
تاريخ الدرجة العلمية : مارس 2011

في هذا العمل، تمت دراسة التأثيرات لمختلف أنواع nanoclay وتركيزها على المرفلوجيا، والنقل ، زحف، الحرارية ، الخصائص الميكانيكية السطحية و السائبة للنانو المركبة .كما جرى التحقق من تطبيق الخطوط الملاحية المنتظمة في خط أنابيب النفط والغاز. تم قياس الخصائص السطحية الميكانيكية باستخدام تقنية nanoindentation. وقد تم اختبار نفاذية CO_2 و CH_4/CO_2 خليط الغاز في الضغوط التي تتراوح 50 حتي 106 شريط ودرجات الحرارة بين 30 و 70 ^oC. كما تم إعداد نموذج رياضي للتنبؤ نفاذية الغازات في nanocomposites البوليمر. تحليل النتائج كشفت أن يتم تحسين خصائص nanocomposites بواسطة إضافة nanoclay. نفادية الغاز تنخفض بنسبة 46،5 ٪ و 11،9 ٪ بإضافة wt٪N1.44P 5 و ٪ wt C15 A1 على التوالي. وهناك زحف للاسترداد من حوالي 93 ٪ يتحقق به N1.44P wt5 ٪. وأظهرت النتائج المتحصل عليها من الاختبارات nanoindentation عن خصائص سطح الميكانيكية اتجاه مماثل لذلك من قياسات كبيرة. لأول مرة، وهذا نموذج نفاذية أن يأخذ في الاعتبار وكان من آثار الضغط ودرجة الحرارة، وتحميل allinitcrysty جزيئات النانو المتقدمة. وأظهرت تناسب نموذج اتفاق جيد مع البيانات التجريبية. عموما، لوحظت خصائص معززة ل C15A nanocomposites التي يوجد مقرها في تحميل طين wt2.5 ٪ في حين كانت في تعزيز wt5 ٪ للبمركب متناهي في الصغر N1.44P مقرها. استنادا على هذه النتائج تم اخيار **nanoclay** المضافة لصف البطانة HDPE/nanocomposite.

CHAPTER 1

INTRODUCTION

1.1 Nanocomposite Materials

A new class of polymer composites has emerged in which the reinforcing phase has the dimensions in nanometric scale (Giannelis, 1996, and Hocine, 2010). These new composites (nanocomposites) offer significantly enhanced mechanical properties due to the high aspect ratio and high surface area of the dispersed nano-sized particles. The reinforcement efficiency of nanocomposites with 2 to 6% of anisotropic nanoparticles can in some situations match that of conventional composites with 40–50% of loading with classical fillers (Pavlidou and Papaspyrides, 2008). Various nano reinforcements are currently being developed; however, layered silicate clay minerals are the most popular due to their availability (natural source), low cost, high aspect ratio, high-surface area and more importantly environmental friendliness (Ray and Okamoto, 2003).

In reality, the mechanical behavior of polymer – nanofiller composites is controlled by several microsructural parameters which include the properties of the matrix and the fillers, as well as the methods of processing employed (Hocine, 2010). Layered silicates are known to be hydrophilic while on the contrary most of the engineering polymers are hydrophobic (Tjong, 2006). Thus, it becomes difficult to obtain a good dispersion of clay particles in most polymers due to the intrinsic incompatibility between the clay and the polymers. In order to have a successful development of clay-based nanocomposites, natural clays are

often chemically modified through an ion exchange reaction (Mittal, 2010; Hwang, et al. 2008). With such modification full advantage of the potential offered by nanoparticles in areas of improved mechanical and thermal properties can be obtained. Up till now, most of the claims regarding the improvement of properties of polymer by the addition of nanocomposite seem to plateau at about 4% clay loadings. Higher loadings of ~7wt% were reported for very few polymers such as Nylon -6 (Nguyen and Baird, 2006). This has been linked to the peresence of hydrogen bonding between amide groups and nanoclay particles. Exfoliation of most organoclays in neat polyolefins such as polypropylene and polyethylene is not very good and far less than that observed in polar polymers like polyamides, polyurethane, and so on. Again, exfoliation can be improved by adding a small amount (about 1 to 2 weight percent) of polyolefins that has been slightly grafted with maleic anhydride to act as a compatibilizer (Paul and Robeson, 2008). For example, polymer – organoclay affinity is increased by adding polyethylene – grafted – maleic anhydride (PE-g-MA). An alternative way to improve clay dispersion is the method of processing. Several studies were conducted on the synthesis and enhancement of properties of polyethylene/nanocomposite but much still need to be done in these areas. Three commonly used methods of synthesizing polymer/clay nanocomposites are intercalation of a suitable monomer and subsequent in situ polymerization; intercalation of polymer from solution; and polymer melt intercalation (Qi et al, 2006). The drawbacks of the first two methods are the requirement of suitable solvent, high cost associated with the purchase of solvents, their disposal and environmental impact. In addition, the method of in situ intercalative polymerization can lead to formation of exfoliated, intercalated or agglomerated structures when the clay loading is higher than 3wt%. With melt intercalation technique, exfoliation

was observed at about 5wt% loading of montmorillonite (Nguyen and Baird, 2006). Consequently, the melt intercalation technique has been employed in this research.

PE is one of the most widely used polyolefin polymers for domestic and industrial applications such as garbage bags, transparency films, clothing and carpeting fibers, automotive and aerospace components, videotapes, packaging films and plastic bottles. Thus, PE–clay nanocomposites have recently attracted considerable attention due to the need for improved mechanical and thermal properties. Variety of research is done on polymer/clay nanocomposite especially on polypropylene nanocomposites. The high density polyethylenes (HDPEs) have been studied to a lower extent (Fujiyama, 2010). Moreover, literature review shows that few of the available research works on polyethylene – clay nanocomposites have not reported the complete behavior and properties of the PE/nanocomposite. For examples, the flammability of PE/nanocomposite was studied by Zang and Wilkie (2003). Lotti, et al. (2008) carried out study on rheological, mechanical and transport properties using clay Cloisite 20A, and Pegoretti et al (2007) investigated the microstructural and mechanical charateristics using clays Cloisite 20A and 15A with focus on the creep behavior. Also, the work of Qi et al (2006) on PE – clay nanocomposite has focussed on low density polyetylene using in situ graft method.

Cloisite C15A, C10A and 30B were reported to be very good reinforcing nanoparticles for some polymers up to a maximum loading of about 3wt% (Innocentini-Mei, 2010). Specifically, C15A has been reported to be suitable for less polar polymer while 30B is suitable for more polar polymers (Pavlidou and Papaspyrides, 2008). For example, C30B was used by González-Vidal, et al. (2010) to investigate the preparation, morphology and properties of poly(hexamethylene terephthalate) – layered silicates. Thus C30B was

employed to study its effect on the compatibilized PE samples produced. Moreover, the effect of the number of alkyl groups attached to the nitrogen of arganic modifier on exfoliation and improvement of mechanical and transport properties was investigated by Hotta and Paul (2004). The authors found out that nanocomposites derived from the organoclay having two alkyl tails (2M2HT) exhibited better dispersion and improvement in mechanical properties than those based on organoclays having one alkyl tail. Similar results were obtained by Samak et al. (2008). Thus C15A with two alkyl tails was one of the organoclays used in this work.

1.2 Nano Indentation

Hardness testing is widely used to study the mechanical properties of metals and ceramics due to a direct correlation between hardness and yield strength of these materials. Vickers indentation tests have been used to measure hardness, toughness, residual stress, yielding stress, modulus of elasticity and thermal shock resistance. Similar studies for viscoelastic materials such as polymers and its composites is less common due to its pronounced degree of elastic recovery and time-dependent properties. However, it has been shown that hardness measurements can be correlated with the mechanical properties (Flores et al, 2000, Giri, et al., 1995, Suwanprateeb, 2000, and Suwanprateeb 2000) and can also be used to observe changes in the surface morphology and microstructure of polymers (Suwanprateeb, 2004). Application of conventional hardness testing techniques for polymer characterization is limited due to their high loads, indenter shapes and high hardness range. In the present study, instrumented nanoindentation was used to determine the mechanical properties of polymer composite surfaces. This technique employs small loads and miniature indenter

tips that can not only measure the hardness but also the modulus of elasticity and creep deformation of the material surface. The objective of nanohardness measurements was to determine the surface mechanical behavior of HDPE nanocomposites and investigate possible correlation between its surface and bulk properties.

1.3 Objectives

The overall objective of this work is the selection of a proper clay additive to be used for PE liners used in gas pipelines. These liners usually fail to isolate the sour gas from steel pipes and eventually this leads to corrosion of the pipeline. It is essential to understand the reasons behind the failure of the PE liners. Possible reasons could be pure mechanical due to stress cycles and creep of polymers or the gas may diffuse in the liner due to high pressure or a combination of these two factors. The use of clay additives was suggested to improve the mechanical properties of the liner with a special focus on creep. Also, the use of clay additives is expected to limit the diffusion of natural gas in the liner. Temperature effects are also examined. Therefore, there is a need to screen clays of diffrent structures for potential application as fillers in PE liners. In addition to the decrease in permeability of the resulting PE-Clay liner, it is also important to ensure that other essential properties such mechanical and thermal properties are not compromised. In this research, the influence of variuos nanoclays on morphological, transport, creep, thermal, surface and bulk mechanical properties of PE-nanocomposite are investigated for possible liner application in oil and gas pipeline network. Four different organically modified nanoclays were used. These are Cloisite® 10A, Cloisite ®15A, Cloisite® 30B and Nanomer® 1.44P. Henceforth, these organoclays shall be referred to as C10A, C15A, C15B and N1.44P in this report. Throughout the review carried out on this work and to the best of our knowledge, we did

not come across a publication in the open literature where N1.44P was studied as reinforcing agent for polyethylene. In addition to the experimental work, a mathematical model was also developed for predicting the permeability of natural gas at high temperature and pressure.

CHAPTER 2

LITERATURE REVIEW

This chapter is devoted to a short review of transport through polymers, mechanical properties and the thermal properties of polymer nanocomposite. The first section gives an introduction to the topic of gas transport, the transport parameters (the permeability, the solubility, and the diffusion coefficients) and the influence of the polymer structure on gas transport. The second section discusses the influence of nanoclay addition on the mechanical properties of the polymer nanocomposite while the last part contains effect of nanoclay on the thermal properties.

2.1 Transport Parameters

Generally, transport processes are described by three coefficients. These include permeability, solubility, and diffusion coefficients.

2.1.1 Permeability Coefficient (P)

This transport parameter is an indication of the rate at which a permeant traverses a polymeric material. It is therefore the critical parameter that researchers are trying to investigate whenever they are involved in the design of new materials. The permeability coefficient is the product of the solubility coefficient (S) and the diffusion coefficient (D). For a component i, the permeability coefficient P is given as (Koros and Madden, 2003):

$$P_i = D_i S_i \qquad 2.1$$

The permeability is often expressed in barrers.

$$1 \text{ barrer} = 10^{-10} \text{cm}^3\text{@STP.cm/cm}^2\text{.s.cmHg.}$$

The value of the permeability coefficient depends on operating conditions, such as temperature, pressure, and composition, as well as on the structural features of the polymeric material. It is mainly dominated by the diffusion coefficient since variations in D are greater than those in S (Vieth 1991, Mohr, et al., 1991, and McHattie and Paul, 1991).

2.1.2 The Solubility Coefficient (S)

Solubility coefficient is a measure of the amount of gas sorbed in a membrane when equilibrated with a given pressure of gas at a particular temperature. It is a thermodynamic parameter that is believed to be dependent on the amount of free volume, the condensability of the penetrant, and on the degree to which the permeant interacts with the polymeric matrix (Baird and Collias, 1995).

2.1.3 The Diffusion Coefficient (D)

This parameter indicates how fast a penetrant is transported through the membrane. It is a kinetic parameter, which is related to the polymer chain mobility or flexibility and to the mobility of the permeant. Diffusion coefficient is also believed to relate to the free volume content, as apparent from the correlations showing an increase in the diffusion coefficient with an increase in the free volume content (Duda and Zielinski 1996, Yampolskii, et al. 1998)

2.2 Laws of Transport Phenomena

The most widely used law of transport phenomena is the laws of diffusion. This law was derived from an analogy with the Fourier's law of conduction in heat transfer. Consider a

polymeric material of thickness *l*, surface *A* that is subjected to a fluid. Let *Q* be the total amount of penetrant which has passed through this polymer during time *t* then*:*

$$J = \frac{Q}{At} \tag{2.2}$$

where *J* is the diffusive flux of a penetrant molecule.

Based on the mathematical theory of diffusion in anisotropic medium, the Fick's first law states that the diffusive flow (J_i) of molecules of specie *i* across a polymeric membrane per unit time and a unitary area is proportional to the concentration gradient between the two sides of the material (Wilkinson, 2000).

$$J_i = -D\nabla C \tag{2.3}$$

where D is the proportionality constant often referred to as the diffusion coefficient.

This first law is applicable in the steady state which is reached when the concentration does not vary with time and the flux is constant. In the unidirectional case, when the diffusion occurred only in one direction *x*, the relation reduces to:

$$J_x = -D\frac{\partial C_i}{\partial x} \tag{2.4}$$

Equation 2.4 is valid when the thickness of the material under consideration is much smaller than the other dimensions (for example, the diameter of a circular material). This condition must hold for the phenomena of diffusion in the other directions to be neglected.

In transient state, the penetrant concentration is a function of position and time. Fick's second law of diffusion is used to describe this unsteady state condition and is given by:

$$\frac{\partial C(x,t)}{\partial t} = \nabla \cdot (D\nabla C_i) \tag{2.5}$$

$C(x,t)$ is the local penetrant concentration at a position coordinate *x* and at time *t*. Above equation can be integrated by taking into account the initial condition $(t=0)$ and boundary conditions $(x=0,l)$ (Klopffer and Flaconnèche, 2001), and constitutes the theoretical reference for numerous problems of common diffusion. Solution to this equation provides the concentration profile in the diffusion zone at different intervals of time.

In most of the penetrant-polymer systems with well defined conditions, *D* can be considered as constant in all the membrane thickness. Thus Equation (2.5) reduces then to

$$\frac{dC}{dt} = D\frac{d^2C}{d^2x} \qquad 2.6$$

However, situation also arises when D is a function of the penetrant concentration. In such case diffusion coefficient can be defined as a mean coefficient over the entire range of concentration (Vieth,1991; and Naito et al, 1993) as:

$$\bar{D} = \frac{\int_{C_v}^{C_m} D(C)dC}{\int_{C_v}^{C_m} dC} = \frac{1}{C_M - C_V}\int_{C_v}^{C_m} D(C)dC \qquad 2.7$$

2.3 Mechanism of Gas Transport Processes in Polymeric Materials

To gain a better understanding of the mechanism of gas transport in polymers, it is important to study the polymer-solute interactions. Generally, there are two principal microsructural conditions of polymeric materials – the glassy and the rubbery states. Polymer structure is an important parameter to take into account because the transport phenomena in a glassy polymer differ totally from those in a rubbery polymer (Vieth,

1991). Polymeric materials in their glassy states are hard, brittle and posses restricted polymer chain mobility, very dense structures, strong intermolecular forces between backbone chains and little internal void space (2 to 10%). Motion within the structure of glassy polymers is largely vibratory. Penetrant diffusivity through their structure is very low. On the other hand, polymers in the rubbery states are tough and flexible with associated free chain movement. In this state, larger amount of free volume through which diffusion can take place are readily accessible. This review will be limited only to transport in rubbery polymers because the polymer matrix under consideration (polyethylene) is rubbery and semi crystalline at room temperature. Details of commonly used models for describing transport in glassy polymer are presented in (Klopffer and Flaconnèche, 2001).

On the basis of relative mobilities of the penetrant and polymer, diffusion in a matrix polymer can be classified into three (Klopffer and Flaconnèche, 2001) - Fickian, Non – Fickian and Anomalous diffusions.

- Case I; Fickian behavior: - the diffusion process has a rate much smaller than that of the relaxation modes of the polymeric matrix. The sorption equilibrium is quickly reached and the boundary conditions are independent of time and do not depend on swelling kinetics;
- Case II; non-Fickian behaviour which relates to a fast diffusion process compared with the simultaneous relaxation processes of the polymer. Here, the sorption phenomena is complicated by a strong dependence with the swelling (plasticizing) kinetics. These deviations from the Fickian behaviour are generally found in the case of the sorption of organic vapours by solid polymers and can persist until

around glass transition temperature (T_g + 15°C). In a nut shell, when a glassy polymer is highly plasticized by the penetrant in such a way that the diffusion coefficient becomes a function of time and of sample history, then non –Fickian behavior is assumed (Stern et al, 1996).

- Anomalous diffusion: this refers to a process when the diffusion and the polymer relaxation rates are comparable. The sorption and the transport of molecules are affected by the presence of pre-existing microvoids in the matrix; the penetrant motion is influenced by the geometrical structure of the polymer.

2.4 Gas Permeation in Rubbery Polymers

Various models have been proposed to describe the diffusion of small molecules through polymers above their glass transition temperature. Some of the models are based upon analysis of the relative mobility of the diffusing molecules and of polymer chains by taking into account relevant intermolecular forces (these are called molecular models). Others relate the diffusion coefficient to the free volume of the system.

2.4.1 Molecular Models

Some of the approaches used in molecular models are based on energy considerations which mean diffusion of gas molecules in polymers is a thermally activated process. In these approaches, the diffusing molecule moves from a position to the other one when a sufficient amount of activation energy is available for the system. That is, certain amount of energy is needed to sufficiently separate the polymer matrix in order to allow the permeant molecule to make a unit diffusional jump (Klopffer and Flaconnèche 2001). The first molecular models were able to predict only the diffusion activation energy and not the

diffusion coefficients (Figure 2.1). In addition, the models sometimes required adjustable parameters whose physical meaning was not always well defined in terms of structure, volume and energy.

In the Activated Zone Theory developed by Brandt in 1959, a molecular model is formulated where the activation energy is decomposed into two terms:

$$E_D = E_i + E_b \tag{2.8}$$

where E_i is the energy required to overcome the attractive forces between chains and create a "hole" in the polymer structure for the penetrant and E_b represents the intramolecular energy used to bend the neighboring chains of the penetrant. Both E_i and E_b are dependent mainly on the molecule diameter (σ_p), the chain length involved in diffusion, and the length of an elementary jump.

$$E_i \propto \sigma_p \tag{2.9}$$

$$E_b \propto \sigma^2{}_p \tag{2.10}$$

Another molecular theory for transport in rubbery zones is that developed by DiBenedetto and Paul (Klopffer and Flaconnèche 2001). In this approach, the activation energy of the diffusion is equal to the potential energy difference between the "normal" dissolved state and the "activated" state in which the cylindrical cavity allowing the penetrant to move is present. This variation of the interaction energy between macromolecules is defined by Lennard-Jones potential.

2.4.2 Free Volume Theory

One of the most promising and earliest free volume models was developed by Fujita and his co-workers in 1961 (Choudalakis and Gohtist, 2009; and Dhoot et al, 2003). The authors suggested that the molecular transport in rubbery polymers is due to a redistribution of free volume and not due to a thermal activation. The basic idea of this theory is that a diffusing molecule can only move from one position to another when there is a space, available in its neighborhood, to receive it. Holes found in this volume are said to have been created by the Brownian movement of the molecular segments of the polymer chains. The dependence of *D* with parameters such as the concentration, the penetrant shape and size, the temperature and the glass transition temperature of the polymer can be explained using the free volume theory.

Free volume fraction is expressed as

$$f = \frac{V_f}{V} = \frac{V_{Tot} - V_{occ}}{V_{Tot}} \qquad 2.11$$

V_f is the free volume, V_{occ} is occupied volume and V_{Tot} is the total volume. There are three possible definitions for the occupied volume (Robertson, 1992).

i. the volume calculated from van der Waals dimensions
ii. the crystalline volume at 0K
iii. the total volume minus the fluctuation volume.

Extensive description of models relating the coefficients *S* and D to free volume fraction in amorphous polymers can be found in Klopffer and Flaconnèche (2001). In this work, review will be limited to models on semicrystalline polymers.

2.4.3 Gas Permeation in Semicrystalline Polymers

In both the glassy and rubbery states, permeability properties can be modified by the presence of crystalline phase or a stress induced orientation. These modifications tend to place an additional constraint on the mobility of the amorphous phase through which the diffusion can take place. The existence of crystalline phase always brings about longer and more tortuous diffusion paths. Having described the two major classes of polymeric materials, this literature study has focus on the understanding of process of gas transport through polyethylene/nanoclay composite. Generally, the diffusion coefficient can be related to the free volume fraction by an expression similar to that of Doolittle (Klopffer and Flaconnèche 2001).

$$D_T = RTA_d \exp\left(\frac{-B_d}{f}\right) \qquad 2.12$$

where A_d a parameter which depends on the penetrant size and shape, B_d a characteristic parameter of the available free volume fraction and f, the fractional free volume of the system is given by

$$f = \phi_1 f_1 + \phi_2 f_2 \qquad 2.13$$

Parameters ϕ_i and f_i are the volume fraction and the free volume fraction of the component *i* respectively.

With an assumption that a semicrystalline polymer can be represented by a two-phase mixture of crystallites and amorphous polymer (Li and Cheng 2003), the free volume

fraction of the amorphous phase, f_a can be predicted. Studies have shown that the sorption and diffusion phenomena took place exclusively in the amorphous phase of the polymer and not in its crystalline zones. Thus solubility coefficient can be expressed in terms of the interaction parameter and fractional free volume as follows:

$$S_a = kf_a \tag{2.14}$$

Thus, the diffusion coefficient can also be rewritten as

$$D_T = A\exp\left(\frac{-bv^*}{f_a}\right) \tag{2.15}$$

v^* is a critical volume related to the penetrant size, *A* and *b* are constants of the system under consideration. All the coefficients have been considered in relative to the amorphous zone because at temperatures well below the melting point, the gas molecules cannot be sorbed and diffuse inside the crystalline zones. Thus ϕ_a is also the amorphous volume fraction. The free volume fraction f_a is defined as

$$f_a = \frac{v - v_0}{v} \tag{2.16}$$

where v and v_0 are respectively the total specific volume of the amorphous phase and the occupied specific volume (of Van der Waals).

2.4.4 Influence of Temperature on Transport Coefficients

Generally, the transport coefficients - *Pe*, *D* and *S* depend on temperature, at a given pressure, via Arrhenius's law on a narrow range of temperatures as follows:

$$S(T) = S_0 \exp\left(-\frac{\Delta H_s}{RT}\right) \quad 2.17$$

$$D(T) = D_0 \exp\left(-\frac{E_D}{RT}\right) \quad 2.18$$

$$P_e(T) = P_{e0} \exp\left(-\frac{E_p}{RT}\right) \quad 2.19$$

The pre-exponential terms represent the limit values of the various coefficients of transport for an infinite molecular agitation $T \to \infty$. E_p is the apparent activation energy for the permeation process. It is related to the apparent activation energy of diffusion process by the relation (Stern et al, 1996):

$$E_P = E_D + \Delta H_S \quad 2.20$$

where ΔH_S is the heat of the solution needed for the dissolution of a permeant mole in the polymer matrix. The above parameters depend on the morphology of the polymer matrix. That is amorphous or semicrystalline structure, value of the temperature relative to the characteristic temperatures T_g and T_f and so on. ΔH_S can be obtained from the relation (Stern et al, 1996):

$$\Delta H_S = \Delta H_{cond} + \Delta H_l \quad 2.21$$

In the above equation:

ΔH_{cond} is the molar heat of condensation, this term is always negative and small for gases;

ΔH_l is the partial molar heat of mixing. This is a small and positive term, which can be estimated from the cohesive energy densities of the penetrant and the polymer using Hildebrand's theory (Klopffer and Flaconnèche, 2001).

$$\Delta H_1 = V_1(\delta_1 - \delta_2)^2 \phi_2^2 \qquad 2.22$$

where δ_1 and δ_2 are solubility parameters which are the square roots of the cohesive energy densities of the penetrant and the polymer. V_1 is the partial molar volume of the penetrant and ϕ_2 the volume fraction of the polymer in the mixture.

The activation energy physically represents the energy level that a molecule should reach to make a jump between one position and another one (Dhoot et al, 2003). It is always a positive quantity. Consequently, *D* is an increasing function of thse increased temperature. This effect may be expressed in terms of an increase in free volume directly related to the bulk expansion of the polymer due to the increased segmental motions and hence, the diffusion process of molecules is facilitated. For a given polymer, the activation energy E_D increases with the penetrant size (more space is required), and reaches an asymptotic limit when the penetrant mobility becomes comparable to that of the polymer segments (Klopffer and Flaconnèche 2001). Experimentally, this theory was verified on many penetrant-polymer systems and values obtained ranged from 10 to 100 kJ/mol.

The pre exponential factor D_o has an entropic character (Krevelen, 1990) and takes into account the length jump and increases with the penetrant size. But, for a given polymer and at a fixed temperature, the diffusion coefficient always decreases with the diffusing

Table 2.1 **Molecular size of CH_4 and CO_2**

Gas	Diameter (nm)	Sources
CO_2	0.330 – 0.389	(Naito et al., 1993; and Koros and Madden, 2003
CH_4	0.380 – 0.41	(Naito et al., 1993; and Koros and Madden, 2003

molecule size. Table 2.1 contains the molecular sizes of some gas molecules. According to Krevelen (1990), the following empirical relation can be obtained:

$$\ln D_o = aE_D + b \qquad 2.23$$

with a and b, coefficients which depend on the considered penetrant type for a given polymer. The activation energy is independent of temperature only over a small range of temperatures (Klopffer and Flaconnèche 2001). It has been shown clearly that, on a wide range of temperatures (from 20° to 100°C), the activation energy is a function of the temperature and is in agreement with the Activated Zone Theory of Barrer. When T increases, the chains entropy grows, the activated zone size is larger and the chains mobility is enhanced, therefore E_D increases. The energy is considered the sum of two terms:

$$E_D = E_D(C \to 0) - \gamma RT \qquad 2.24$$

The term $E_D(C \to 0)$ represents a measure of the apparent activation energy for diffusion in a polymer matrix which is otherwise unaffected by the presence of the penetrant in terms of segmental motions. The second term is to take care of the amount by which the apparent activation energy is reduced by the sorption of the penetrant (plasticization). Generally, the diffusion of small, non-reactive molecules with the polymer leads to lower values of activation energy at $T < Tg$ than at $T > T_g$. However, recent research by Tonge et al. (2001) on PMMA in a range of temperatures near the glass transition temperature (above and below) did not show the same behavior for E_D as earlier mentioned in the vicinity of Tg. On the other hand, D_o varied sharply. In summary, the activation energy is influence by the rigidity of the polymer backbone, the cohesion energy of the polymer and the penetrant size (Weinkauf and Paul, 1990).

2.4.5 Influence of Concentration on Transport Coefficients

Equations for representing the influence of concentration on transport coefficient are based on whether the system obeys Henrys law or not. For systems in which the solubility essentially obeys Henry's law (for example hydrocarbons in elastomer), the diffusion coefficient on the sorbed penetrant concentration has been empirically represented, at a given temperature, by a linear equations of the form (Klopffer and Flaconnèche 2001):

$$D(C) = D(0)(1 + \beta C) \qquad 2.25$$

The dependence can also be represented with an exponential model:

$$D(C) = D(0)e^{\beta C} \qquad 2.26$$

$D(0)$ is the limit of D when C tends towards zero and ß is a constant parameter at a fixed T, characterizing this dependence. When the systems under consideration do not follow exactly Henry's law, the isotherm of Flory-Huggins type (high-soluble gases in rubbery polymers) is used. Thus, the following expression for S was proposed by Naito *et al.* (1996):

$$S(C) = S(0)e^{\sigma C} \qquad 2.27$$

with $S(0)$, the limit value of the solubility when the concentration is close to zero. This term is in fact the Henry's law coefficient k_D which is a characteristic parameter at a given temperature (Klopffer and Flaconnèche 2001). σ is a constant relating to polymer-penetrant interactions.

For the diffusion coefficient, the concentration dependence can be represented as:

$$D(C) = D(0)e^{\left[\beta C / (1+\sigma C)\right]} \qquad 2.28$$

At a given temperature, the local concentration C of the gas dissolved in the polymer can be related to the pressure by the following relation:

$$C = S(C)\,p \qquad 2.29$$

where $S(C)$ is the solubility coefficient (which is a function of either C or p). This coefficient depends on the polymer-penetrant interactions as well as on the gas condensibility. For low pressures and ideal gas, Henry's law is obtained from 2.29

$$C = k_D\,p \qquad 2.30$$

where k_D is the proportionality constant of Henry's law. It is, in fact the solubility coefficient when there is no concentration dependence.

In practice, for the permeation of simple gases of low molecular weight in rubbery polymers, and under relatively moderate pressures, the diffusion mechanism is Fickian and the departures from Henry's law for the sorption are negligible (Scheichl et al., 2005). However, in this work, this assumption will not be applicable because permeability studied is carried out at very high pressure. Cases of high pressure gas permeation have not yet been given much attention in literature (Scheichl et al., 2005).

2.4.6 Influence of Pressure on Transport Coefficient

The effect of pressure on gas diffusion through rubbery polymers was first studied using the free volume theory. The results of these studies showed that the evolutions of the permeability coefficient with pressure depend on the diffusing molecule type. For organic vapours or very soluble gases such as CO_2, *Pe* increases whereas it decreases for little soluble gases such as He, N_2 (Klopffer and Flaconnèche 2001). Thus, it was concluded that the pressure influence could be explained as the result of two opposing phenomena as follows

- phenomenon related to the hydrostatic pressure which in turn leads to an increase of the polymer density, *via* polymer compaction, thereby reducing the free volume inside the polymer
- phenomenon due to the diffusing molecule concentration within the matrix where the pressure increase corresponds to an increase of the penetrant concentration in the polymer. The diffusing molecules can plasticize the macromolecular chain, which means an increase free volume.

Each of the above effects leads to a different evolution of *Pe*. Obviously, the first one of these two mechanisms tends to retard the diffusion process by reducing the segmental motions whereas the second enhances it. The simultaneous but opposite effects of at a given temperature was described by Naito *et al.* (1991, 1993) using the following model::

$$D(C,p) = D(0,0)e^{\beta_h p + \alpha C} \qquad 2.31$$

In the above relation:

$D(0,0)$ is the diffusion coefficient at $C = 0$ and $p = 0$; the exponential term $e^{\beta_h p}$ represents the hydrostatic pressure effect, where β_h is negative because it expresses the drop of D. The term $e^{\alpha C}$ characterizes the increase of dissolved molecules in the polymer resulting from the plasticization, and hence, the more important available free volume.

This model is valid for pressures that never exceeded 10 MPa. The pressure effect (up to 10 MPa) on permeabilities of some pure gases (with various molecular sizes and solubilities) in rubbery polymers such as LDPE, PP, poly(ethylene-co-vinyl acetate) and polybutadienes have been investigated by Naito *et al.* (1991, 1993, 1996). Also, base on the kinetic theory for diffusion in liquids, the coefficient β_h is related to the activation volume V^* of the diffusion process, by means of the following relation (Naito *et al.*, 1991):

$$V^* = -RT\beta_h \tag{2.32}$$

with R the gas constant.

Above relation is valid when the compressibility of the amorphous fraction of the polymer (the rubbery state is comparable to a liquid) is assumed to be negligible.

The following relation was also proposed to express the dependent of V^* on the molecular size of the penetrants (Naito *et al.*, 1993):

$$\beta_h = -A\bar{d}^n \tag{2.33}$$

$\bar{d}$ is the average molecular diameter of the gas, *A* a constant and *n* a constant between 2 and 3 (for LDPE and PP). As for α, it is proportional to the partial molar volume and then, to the penetrant diameter.

The simplified form of the Flory-Huggins equation can be used to describe the mean solubility coefficient as follow:

$$S = S(0,0)\exp(\sigma C_\infty) \tag{2.34}$$

where *S*(0,0) is the solubility value when both values of *C* and *p* tend towards 0 (Henry's constant). Thus, the mean permeability coefficient is written as (Naito *et al.*, 1996):

$$\bar{Pe} = D(0,0)k_D \exp\left[\beta_h p + \left(\sigma + \frac{\alpha}{2}\right)k_D p\right] \tag{2.35}$$

Equation (2.35) can be used to a pressure up to 20MPa. A general equation that describes the dependence of *D* on the concentration, pressure and temperature was suggested by Benjelloun-Dabaghi *et al.* (2001):

$$D(T,C,p) = D_{00}(p)e^{\frac{-E_D}{RT}}e^{\beta C} \tag{2.36}$$

The term $D_{00}(p)$ is expressed in terms of pressure effect of diffusion as shown below:

$$D_{00}(p) = D_{00} \exp\left(\beta_h^L p + \beta_h^Q p^2\right) \quad 2.37$$

$\left(\beta_h^L\right)$ and β_h^Q are coefficients (linear and quadratic) relative to the pressure dependence. Their dimensions are MPa^{-1} and MPa^{-2}. This model has been validate with PVDF-CO_2 system by Benjelloun-Dabaghi *et al.* (2001).

2.4.7 Influence of Crystallinity on Transport Coefficient

The impact of crystallinity is evidence from the two phase model. For isotropic HDPE with spherulitic structures, it has been shown that the sorption and diffusion took place exclusively in the amorphous regions (Baird and Collias, 1995). The dispersed crystalline phase presents a resistance to the permeant passage. Specifically, these crystalline zones have two effects on the gases diffusion. First, they increase the effective path length of diffusion, and, second, they seem to reduce the polymer chains mobility in the amorphous phase (because chain ends are trapped in the neighbouring crystalline lamellae) and, then, lead to higher activation energy of diffusion. To account for these effects, a tortuosity factor (τ) and a chain immobilisation factor (β) were introduced by Michael and his coworkers. The following expressions were proposed for the coefficients of solubility and diffusion (Dhoot et al, 2003):

$$S = S^* \phi_a \quad 2.38$$

$$D = \frac{D^*}{\beta\tau} \quad 2.39$$

where S^* and D^* are the coefficients of solubility and diffusion in a completely amorphous polymer, and ϕ_a is the volume fraction of the amorphous phase. β is the factor relating to chain immobilization.

Diffusion coefficient can also be expressed in terms of the amorphous volume fraction as follows:

$$D^* = D_a \phi_a^n \qquad 2.40$$

where $1 < n < 2$ for unoriented and $\beta = 1$.

For polymers where the amorphous chains are restrained in mobility by their ends fixed in the adjacent crystals, the following expressions for the coefficients of diffusion and permeability have been proposed:

$$D = \frac{\psi}{B} D_a \qquad 2.41$$

where ψ is the detour ratio. It describes the detour that the penetrant should make to avoid the impermeable crystalline zones ($0 < \psi < 1$). B, is called the "blocking factor". It underlines that the amorphous regions included between two crystalline zones are sometimes too narrow and prevent the passage of the penetrant ($B > 1$).

Permeability is expressed in a similar manner as

$$Pe = \frac{\psi \phi_a}{B} D_a \qquad 2.42$$

where ϕ_a is the amorphous volume fraction and Pe is the permeability coefficient in the completely amorphous polymer. Among the main limitations in the understanding of the transport mechanisms in the semicrystalline polymers is that D^* and S^* cannot be measured directly. For this reason 100% amorphous state are sometimes assumed. Indeed, the transport properties are influenced by size and shape of crystallites, their spatial distribution, the crystalline morphology (which depends on the molecular weight, polydispersity index, processing conditions), the degree of crystallinity and the presence of

short ramifications (Klopffer and Flaconnèche 2001). The following expression was formulated to relate permeability and polymer density ρ (Klopffer and Flaconnèche 2001):

$$Pe = K(1-\rho) \qquad 2.45$$

where K and n are constants, n is close to 2.

2.4.8 Influence of Polymer Structure on Transport Coefficient

Researchers, over the year, have not found it easy to correlate the diffusivity of gases with the nature of the polymer. This is because it is impossible to change one feature of the polymer without affecting the others (Flaconnèche et al, 2001). There are some various parameters that may be linked together, some of which include the degree of chains packing, the segmental chain mobility, the polymer cohesive energy, the thermal expansion coefficient, the glass transition temperature, the crystallinity, the addition of plasticizers or reinforcing fillers and chain flexibility to mention but a few. Thus, introduction of lateral methyls in elastomers decreases the value of D because the flexibility also falls (due to increase in the cohesive energy between chains). On the other hand, side-chain groups may provoke steric hindrances. For example, the introduction of polar side-chains causes an increase of the energies of cohesion, thus resulting in a lower diffusion coefficient value. Indeed, the chain flexibility and the cohesive energy between macromolecules influence directly the glass transition temperature. The value of the diffusion activation energy is more important because the existing cohesive forces between chains are strong and as the gas molecule dimensions are also large. The average molecular weight of the polymer seems to have no influence on S, D and Pe, except for the case of very low values where the chain ends have a significant influence on the free volume.

2.5 Overview of Gas Barrier Properties in Polymer\Clay Nanocomposites

Clays incorporation into polymer matrix are believed to increase the barrier properties by creating a maze or ‘‘tortuous path’’ that retards the progress of the gas molecules through the matrix resin (Hu et al., 2008). The direct benefit of the formation of such a path is clearly observed in near to exfoliated nanocomposites (Sinha Ray et al., 2003a).

The gas barrier properties of nanocomposites primarily depend on the dimension and dispersion of layered silicate particles in the polymer matrix. When the degree of dispersion of layered silicate in the matrix is the same, barrier property of nanocomposite directly depends upon the layered silicate aspect ratio. Gusev and Lusti (2001) suggested that changes in the local permeability in the presence of silicate layers are also responsible for the improved gas barrier property. This factor is directly related to the molecular level interaction of polymer matrix with the silicate layers.

Chang et al. (2003) reported the oxygen gas permeability of polymer nanocomposites prepared with three different kinds of nanoclays using a melt intercalation technique. The results show that O_2 gas permeability of nanocomposites had systematically decreased with increasing clay content. At 10% clay loading, the permeability value of nanocomposites decreased to half of its original values for untreated polymer, regardless of the type of nanoclay. This is attributed to the increase in the lengths of the tortuous paths in nanocomposites in the presence of high clay content (Sinha ray Okamoto, 2003). Recently, Gorrasi et al. (2003) reported the morphology dependent vapor barrier properties of polycaprolactone/clay nanocomposites. The water sorption increases with the increase in the clay content, particularly for the composites containing the unmodified clay.

The permeability of O_2 in the cross-linked polyester nanocomposite films as a function of the volume fraction of clay was studied by Bharadwaj et al (2002). The permeability of O_2 through the cross-linked polyester nanocomposites films decreased relative to the pure cross-linked polyester film. More interestingly, it was observed that the decrease in permeability at 2.5 wt% clay content was greater than at other concentration, and this result was found to be consistent with the results of their mechanical testing. Their results suggest that the morphology is composition dependent.

In a similar experiment, the transport of O_2 and N_2 gases through poly (ethylene-co-vinyl acetate) – clay nanocomposites were studied by Kumar et al (2008). They analysed the morphology of the nanocomposite using X-ray diffraction and transmission electron microscopy. Their results showed that samples with 3wt% filler loading showed the least free volume and hence a considerable reduction in gas transport. Also, it was found that permeability increased for nanocomposites containing more than 3wt% due to agrregation of clay fillers at higher loading. The thermal stability also found to improve on incorporation of the clay filler.

Moreover, Muralidharana et al (2008) prepared poly(ethylene-*co*-vinyl acetate)/clay nanocomposite membranes with different clay loadings. The morphology of the nanocomposites was investigated using X-ray diffraction technique and transmission electron microscopy. The dispersion of layered silicates decreased with increasing filler loading. Samples with low filler content showed excellent dispersion of layered silicates resulting in a partially exfoliated structure. The transport characteristics of aromatic

hydrocarbons through the nanocomposite membranes were studied by the simple sorption gravimetric analysis in the temperature range

28–70◦C and the results were compared with unfilled membrane. The solvent uptake nature of the nanoclay filled polymer samples was found to be much reduced. The solvent uptake was minimum for composites with 3 wt% of filler and increased with increasing filler content, which is presumably due to aggregation of clay filler at higher loading. The influence of free volume on the transport properties of the membranes was studied using positron annihilation lifetime spectroscopy. The transport phenomenon was found to follow an anomalous mode. Activation parameters were estimated and the molar mass between crosslinks was calculated using Flory–Rehner Theory. The experimental data were compared with theoretical predictions. Thus the barrier property of nanocomposites was profoundly impacted by the degree of dispersion of intercalated layers in the polymer matrix. Strawhecker and Manias (2000) measured the water vapor transmission (WVT) rates of pure PVA and its nanocomposites. The permeability decreased to about 40% of the pure WVT values for silicate loadings of only 4–6 wt%. So, it is clear that nanoclay composites show enhanced barrier properties. On the other hand, nanocomposites with higher clay concentrations, showed a increase in permeability (Bharadwaj et al., 2002). However, the dependence on factors such as the relative orientation and dispersion (intercalated, exfoliated or some intermediate) is not still well understood.

Matteucci et al (2008) also shed more light on the anomalous permeability behavior of nanocomposite at higher clay concentration from the results of their investigation on gas permeability, solubility, and diffusion coefficients in 1,2-Polybutadiene/Magnesium Oxide

nanoparticles (3nm). It was observed that the nanocomposite density was consistently lower than that anticipated on the basis of an additive model, suggesting the presence of voids in the nanocomposites. It was also observed that acid gas (i.e., CO_2) and nonpolar gas (i.e., CH_4, N_2) permeability increased with increasing particle loading following the incorporation of nanoparticles into the polymer. For instance, CO_2 permeability increased from 52 barrer in the unfilled polymer to 650 barrer in a nanocomposite containing 27 vol % (nominal) MgO, at 35 °C and a feed pressure of 12 atm. Gas solubility increased systematically with increasing particle loading. In contrast, gas diffusion coefficients initially decreased with increasing particle loading and then increased with increasing loading at particle loadings greater than 10 vol% (nominal). According to the authors, the exhibited higher permeability was said to have resulted from the presence of voids in the nanocomposite films. Thus as the void concentration increased, gas permeability also increased. This phenomenon was due to increase in both gas solubility and permeability. Diffusion coefficients were lower than in the unfilled polymer at low particle loading but increased at higher loadings to levels that were higher than the unfilled polymer at the highest particle loadings considered. For instance, in a PB film containing 27 vol% (nominal) MgO, about 60% of the CH_4 permeability increase, relatively to an unfilled sample, can be attributed to an increase in solubility, while the remaining 40% of the increase can be attributed to an increase in the methane diffusion coefficient.

Bharadwaj (2001) addressed the modeling of barrier properties in nanoclay composites based upon the tortuosity arguments described by Nielsen in 1967. These models predict the minimum permeability that can be expected for a polymer filled with plate like particles. The correlation between the sheet length, concentration, relative orientation, and

state of aggregation is expected to provide guidance in the design of better barrier materials using the nanocomposite approach. The presence of filler, spherical, plate, cylindrical, and so on, introduces a tortuous path for a diffusing penetrant. The reduction of permeability arises from the longer diffusive path that the penetrants must travel in the presence of filler. A sheet-like morphology is particularly efficient at maximizing the path length.

The effect of pressure on the solubility, diffusivity, and permeability of He, H_2, O_2, N_2, CO_2, CH_4 , C_2H_4, C_2H_6, C_3H_6 and C_3H_8 in poly(ethylene oxide) (PEO) at 35 ◦C was reported by Lin and Freeman (2004). Additionally, the temperature dependence of permeability was also reported. The effect of polar ether linkages in PEO on gas transport is illustrated by comparing transport properties in PEO with those in polyethylene (PE). For example, at 35^0C and infinite dilution, semi-crystalline PEO exhibits CO_2 permeability coefficient of 12 barrers, and CO_2/H_2 and CO_2/N_2 pure gas selectivities of 6.7 and 48, respectively. In contrast, at similar conditions, the permeability of PE to CO_2 is 13 Barrers, but the CO_2/N_2 selectivity is only 13. In addition to good separation properties for quadrupolar – nonpolar gas pairs, PEO also shows interestingly high selectivity for olefins over paraffins, which is ascribed to favorable interaction between the polar ether groups in PEO and olefins. For example, the infinite dilution permeability of PEO to propylene is 3.8 Barrers and pure gas propylene–propane selectivity is 2.7 at 35 ◦C.

A simple renormalization group model was proposed by Lu and Mai (2005) to assess the influence of geometric factors (such as aspect ratio, orientation, and extent of exfoliation) of layered-silicate fillers on the barrier properties of polymer-clay nanocomposites. The barrier properties of polymer-clay nanocomposites, with far less inorganic contents of

layered silicate fillers, are remarkably superior to those of neat polymers or their conventional counterparts. The results show that the aspect ratio of exfoliated silicate platelets has a critical role in controlling the microstructure of polymer-clay nanocomposites and their barrier properties. The estimated percolation thresholds of clay content for minimum permeability are in good agreement with experimental data.

Frounchi et al (2006) carried out a study on nanocomposites of polypropylene (PP)/ ethylene-propylene-diene rubber (EPDM) blend with montmorillonite-based organoclay prepared in a solvent blending method. The authors used permeability model for flake-filled polymers to estimate the aspect ratio of nanoclay platelets in the blend nanocomposites. According to the permeability model, very high barrier property could be obtained if the aspect ratio of the flakes or platelets of the organoclay could be significantly increased in the blend. In the same research, differential scanning calorimetry measurements was used to study crystalinity and the results indicated a decrease in crystallinity up to 27% suggesting a reduction in spherulites growth. However, the melting temperature remained unchanged. The increase in barrier property of the blend, despite a decrease in crystallinity, indicated the dominant role of organoclay platelets in barrier improvement.

Gas barrier properties of polyethylene-layered silicate nanocomposites have been examined by Maged et al. (2005). The gas permeability was measured as a function of the filler loading. The authors report that oxygen permeability in HDPE with 2.8% nano clay loading decreased to almost half that of neat HDPE. Zhong et al (2005) studied the oxygen barrier properties of organoclay-polyethylene nanocomposite films. An organically modified montmorillonite was compounded with ethylene vinyl acetate copolymer (EVA), low

density polyethylene (LDPE), and high density polyethylene (HDPE) in a twin-screw extruder. Oxygen permeability of these nanocomposite films was investigated to understand the effects of organoclay on different types of polyethylene. It was found that the clay enhancing effects are strong function of the matrix. The oxygen barrier properties of clay/EVA systems increased with clay loading. The oxygen barrier of EVA doubled at 5 wt% clay. Maleic anhydride grafted polyethylene (MAPE) usually is used as a compatibilizer for LDPE and HDPE-based nanocomposites. However, the MAPEs were found to weaken the oxygen barrier of the PEs, especially for HDPE. This is believed to be a result of less compactness caused by the large side groups and the increase in polarity of the MAPEs. Incorporating 5 wt% clay improves the oxygen barrier by 30% for the LDPE/MAPE system. The tortuous path equation was used to model the oxygen permeability of the clay/EVA nanocomposite films.

Polyamide 6-montmorillonites membranes have been prepared and studied for a large range of clay content (from 0 to 18 wt%) by Picard et al (2007). The barrier properties of these systems have been determined for different diffusing molecules varying by their kinetic diameter and their interaction capacity. The relative permeability has been found to be independent on the diffusing molecule showing that a tortuosity effect is at the origin of the improved barrier properties. The crystalline morphology of the polyamide matrix has been shown to be only slightly dependent on the nanocomposite composition. Consequently, the permeation properties have been related to the clay content and dispersion. From a quantitative description of the montmorillonite particle dispersion, the ability of different geometrical models to describe the experimental relative permeability data is discussed. This modelling leads to the conclusion that it is necessary to consider the polydispersity of

the impermeable filler shapes and to take into account the presence of surfactant located at the inorganic surface to appropriately model the transport properties of the nanocomposites in a large range of nanoclay contents.

Permeation properties of the nanocomposites were studied as a function of processing methodology by Herrera-Alonso et al (2009) to evaluate the use of polyurethane/clay nanocomposite films as potential barrier membranes to gas permeation. The montmorillonite clay was intercalated with different alkylammonium ion surfactants before being introduced into the polymer matrix and the permeation properties of the nanocomposites obtained were studied as a function of processing methodology. Their results showed that permeation was highly sensitive to the preprocessing method. Membranes with sonicated particles in the polymer matrix had significantly lower permeation than membranes with stirred clay particles. This improvement in barrier properties was attributed to a better dispersion of the sonicated clays in the polymer matrix.

Recently, it has just been reported that nanocomposites with higher degree of exfoliation and higher glass transition temperatures, better mechanical properties and higher flame resistance can be produced by combining two procedures of in situ ringopening polymerization and melt blending of nanoclay. The synthesis of poly(hexamethylene terephthalate) (PHT) and montmorillonite organo-modified with alkylammonium cations bearing two primary hydroxyl functions was carried out by González-Vidal et al (2010). PHT /layered silicate nanocomposites were prepared by dispersing Cloisite 30B into the polymer matrix by two procedures - in situ ringopening polymerization of cyclic hexamethylene oligomers and melt blending of the nanoclay within the molten PHT. These two procedure were then combined using a highly filled PHT–CL30B premix a as

masterbatch to prepare the nanocomposites. The nanocomposite containing 25% (w/w) of inorganics was obtained by in situ ring-opening polymerization and then blended within molten PHT yielding a nanocomposite with 3% (w/w) of inorganics. Their results showed a partially exfoliated structures for samples prepared by melt blending while exclusively intercalated nanocomposites was obtained for samples produced by ring-opening polymerization. The two-step preparation method led to a nanocomposite with semi-exfoliated/semi-intercalated morphology exhibiting higher extent of clay platelet delamination. It was also revealed that clay delamination was favored by the grafting of PHT chains onto the nanoclay along the blending process. A slightly increase in Tg and a moderate decrease in melting enthalpy of PHT were observed upon addition of CL30B whereas Tm was maintained almost unchanged. Increases in the stiffness and storage modulus up to 20% and 40%, respectively, were attained while maintaining the elongation to break almost unchanged. A flame retardancy test showed a drastical enhancement in the behavior for the case of the masterbatch-based nanocomposites. It was concluded that partial exfoliation of clay platelets in nanocomposites, and in a higher degree in the masterbatch nanocomposite, is responsible for the improved mechanical properties that were observed with respect to the unfilled PHT.

Xu et al. (2006) theoretically analyzed the effects of clay layers on the barrier properties of polymer/clay nanocomposites containing impermeable and oriented clay layers. Using the relative permeability theory in combination with the detour theory, they obtained new relative permeability expressions that allow investigating the relative permeability as a function of different geometric parameters. It was found that intercalated and/or incomplete exfoliated structures and dispersed tactoids with several layers can effectively

enhance the barrier properties of the materials. Furthermore, the authors developed the chain-segment immobility factor to briefly discuss the chain confinement from clay layers. The results showed that the chain confinement enhanced the barrier properties of the intercalated nanocomposites.

To sum up, all of the above permeability studies are done at atmospheric pressure and for pure gases, which are hardly ever to be the actual conditions in the field. However, in this work, the permeability was studied at high pressure and for mixture of gases, in order to simulate the actual field conditions.

2.6 Mechanical and Physical Properties of Polymer/Clay Nanocomposite

Wu et al. (2004) investigated the influence of chlorinated polyethylene (CPE) on mechanical properties, morphology, and rheology of nanocomposites of poly(vinyl chloride, PVC) and nanometric calcium carbonate particles. Nanocomposites of PVC and nano-calcium carbonate ($CaCO_3$) particles were prepared via melt blending, and CPE as an interfacial modifier was also introduced into the nanocomposites. The mechanical properties, morphology, and rheology were studied. The elongation at break and Young's modulus also increased with increasing the nano $CaCO_3$ concentration. Also, the notched Izod impact strength achieved a significant improvement by incorporating CPE into the nanocomposites, and obtained a value of 745 J/m. Morphology investigation indicated that the nano $CaCO_3$ particles in the PVC matrix were encapsulated with a CPE layer.

Dynamic mechanical analysis (DMA) measures the response of a given material to an oscillatory deformation as a function of temperature or frequency. DMA results are composed of three parameters: (a) the storage modulus (G′ or E′), (b) the loss modulus (G″

or E″), and (c) tan δ, the ratio (G″/G′ or E″/E′), useful for determining the occurrence of molecular mobility transition, such as the glass transition temperature (Tg). DMA has been used to study temperature dependence of G′ of polymers upon nanocomposite formation under different experimental conditions (Sinha Ray et al., 2003). The enhancement of G′ at high temperature was observed by Maiti et al. (2002) and suggested to be due to mechanical reinforcement by the silicate layers as well as extended intercalation at high temperature. Above T_g, when materials become soft, the reinforcement effect of the silicate layers becomes prominent due to the restricted movement of the polymer chains.

The tensile modulus of a polymeric material has been shown to be remarkably improved when nanocomposites are formed with layered silicates (Sinha Ray and Okamoto, 2003). The dramatic enhancement of the modulus for such extremely low clay concentrations cannot be attributed simply to the introduction of the higher modulus inorganic filler layers. A theoretical approach is assuming a layer of affected polymer on the filler surface, with a much higher modulus than the bulk equivalent polymer (Shia et al., 1998). This affected polymer can be thought of as the region of the polymer matrix that is physisorbed on the silicate surface, and is thus stiffened through its affinity. Obviously, for such high aspect ratio fillers as silicate layers, the surface area is exposed to the polymer.

Bandyopadhyay et al. (1999) reported the first improved thermal stability of polymer nanocomposites that included clay. These nanocomposites were prepared by melt intercalation. Authors argue that the silicate layers act as a barrier for both the incoming gas and also the gaseous by-products, which in one hand increases the degradation onset temperature and also widens the degradation process. The addition of clay enhances the performance of the char formed, by acting as a superior insulator and mass transport barrier

to the volatile products generated during decomposition. Recently, there have been many reports concerned with the improved thermal stability of polymer nanocomposites prepared with various kinds of organically modified layered silicate (Paul et al., 2003).

Liu and Wu (2002) investigated polyamide 66/Clay nanocomposites via melt intercalation. Polyamide 66/clay nanocomposites (PA66CN) were prepared via a melt compounding method using a new kind of organophilic clay, which was obtained through co-intercalation of epoxy resin and quaternary ammonium into Na modified clay. The dispersion effect of silicate layers in the matrix was studied by means of XRD and TEM. The silicate layers were dispersed homogeneously and nearly exfoliated in the matrix as a result of the strong interaction between epoxy groups and PA66. The mechanical properties and heat distortion temperature of PA66CN increased dramatically. The finely dispersed silicate layers and the strong interaction between silicate layers and the matrix reduced the water absorption, at 10 wt% clay content; PA66CN only absorbs 60% water compared with PA66. The addition of silicate layers changed the crystal structure in PA66CN.

Zhang et al. (2005) investigated PE and PP nanocomposites based upon an oligomerically modified clay (lauryl clay). Nanoclay was modified with an oligomeric surfactant, which was then melt blended with PE and PP in a Brabender mixer. The morphology was characterized by XRD and TEM, while thermal stability was evaluated from TGA and the fire properties by cone calorimetry. The nanocomposites were best described as mixed immiscible/intercalated/delaminated systems and the reduction in peak heat release rate is about 40% at 5% inorganic clay loading.

Tjong and Meng (2003) reported their results on preparation and characterization of melt-compounded polyethylene/vermiculite nanocomposites. PE-layered vermiculite (VMT) nanocomposites were fabricated via direct melt compounding in a twin-screw extruder followed by injection molding. Exfoliated PE/VMT nanocomposites were readily prepared via *in situ* melt mixing of maleic anhydride modified VMT with PE. Maleic anhydride acts as either the intercalation agent for VMT or as a compatibilizer for the PE and VMT phases. XRD and TEM observations revealed the formation of exfoliated PE/VMT nanocomposites. The experimental results showed that the storage modulus and strength of nanocomposites tend to increase with increasing VMT content. Nearly 25% increment in the tensile strength and 50% increment in the storage modulus were achieved by incorporating 4 wt % VMT into PE. The thermal properties of the nanocomposites were investigated by DMA and DSC. The glass-transition temperature of PE/VMT nanocomposites appeared to increase upon the introduction of VMT into the PE matrix.

Osman and Rupp (2005) studied the interfacial interactions and properties of PE-layered silicate nanocomposites. Organically modified nanoclay, carrying alkyl chains, phenyl groups, or a combination of both, were prepared and compounded with PE. The oxygen permeability coefficients and tensile properties of the nanocomposites were correlated to the exfoliation of the organically modified nanoclay. Partial exfoliation was achieved, although no intercalation was observed. Aromatic moieties attached to the clay surface led to a stronger interaction between the OMMT layers and reduced exfoliation.

Hotta and Paul (2004) analyzed the nanocomposites formed from LLDPE and organoclays. PE-clay nanocomposites were prepared by melt compounding various combinations of a maleic anhydride grafted LLDPE (LLDPE-g-MA), a LLDPE, and two organoclays. The

two types of organoclays were selected to show the effect of the number of alkyl groups attached to the nitrogen of the organic modifier on exfoliation and improvement of mechanical properties. Nanocomposites derived from the organoclay having two alkyl tails, exhibited better dispersion and improvement of mechanical properties than nanocomposites based on the organoclay having one alkyl tail. This result was the opposite of what was observed for nylon-6 nanocomposites. In addition, the rheological properties and gas permeability of the nanocomposites derived from the organoclay having two alkyl tails were investigated. Both melt viscosity and melt strength increased with increased content of clay (MMT) and LLDPE-g-MA. Gas permeability was decreased by the addition of MMT.

Yang et al. (2003) prepared PE/ Montmorillonite nanocomposites by in situ coordination polymerization using a nanoclay/$MgCl_2$/$TiCl_4$ catalyst activated by Al(Et)3. The catalyst was prepared by first diffusing $MgCl_2$ into the swollen MMT layers, followed by loading $TiCl_4$ on the inner/outer layer surfaces of MMT where $MgCl_2$ was already deposited. The intercalation of nanoclay layers by $MgCl_2$ and $TiCl_4$ was demonstrated by the enlarged interlayer spacing determined by WAXD. The nanoscale dispersion of nanoclay layers in the PE matrix was characterized by WAXD and TEM. As a consequence, the crystallinity of the nanocomposite decreased sharply, whereas the tensile strength was significantly improved compared to that of virgin PE of comparable molecular weight. The confinement of the nanodispersed clay layers to molecular chain and the strong interaction between the nanoscale nanoclay layers and the resin matrix were thought to account for the decrease of crystallinity and the remarkable enhancement of strength.

Gopakumar et al. (2002) investigated the influence of clay exfoliation on the physical properties of nanoclay/polyethylene composites. Melt compounding was used to prepare conventional composites of Montmorillonite clay and PE as well as nanocomposites of exfoliated nanoclay platelets dispersed in a maleated polyethylene (PE-g-MAn) matrix. The extent of clay platelet exfoliation in the PE-g-MAn nanocomposites was confirmed by XRD and resulted in a significant reduction of the degree of crystallinity and increased polymer crystallization rates. Studies of non-isothermal crystallization kinetics suggested that the exfoliated clay promotes heterogeneous nucleation and two-dimensional crystallite growth. PE/clay composites behaved in a similar manner as conventional macro composites, exhibiting modest increases in their rheological properties and Young's modulus. Conversely, the nanoscale dimensions of the dispersed clay platelets in the nanocomposites led to significantly increased viscous and elastic properties and improved stiffness. This was attributed to the high surface area between the polymer matrix and the exfoliated clay, which resulted in enhanced phase adhesion.

CHAPTER 3

EXPERIMENTAL

3.1 Materials

A high density polyethylene (HDPE) HE3490-LS with melt flow index of 0.25 g/10 min (190^{o}C/2.16 kg) and density 959kg/m^{3} supplied by Borouge Company, UAE was used as matrix. This grade is usually used for liner applications. Polyethylene-grafted-maleic anhydride (PE-g-MA) used was acquired from Aldrich. PE-g-MA contained ~3wt% maleic anhydride; its viscosity is 1700-4500 cP and melt temperature is 105°C.

Commercial organoclays – Closite C10A, C15A and C30B were supplied by Southern Clay Products Inc and N1.44P by Nanocor, Inc. C10A contains dimethyl, benzyl, hydrogenated tallow, quaternary ammonium (2MBHT) at 125meq/100g Clay concentration as organic modifier while 15A contain dimethyl dehydrogenated tallow ammonium (2M2HT) at the same concentration. C30B contains methyl, tallow, bis-2-hydroxyethyl, quaternary ammonium (MT2EtOH) at 90 meq/100g clay. N1.44P nanoclay has a quaternary ammonium chemistry-based surface modification.

3.2 Sample Preparation

The same preparation process was used for all the composites. In accordance with procedure employed by Barick and Tripathy (2010), the clay samples were first dried for 24 hours at about 100^{o}C prior to blending them with the polymer. Sample of a new polymer of

PE and PE-g-MA was produced by melt blending 98wt% HDPE with 2wt% PE-g-MA (Zhang and Wilkie, 2003). Variuos research works has been done using different content of compatibilizer in nancomposite preparations (Hotta and Paul, 2004; Usuki, et al, 2005; Pegoretti, et al, 2007; Pavlidou and Papaspyrides, 2008; and Lee, et al., 2005). In this work, 2wt% of PE-g-MA was used for preparing the new polymer blend which henceforth will be reffered to as BHDPE. Masterbatches with higher concentration of organoclay were first prepared. These masterbatches were then diluted by melt blending with more BHDPE to attain a final composition of 1, 2.5 and 5wt% of organoclays with Brabender mixer operating at a blending temperature of 190^{o}C for 10 min at 50rpm. Sheets of various shapes were finally obtained by compression moulding in a Carver press.

3.3 Morphology Characterization

Degree of clay dispersion in the composites was first investigated by X-ray diffraction (XRD). The test was conducted on nanoclay powders, pure HDPE and the nanocomposites using a diffractometer with Cu Kα radiation of λ=1.5406Å, voltage of 40.0 kV, and current of 30.0 mA. Samples were scanned in 2θ from 1.8 to 10^{o} at the rate of 1^{o}/min. The XRD patterns were used to calculate d-spacings of the nanocomposites layers using Bragg's law. Relative intercalation (RI) of the clay in the polymeric matrix was calculated using equation (1).

$$RI = \left(\frac{d - d_o}{d_o} \right) 100 \qquad 3.1$$

where d_o and d are the d-spacings of the pure clay and the clay in the nanocomposites, respectively (Pegoretti et al, 2007).

SEM was done by first etching the polymer samples. Surfaces of theses sample were then coated with gold on a JEOL Fine Coat Ion Sputter JFC -1100m sputtering equipment. Morphological studies were performed on the chemically etched and gold sputtered samples using Scanning Electron Microscope.

3.4 Mechanical Testing

Tensile tests were performed using an Instron 5560 Mechanical Testing Machine on dumbbell specimens according to ASTM test standard D-638. All tests were conducted at cross - speed of 60 mm/min and gage length of 30 mm. The measured stress / strain data was used to find all the mechanical properties. The Young's modulus was calculated at 0.20% strain. Minimum of five samples were tested for each composition.

3.5 Differential Scanning Calorimetry (DSC)

DSC measurements were performed using a TA Q1000 instrument equipped with a liquid nitrogen cooling system and auto sampler. Nitrogen at a flow rate of 50 ml/min was used to purge the instrument to prevent degradation of samples upon thermal treatments. The DSC was calibrated in terms of melting temperature and heat of fusion using a high purity indium standard (156.6ºC and 28.45 J/g). Universal Analysis software was used to calculate the percentage crystalinity using 293J/g heat of fusion for a 100% polyethylene crystal (Blaine, 2010).

Nanocomposite samples (5–10 mg) were sliced and placed in a non-hermetic aluminum pans. To minimize the thermal lag between the sample and the pan, samples with flat surface were used. An empty aluminum pan was used as a reference. First, the baseline was calibrated using empty crimped aluminum pans. All testing was performed in the standard

DSC mode between 30°C and 200°C using the procedure described in Blaine (2010) and Cui and Tao (2010).

3.6 Dynamic Mechanical Analysis

The dynamic mechanical behavior of the PE/clay nanocomposites samples obtained from Carver press was measured using TA Q800 DMTA. The dimensions of the rectangular specimens used are 1 mm × 10 mm × 4 mm (thickness × width × length). Temperature step/Frequency sweeps and creep tests were performed.

3.7 Surface Mechanical Properties

Surface mechanical properties of the samples were measured using a nanoindenter. In a typical instrumented nanoindentation test, the applied normal load and the depth of penetration is recorded during the measurement while the area of the indent is calculated from the known geometry of the indenter tip. These values can be plotted to result in load-displacement curves. In the present study, three sided diamond pyramid Berkovich indenter was used. The indenter penetrated the sample at a maximum load of 20 mN with load/unload speed of 40 mN/min. The indenter remained stationary for 90 seconds between each loading and unloading cycle. The hardness, elasticity and creep data were acquired from the normal force versus penetration depth curves generated by the computer. A set of four indentations was acquired for each test. The nanoindentation method is used to correlate the bulk with nano mechanical properties.

3.8 Measurement of gas permeability

Natural gas is mainly composed of CH_4 with variable amounts of mainly CO_2. In this study, two compositions were used: 100% CH_4 (AGA, 99.5%) and a mixture of 80% CH_4

and 20% CO_2 (AGA, 99.5%). Pure CH_4 and mixed CH_4 and CO_2 permeabilities were determined using a high pressure 2-D permeation cell as shown in Figure 1. The operating conditions of the cell are up to 150 ºC and 700 bar. The cell consists of two chambers; a high pressure chamber (upstream) and a low pressure chamber (downstream). The molded polymer samples were sandwiched; one after the other, between the two chambers and they were supported by two porous plates that allow gas to freely contact the sample and at the same time prevents sagging of the polymer sample. The downstream chamber has a free internal volume of 22.057 cm^3 whereas the upstream chamber has a variable volume due to the metal bellow placed inside the chamber. By injection to- or withdrawal of water from the bellow using an ISCO pump (Teledyne 100DX syringe pump), it is possible to decrease or increase the volume of the upstream chamber. Due to this construction it is possible to perform permeability experiments at constant differential pressure across the polymer membrane. The two chambers are held together by two stainless steel flanges which are securely fastened by use of 8 heavy-duty stud bolts. The temperature in the chambers is controlled by circulating hot glycerine inside two heating jackets surrounding the chambers. The temperature is measured by a Pt-100 thermocouple (RS Components, ±0.1 ºC) which is placed in the gap between the two chambers close to the location of the polymer membrane. The pressures in the two chambers are measured by two Fisher-Rosemount pressure transducers. For safety reasons, the upstream side is connected to a pressure transmitter-switch system which shuts down the heating bath and the ISCO pump in case the pressure exceeds the cell limit. The entire cell is mounted on a frame in a fume hood after assembly. The up- and downstream pressures, the temperature and the amount

of liquid injected by the ISCO pump is computer recorded continuously during the whole experiment.

The polymeric sample was initially evacuated of any residual gas by applying vacuum to both sides of the membrane for several hours. The gas (CH_4 or CH_2/CO_2) is then charged to the upstream side; in this case the pressure difference between the upstream and downstream sides was varied between 50 and 106 bar. The temperature of the cell is set to 30, 50 or 70ºC. The pressure in the downstream chamber increases as the gas permeates through the polymer sample. Consequently, the pressure in the upstream chamber also increased since the experiments are performed at a constant differential pressure across the polymeric membrane. In practice, this is done by running the ISCO pump at constant pressure mode, using the upstream and downstream pressure difference as an input to the pump. The thickness of the polymer samples was measured using a micrometer screw. The thickness was measured on 15 different spots on the sample and from that an average was obtained.

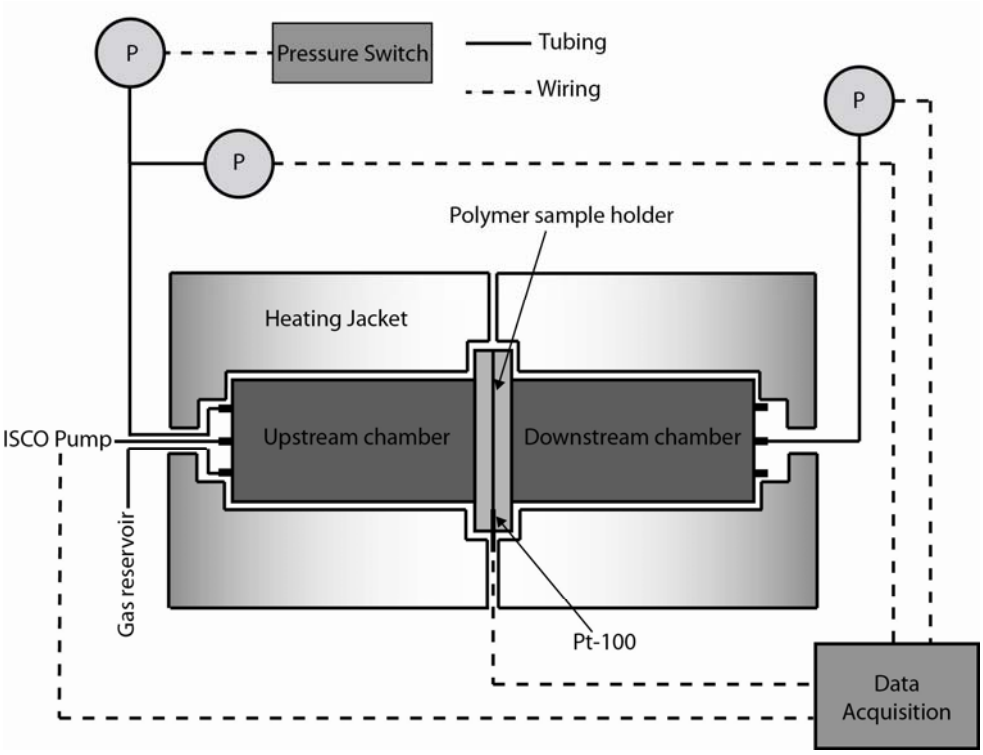

Figure 3.1: Schematic of the 2-D permeation cell, with pressure and temperature monitoring and control and data acquisition.

CHAPTER 4

RESULTS AND DISCUSSION: MORPHOLOGY, MECHANICAL, THERMAL AND TRANSPORT PROPERTIES

The results obtained from various mechanical, thermal and transport tests are discussed in the following.

4.1 X-ray Diffraction Analysis

Both X-ray diffraction (XRD) and SEM have been reported to be very good techniques to study the morphology of polymer nanocomposites. The intensity obtained from XRD is generally used as a means for classifying nanocomposites as either intercalated or exfoliated. For example, Figure 4.1 (a) shows the XRD patterns of BHDPE+C15A, while Figure 4.1 (b) provides similar information for BHDPE+N1.44P. In both cases, XRD results for neat organoclays (C15A and N1.44P) were also included for comparison. From these Figures, it can be seen that the organoclay pattern shows an intense peak at around $2\theta=4.02^{o}$ for N1.44P, corresponding to a basal spacing of 21.96 Å and $2\theta=4.6^{o}$ which is equivalent to a spacing of 19.19Å for C15A. Addition of 2.5wt% of C15A to BHDPE increase the basal spacing to 34.75 Å ($2\theta=2.54$), an increase equivalent to 81.08% compare to the neat organoclay. The basal spacing also increased to 31.30 Å ($2\theta=2.82^{o}$) corresponding to 42.53% relative intercalation, by adding 2.5% of N1.44P. Prevalent proposals from literature revealed that shifting of peaks to lower angles is an indication of

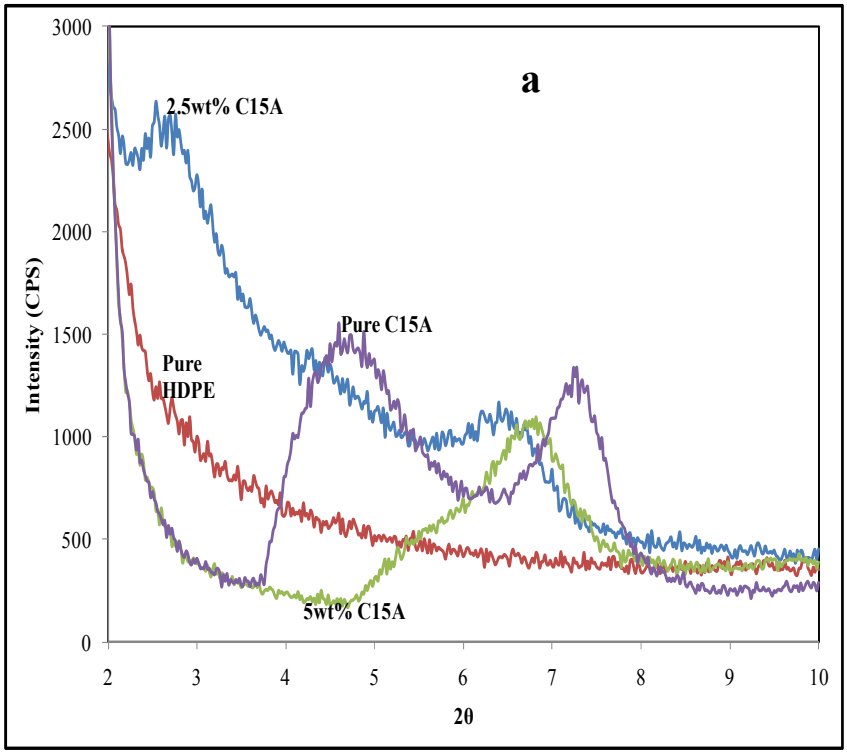

Figure 4.1a : XRD patterns for clay and polyethylene/clay nanocomposite for BHDPE+C15A

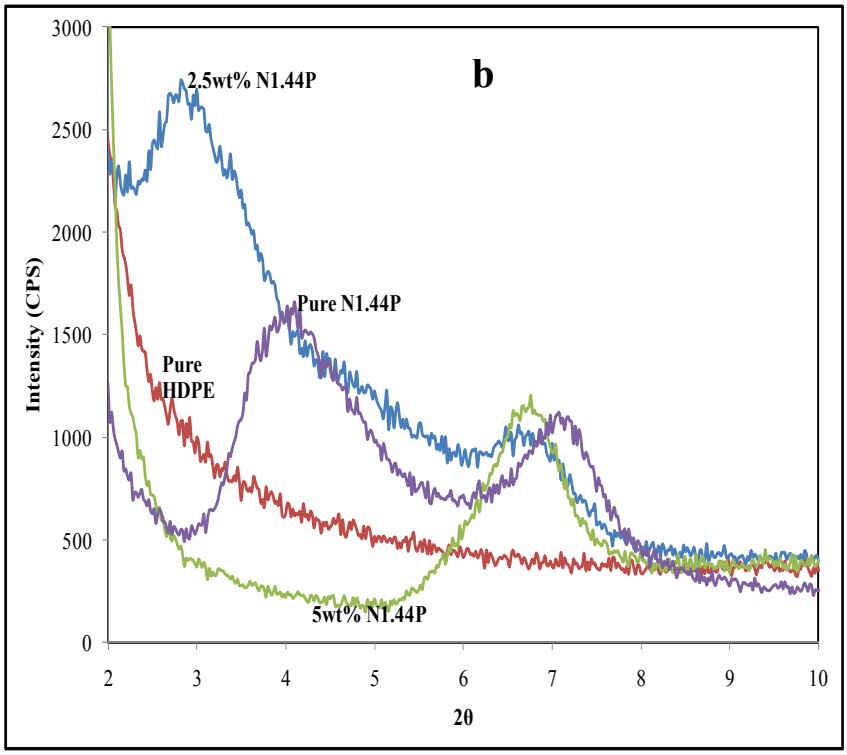

Figure 4.1b: XRD patterns for clay and polyethylene/clay nanocomposite BHDPE+N1.44P

penetration of the polymer chains into the clay gallery. Thus, these results suggest the formation of intercalated clay structure (Cui et al, 2007 and Herrera-Alonso et al, 2009). Also, the absence of peaks for nanocomposites with 5wt% C15A and 5wt% N1.44P can either be taken to be indicative of highly exfoliated structure or immiscible composites (Paul and Robeson, 2008; and Mittal, 2010). In this work, it is rather taken as an indication of finely distributed tactoids which is evident in the SEM results.

Secondary reflections were observed at high 2θ for the samples except the neat polymer. Such secondary diffractions have also been observed in results reported by Gopakumar et al (2002), Hotta and Paul (2004), Kannan and Bhagawan (2009), Mittal (2010), and Fujiyama (2010) for variety of polymer/clay nanocomposites. The presence of these peaks is an indication of the formation of conventional composites. Moreover, it is worthy of note that XRD signals are qualitative in nature. Any idealized classification of the composite morphologies as intercalated or exfoliated based on XRD results is entirely arbitrary Mittal (2010). Thus SEM tests were also performed to compliment these results.

4.2 SEM Analysis

SEM micrographs of chemically etched surfaces of the nanocomposites are shown in Figure 4.2 (a-d). It can be observed that the nanoclay are well dispersed as shown in Figure 4.2a for BHDPE+C15A with 2.5wt% loading and Figure 4.2c representing BHDPE+N1.44P with 2.5wt% loading. SEM results in Figures 4.2 (b and d) revealed agglomeration of the matrix particles. However, this agglomeration seems to be more intense in sample with 5wt% C15A (Figure 4.2b) than that of 5wt% N1.44P (Figure 4.2d). In Figure 2b, the agglomerated region is composed of a large number of C15A clay present within the composite matrix. The agglomeration was not localized at a particular region but

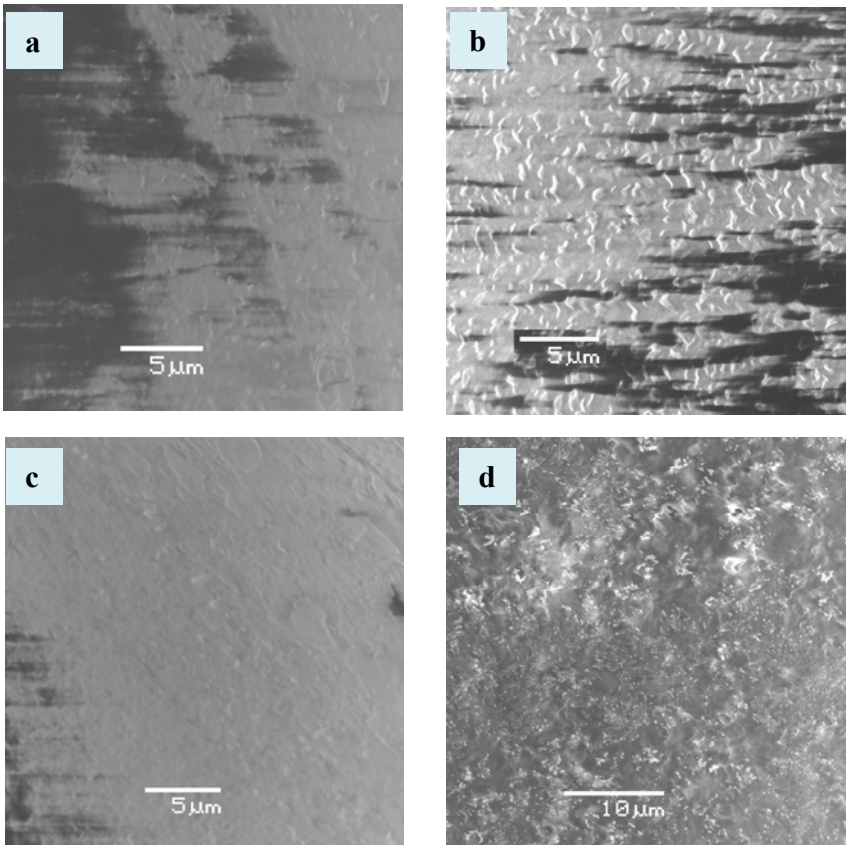

Figure 4.2: SEM micrographs of polyethylene/clay nanocomposites (a) BHDPE+C15A-2.5wt% (b) BHDPE+C15A-5wt% (c) BHDPE+N1.44P-2.5wt% (d) BHDPE+N1.44P-5wt%.

was seen to be distributed across the matrix of the composite. Like C15A, the nanocomposite of N1.44P is composed of agglomeration well distributed but with tactoids smaller than that of C15A.

4.3 Mechanical Testing

Table 4.1 shows the results for mechanical testings. It is evident that mechanical properties were markedly promoted by addition of PE-g-MA compatibilizer. The new polymer (BHDPE) is stiffer and tougher than pure HDPE. Young modulus increased by ~5%, elongation by ~20% and toughness by 35%. Percentage increments of ~25% and ~3% in ultimate strength and yield strength respectively were also observed. These results are in agreements with experimental works on polyolefin –clay nanocomposites (Hotta and Paul, 2004; Usuki, et al, 2005; Pegoretti, et al, 2007). In particular, Hotta and Paul (2004) reported approximately 8% and 28% increments in tensile modulus and tensile yield strain by adding 5wt% LLDPE-g-MA to LLDPE. No increment was observed for tensile yield strength. Also, Pegoretti, et al (2007) studied the tensile mechanical response of polyethylene nanocomposites and 0.33% and ~3% increase in yield stress and strain at break, respectively, were recorded upon the addition of 10wt% PE-g-MA to HDPE.

Tensile properties of the nanocomposite were also sumarized in Table 4.1. As usual, the effect of clay addition is markedly dependent on the polymer-clay intercalation level. The Young's modulus improvement was highest for C15A based polymer than all other clays. The 2.5wt% C15A filled BHDPE sample shows an enhancement of about 4% in Young's modulus, compared to the pure HDPE, while the increase for the BHDPE sample filled

Table 4.1 : Tensile Mechanical Properties of the HDPE and Nanocomposites

Polymer Type	% Loading	Young's Modulus (MPa)	Yield Strength (MPa)	Ultimate Strength (MPa)	% Elongation	Toughness (MJ/m^3)
PURE HDPE	0.0	644 ± 32.4	39 ± 1.2	48 ± 1.3	1002 ± 23.1	34 ± 1.2
BHDPE	0.0	663±20.4	41±1.5	60±2.1	1207±39.5	46±2.2
BHDPE +C15A	1.0	617 ± 25.0	40 ± 0.6	46 ± 4.5	862 ± 137.5	29 ± 6.1
	2.5	670 ± 16.8	38 ± 0.2	44 ± 3.2	906 ± 149.8	28 ± 5.8
	5.0	581 ± 19.6	35 ± 1.4	36 ± 2.0	716 ± 82.1	20 ± 3.2
BHDPE +C10A	2.5	600 ± 28.5	35 ± 0.2	40 ± 2.7	977 ± 71.7	28 ± 2.6
BHDPE +N1.44P	1.0	569 ± 13.5	33 ± 1.1	42 ± 2.4	1074 ± 10.8	31 ± 1.5
	2.5	621 ± 11.5	34 ± 0.2	38 ± 3.5	921 ± 111.1	26 ± 4.0
	5.0	664 ± 1.6	35 ± 0.3	35 ± 0.3	570 ± 62.8	17 ± 1.8
BHDPE +C30B	2.5	543 ± 9.5	35 ± 0.5	39 ± 2.1	870 ± 94.7	25 ± 3.2

with 5wt% N1.44P is 3%. The modulus decreased for both C10A and C30B based nanocomposites. The fluctuation in the change in modulus due to the addition of C15A is likely due to agglomeration which is apparent as the C15A loading was increased from 2.5 to 5wt%. Nanofillers are prone to both agglomeration as well as reagglomeration even after dispersion (Fujiyama, 2010). Logically, one may expect that higher stiffness can be obtained within 2.5 and 5wt% for C15A and above 5wt% for N1.44P. Generally, the improvement in Young's modulus is more effective for C15A at low loading and for N1.44P at higher loading. Both X-ray diffraction (XRD) and SEM were used to qualitatively describe the intercalation/dispersion of C15A and N1.44P nanaoclays in BHDPE matrix as discussed earlier.

There was a general decrease in the yield strength and ultimate strength as the nanoclay was added except for C15A at 1wt% loading where the yield strength increased by about 3% compared to pure HDPE. The yield strength continues to decrease gradually as the weight of C15A is increased. Similar results were reported by Goettler (2005), Zhao, et al. (2005), and Alexandre and Dubois (2000). This is expected since the composite becomes stiffer with the addition of clay. On the other hand, there was a decrease of about 18% in yield strength when 1% N1.44P was added and the yield strength increased as the wt% of the N1.44P was increased. Coinsidentally, addition of 2.5wt% C10A as well as C30B brought about the same decrease in yield strength (about 11%) but the ultimate strength decreased by 20% and 23%, respectively. This decrease is typical for C30B as reported by Finnigan, et al. (2004) and Pavlidou and Papaspyrides (2008).

The effect of nanocomposite formation on tensile strength is not yet clear since both reductions as well as increase of tensile strength upon nanocomposite formation have been reported. However, the decrease in the tensile strength observed in this work may be associated to the synergistic effect of the difference in polarity between PE and the clay, and the fact that there is an optimum clay concentration up to which nanocomposite tensile strength improvement can be achieved. Beyond this concentration, further increase in clay loading causes a moderate decrease of tensile strength since the tensile strength is usually sensitive to the degree of dispersion (Phang, et al. 2005, and Hocine, 2010). Thus, a decrease in yield stress accounts for a weaker polymer – clay interaction while its enhancement, even if small, is an indication of a good filler interaction (Pegoretti, et al, 2007).

Also, the elongation of all nanocomposites decreased except for N1.44P (at 1wt% loading). The toughness of all nanocomposites decreased in comparison with the pure HDPE. At the same loading, the decrease in elongation for C10A and C30B are different. The drop is more for C30B than C10A. This is most likely due to the fact that C30B is suitable for polar polymers (Pavlidou and Papaspyrides 2008). All these variations are similar to what was reported for other polymers by Finnigan, et al. (2004), Goettler (2005) and Fornes, et al. (2001). The slight deterioration in toughness accompanying the enhanced stiffness and strength has been reported by Fujiyama (2010). Generally, nanocomposite stiffness usually increases by significant factor over that of virgin matrix when uniform dispersion is achieved. However, literature also revealed that nonlinear mechanical properties such as tensile strength and elongation at break may decrease beyond critical proportion of reinforcing particles. This phenomenon may be explained by the fact that Young's

Table 4.2 Thermal Properties of Nanocomposites for various clay contents

Polymer type	**Nanoclay loading (wt%)**	**X_c, (%)**	**T_{onset}** (^oC)	**T_{peak}** (^oC)
PURE HDPE	0	65.32	116.34	131.6
BHDPE	0	67.05	116.23	132.81
BHDPE +C15A	1	63.56	115.81	133.72
	2.5	63.69	116.14	132.23
	5	60.36	115.78	133.23
BHDPE +C10A	2.5	62.32	115.93	133.45
BHDPE +N1.44P	1	62.35	115.88	134.39
	2.5	62.91	116.03	134.8
	5	63.87	115.8	135.03
BHDPE +C30B	2.5	65.14	116.06	133.48

modulus (stiffness) is evaluated at low strains (about 2%) whereas other properties are determined beyond catastrophic break where load transfer between the polymer and nanofiller is important.

4.4 DSC Analysis

The variation in thermal properties of the nanocomposites with clay loading is presented in Table 4.2. First, the comparison of the unfilled polymers, with and without the compatibilizer (PE-g-MA) is made. Here, the crystallization and peak temperature increased by about 3 and 1%, respectively while the onset temperature practically remained constant for BHDPE. Similar

results were reported by Jacquelot, et al. (2006) and Abbasi et al (2011) where the crystallinity increased by about 6.5% on addition of 20wt% LDPE-g-MA to metallocene – HDPE .

In agreement with previously reported results (Lee, et al., 2005), the temperature for the onset of thermal decomposition decreased with increasing clay content. The decrease is because the amount of PE- g-MA was fixed for various clay contents and the decrease in temperature might have been caused by difference in the amount of octadecylamine accompanied by an increase in the clay content. There was a decrease in crystalinity for all nanoclay except C30B which remain almost constant (0.18% decrease). For C15A, there was practically no change in crystallinity as the loading was increase from 1 to 2.5%. Thereafter a decrease of 3.33% was obtained. In the case of N1.44P, the crystallinity first dropped and then gradually increased with increase in the percent loading. The increase was more pronounced at higher loading. For example, about 0.9% increase in crystallinity was obtained by increasing the wt% N1.44P loading from 1 to 2.5 whereas 1.53% resulted when

the wt% was increased from 2.5 to 5. Similar flunctuation in the degree of crystallinity has also been reported by (Khumalo et al, 2010). According to the authors, flunctuations are due to the efficiencies of the nanoparticles as nucleating agents. Also, the presence of nanoclay such as montmorillonite in a polyolefin enhances its crystallization rate and reduces its crystalline (spherulite) size, since it functions as a nucleating agent (Abbasi et al, 2011). Moreover, comprehensive expalanations for dramatic changes in the crystalinity have been reported by Fujiyama (2010) and Paul and Robeson (2008). According to Paul and Robeson, the complex process of crystallization is influenced by many competing factors. Thus incorporation of nanoparticles into a polymer matrix can bring about both nucleation as well disruption of attainable spherulite size.

The melt peak temperature increased with loading. The highest melt peak temperature of 135.03^{o}C was obtained with the addition of 5wt% N1.44P. Moreover, when comparing the melting point for the nanocomposites with that of virgin polyethylene, it was observed that the melting point decreased with the addition of all nanoclays and hence the degree of crystallinity. This is a much expected result since it is well known that the incorporation of nanoclays in a semicrystalline polymer (such as polyethylene) constitutes a physical obstacle to the molecular chain movement that hinders the crystallization process (González-Vidal, et al. 2010).

4.5 Dynamic Mechanical Analysis (DMA)

4.5.1 Effect of temperature

Generally, DMA results are expressed by three main parameters: (a) the elastic response to the deformation termed as the storage modulus (E'), (b) the plastic response to the deformation corresponding to the loss modulus (E''), and (c) the $\tan\delta$ (ratio E''/E') which

is a measure of the damping behavior responsible for determining the occurrence of molecular mobility transitions such as the glass transition temperature. In this work, DMA was carried out to monitor the temperature and frequency dependence of these three factors as shown in Tables 4.3, 4.4 and 4.5, respectively. The significant enhancement of storage modulus ($E^{'}$) in the investigated temperature range for all BHDPE nanocomposites over that of pure HDPE matrix (Table 4.3) indicates that nanoclay has a strong effect on the elastic properties of the neat HDPE due to the restricted movement of HDPE chains that resulted from the dispersion of clay layers. Within the clay types, the storage modulus increased with the addition of nanoclay. For example the moduli increased by 90% with the addition of 1wt% C15A and by 96%, and 122% when 2.5wt% and 5wt% clay were added respectively. For N1.44P, the increases were 29%, 135% and 93% for 1wt%, 2.5wt% and 5wt% clay loadings respectively over that of HDPE. The drop in storage modulus for 5wt% N1.44P is due to the formation of base resin. The drop in modulus was observed for all the samples as the temperature increased is said to be typical of polyethylene (Peacock 2000). The values of storage modulus at 30^{o}C are about six times that at 90^{o}C. This is due to disordering of the crystalline domain and increase in the chains freedom of movement owing to an increase in free volume that usually accompanies temperature increase.

The loss modulus, as presnted in Table 4.4, increased with increased loading of C15A but fluctuate with increase in loading of N1.44P at 30^{o}C. For both nanoclays, the loss modulus fluctuated at 50, 70 and 90^{o}C. The highest modulus was obtained at 5wt% loading for C15A and 2.5wt% loading for N1.44P nanocomposites. The trend observed for the damping factor is shown in Table 4.5. It is interesting to note that $\tan\delta$ remained

practically unchanged with increase in clay loading but increased slightly with increase in temperature.

4.5.2 Effect of frequency

Also shown in Table 4.3, 4.4 and 4.5 is the frequency dependence of storage modulus ($E^{'}$), loss modulus ($E^{''}$), and $\tan\delta$ of the BHDPE/nanocomposites and the HDPE at room temperature. The storage and loss moduli of the nanocomposites are substantially higher than that of their pristine counterpart for all frequencies due to the strong dimensional stability and rigidity of the nanoscopically dispersed nanoclay in BHDPE matrix. The nanocomposites containing higher filler concentration (5wt%) show highest modulus at all measured frequencies for C15A as organoclay may restrain the relaxation phenomenon of every segment in HDPE chains as a result modulus increases. Highest modulus was obtained for N1.44P nanocomposite at intermediate concentration (2.5wt %).

Unlike, the storage modulus, the change in loss modulus does not follow a definite pattern. At lower frequencies (0.1 and 1Hz) loss modulus increased generally at all temperatures except for N1.44P clay aggregates (Innocentini-Mei, 2010). This result is supported by the results of microstructural investigation (SEM and XRD) which is discussed later in this work. Also, the stability changes observed is in agreement with the results reported by Lim et al (2002) and Paul et al. (2003). However, our results are slightly different from what was reported by Zhai et al. (2004) where only a system with 1wt% of organoclay has good thermal stability compared to the few cases such as BHDPE, BHDPE+10A and BHDPE+1wt% N1.44P. Generally, the loss and storage moduli of nanocomposites are significantly higher than that of the neat HDPE for all the measured frequencies. These results are in agreement with that of Barick and Tripathy (2010) for storage and loss

Table 4.3 Storage modulus of Pure HDPE and HDPE/Clay Nanocomposites as a function of Temperature

	PURE HDPE	BHDPE	BHDPE+C15A			BHDPE+N1.44P		
			1%	2.50%	5%	1%	2.50%	5%
^{o}C	Storage modulus (MPa) at Frequency = 0.1Hz							
30	303.8	671.9	578	596.2	676	390.4	715.1	586.3
50	203.6	372.7	404.6	386.7	437	221.3	536.4	378.3
70	110.5	210.5	210	219.8	239	120.1	285.4	200.3
90	52.25	108.1	98.13	96.75	114	54.66	121.2	90.54
	Storage modulus (MPa) at Frequency =1Hz							
30	381.7	793.3	738.3	756.3	864	461.2	911.8	750
50	262.8	490.3	520.2	495.8	565	281.7	692.5	488.3
70	152.5	295.3	300	283.2	319	161	374.4	269.7
90	70.36	146.7	149.6	142.1	162	76.79	182.7	136.5
	Storage modulus (MPa) at Frequency =10Hz							
30	454.6	907.5	880	902.6	1039	527.1	1095	900
50	326.7	644.7	649.7	620.8	717	344.5	866.4	614.4
70	185.8	383.9	390.6	353.2	413	207.5	464.3	351.8
90	93.32	194.2	202.1	197.3	217	102.9	246.3	189.2

Table 4.4 Loss modulus of Pure HDPE and HDPE/Clay Nanocomposites as a function of Temperature

	PURE HDPE	BHDPE	BHDPE+C15A			BHDPE+N1.44P		
			1%	2.50%	5%	1%	2.50%	5%
^{o}C	Loss modulus (MPa) at Frequency =0.1Hz							
30	53.4	131.8	103.5	106.6	122.9	71.82	130.1	106.9
50	38.2	82.74	77.04	75.62	92.79	50.68	105.8	77.3
70	27.25	53.34	50.47	54.12	59.54	30.13	70.71	50.79
90	14.59	29.93	29.46	27.51	31.09	15.5	35.95	26.38
	Loss modulus (MPa) at Frequency =1Hz							
30	55.84	114.7	111.1	113.6	134.5	61.15	140.1	116.2
50	45.33	93.26	92.21	89.29	104.6	52.12	126.7	90.58
70	30.96	61.54	62.47	58.31	64.53	33.02	79.09	56.58
90	16.48	34.71	36.65	34.92	38.15	18.37	45.78	33.45
	Loss modulus (MPa) at Frequency =10Hz							
30	41.27	79.27	81.73	88.8	107.3	40.47	106.3	92.27
50	41.32	88.65	84.53	83.9	100.5	45.91	119.1	84.97
70	32.18	68.18	69.42	61.74	72.25	36.01	84.13	63.51
90	18.38	38.53	41.24	40.17	42.52	20.16	51.65	39.29

Table 4.5 Tan δ of Pure HDPE and HDPE/Clay Nanocomposites as a function of Temperature

	PURE HDPE	BHDPE	BHDPE+C15A			BHDPE+N1.44P		
			1%	2.50%	5%	1%	2.50%	5%
°C	Tan δ at Frequency =0.1Hz							
30	0.1758	0.1962	0.1792	0.1787	0.1817	0.184	0.182	0.1824
50	0.1876	0.222	0.1904	0.1956	0.2121	0.2291	0.1972	0.2043
70	0.2467	0.2534	0.2403	0.2462	0.2488	0.2509	0.2478	0.2536
90	0.2793	0.277	0.3002	0.2843	0.2726	0.2836	0.2967	0.2913
	Tan δ at Frequency =1Hz							
30	0.1463	0.1446	0.1505	0.1502	0.1557	0.1326	0.1536	0.1549
50	0.1725	0.1902	0.1773	0.1801	0.1853	0.1851	0.1829	0.1855
70	0.203	0.2084	0.2082	0.2059	0.2026	0.2051	0.2113	0.2098
90	0.2342	0.2366	0.245	0.2457	0.2361	0.2392	0.2505	0.2451
	Tan δ at Frequency =10Hz							
30	0.0908	0.08735	0.0929	0.0984	0.1033	0.0768	0.097	0.1025
50	0.1265	0.1375	0.1301	0.1352	0.1401	0.1333	0.1375	0.1383
70	0.1733	0.1776	0.1777	0.1748	0.1748	0.1736	0.1812	0.1806
90	0.197	0.1984	0.2041	0.2036	0.1956	0.1959	0.2097	0.2077

moduli of thermoplastic polyurethane/organoclay. According to the authors, the increase in the moduli is due to strong dimensional stability and rigidity of nanoscopically dispersed nanoclay in the neat matrix. Tan δ was found to increase with increase in temperature, decrease with increase in frequency and remain practically unchanged with increase in clay loading. However, the nanocomposites have higher $\tan\delta$ than that of neat HDPE especially at high frequencies.

4.5.3 Cole–Cole plot

The Cole Cole plots are usually represented as loss modulus vs storage modulus as function of frequency or time element (Hussein et al, 2006). The plots have been applied for the study of linear viscoelastic mechanical properties of polymers, especially in the vicinity of the glass transition (Sperling, 2006). It is also used to study the phase behavior and structural changes taking place after addition of nanofiller to polymeric systems (Barick and Tripathy, 2010) and have been reportedly employed as useful tool to offer indirect proof of considerable exfoliation that takes place during the processing of polymeric materials (Dominkovics and Pukanszky, 2007). In this work, the dynamic mechanical properties which were examined as a function of temperature and frequency are represented on the Cole–Cole plots. Figures 4.3 (a - d) show the Cole–Cole plots. The nature of the plot is reported to be indicative of the nature of the polymer filler system. For example, a smooth semicircular diagram is indicative of homogeneous systems (Barick and Tripathy, 2010; Watanabe et al, 2009; and Joshi et al, 2006). The Cole–Cole diagrams presented in Figures 4.3 (a - b) are imperfect semicircular plots indicating some degree of miscibility of the nanocomposites with 1, 2.5 and 5 wt% of nanoclay. The curves in Figures 4.3 (c and d) are not as perfect as that of Figure 4.3 (a and b) likely due to the type

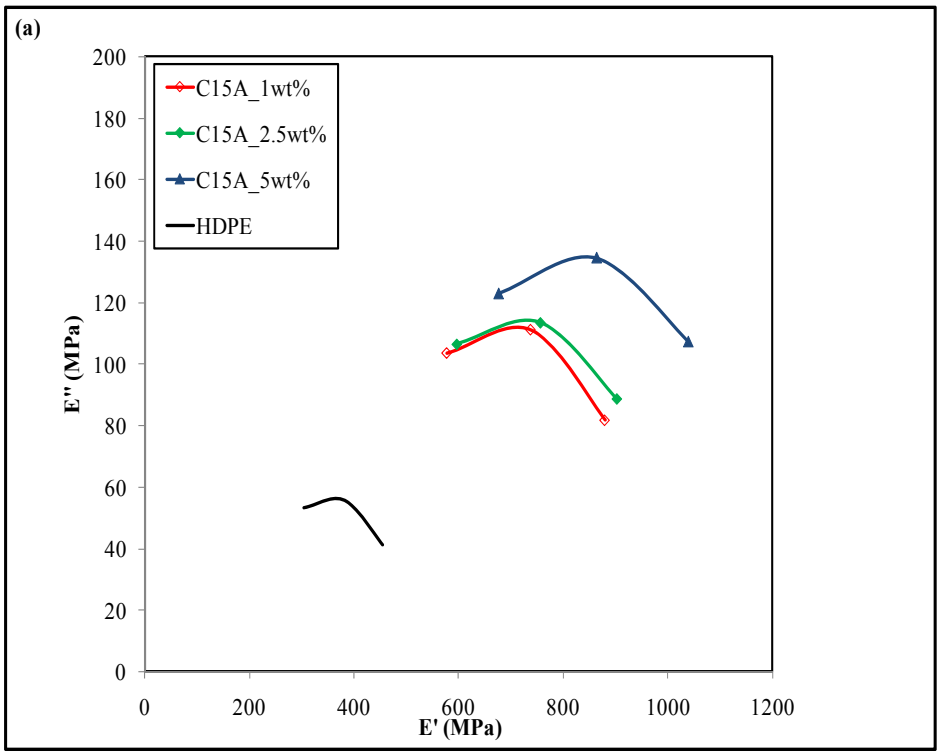

Figure 4.3a Cole – Cole plot of the HDPE and BHDPE+C15A nanocomposites as a function of frequency (at constant temperature of 30^{o}C)

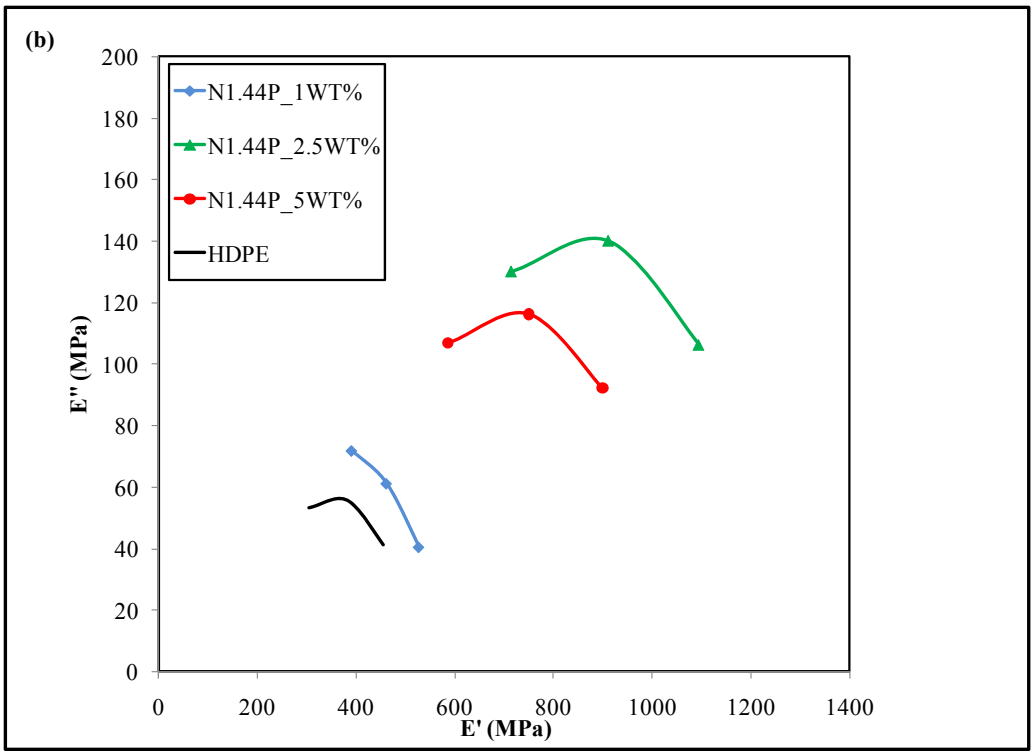

Figure 4.3b. Cole – Cole plot of the HDPE and BHDPE+N1.44P nanocomposites as a function of frequency (at constant temperature of 30^{o}C)

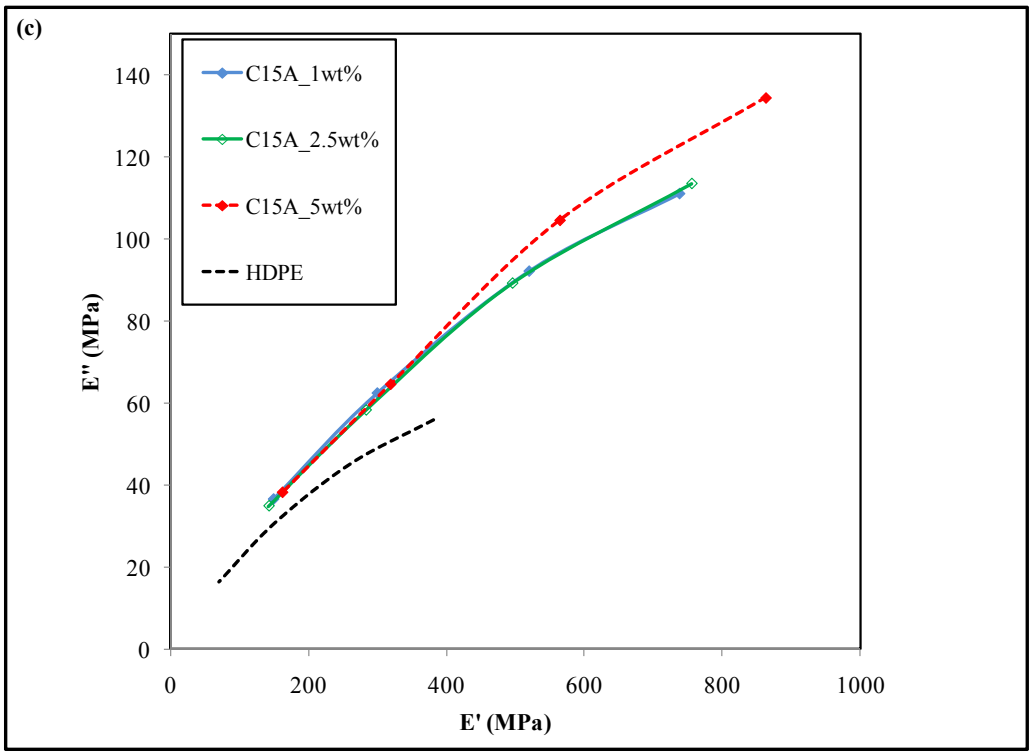

Figure 4.3c. Cole – Cole plot of the HDPE and BHDPE+C15A nanocomposites as a function of temperature (at constant frequency of 1Hz)

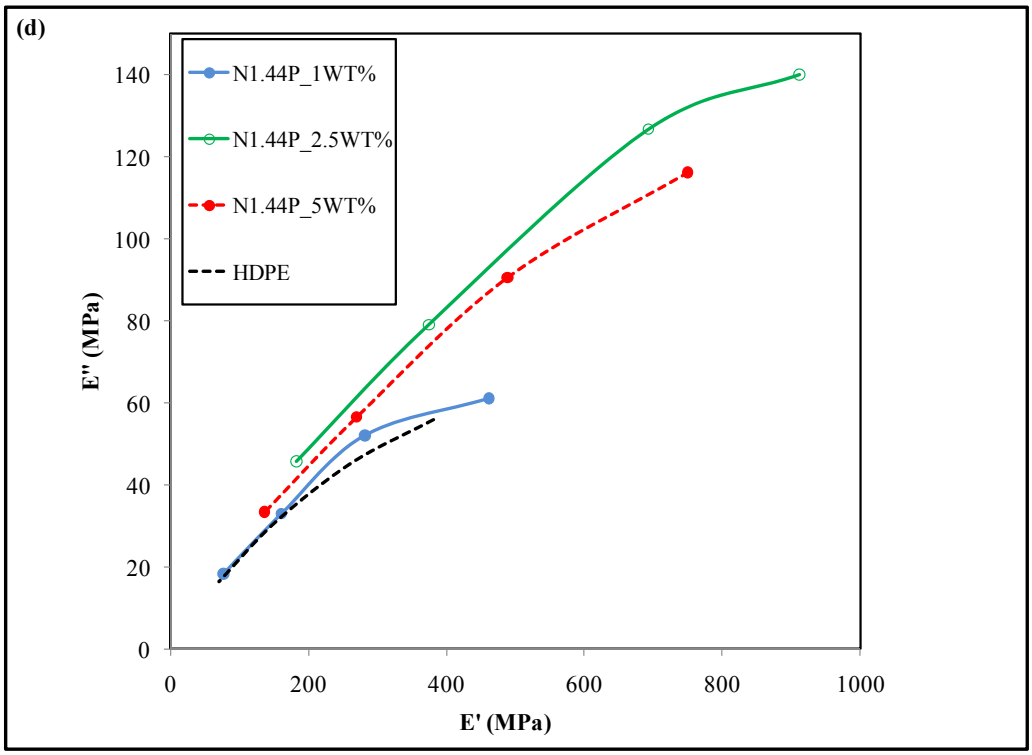

Figure 4.3d. Cole – Cole plot of the HDPE and BHDPE+N1.44P nanocomposites as a function of temperature (at constant frequency of 1Hz)

and range of experimental conditions considered. The former is as a function of frequency while the latter is as a function temperature above the glass transition. These curves are in agreement with results that were reported in previous Cole – Cole plot for variety of nanocomposites prepared by various methods. Specifically, similar curves have been reported by Joshi et al (2006) for HDPE/Octamethyl-POSS nanocomposites prepred by melt blending, Madbouly et al (2007) for POSS/Polyurethane –urea nanocomposite prepred by solution polymerization and by Barick and Tripathy (2010) for polyurethane/organoclay nanocomposites prepared by melt compounding. Thus, the shape of the curve points towards a relatively good clay polymer interaction which means the clays were at least finely dispersed. The positions and sizes of these curves are due to properties change resulting from varying nanoclay loadings. Consequently, it can be concluded that BHDPE/clay nanocomposites systems posses some degree of homogeneities for different amount of organoclay loadings.

4.6 Surface Mechanical Properties

Instrumented nanoindentation technique involves the use of small loads and indenter tips which result in shallow indents. This allows study of surface properties of materials. For instance in the present study, information was obtained from HDPE polymers from a depth range of merely 2-4 μm. For metals and alloys, indenter penetration could be as low as tens or few hundreds of nanometers. Typical indent obtained from pure HDPE sample is shown in Figure 4.4a. During instrumented nanoindentation, load and depth of penetration is recorded and the area of the indent is determined using the known geometry of the indentation tip. These values are plotted on a graph to create a force-displacement curve

which is used to extract mechanical properties of materials as shown in Figures 4.4b and 4.4c.

Hardness is calculated using the depth of penetration of indenter and modulus of elasticity is measured from the slope of the unloading curve. This technique can also be used to measure creep for certain materials such as polymers and soft metals. Creep is commonly measured by maintaining the force at a constant maximum level and measuring the change in the depth of the indenter as a function of time. The relative change in the indentation depth is taken as the creep of the specimen. For polymers, if indenter is held at constant force for a certain period of time, the indenter continues to penetrate the sample due to creep. This appears as the flat area on top in the force-displacement curves as shown in Figure 4.4c. The flat region indicates that the material continues to deform at constant force which is defined as creep. During loading, the size of the indent increases with time as a result of viscoelastic flow and relaxation processes occurring within the polymer. Shape of indents obtained in this study are typical of those obtained for polymer materials where the edges of the indent appear to cave inwards indicating significant recovery of the polymer material upon unloading (see Figure 4.4a). These indents are sometimes called 'pincushioned' indents which suggest that elastic recovery has taken place on the edges or faces, but not along the diagonals of the indent. Absence of elastic recovery along the diagonals of the indents suggests that nanoindentation is an appropriate tool to study the nanohardness and viscoelastic behavior of polymers (Low, 1998). Small amount of elastic deformation occurs during the course of indentation which is then followed by viscoelastic flow. When the indenter is removed, instantaneous elastic recovery occurs followed by

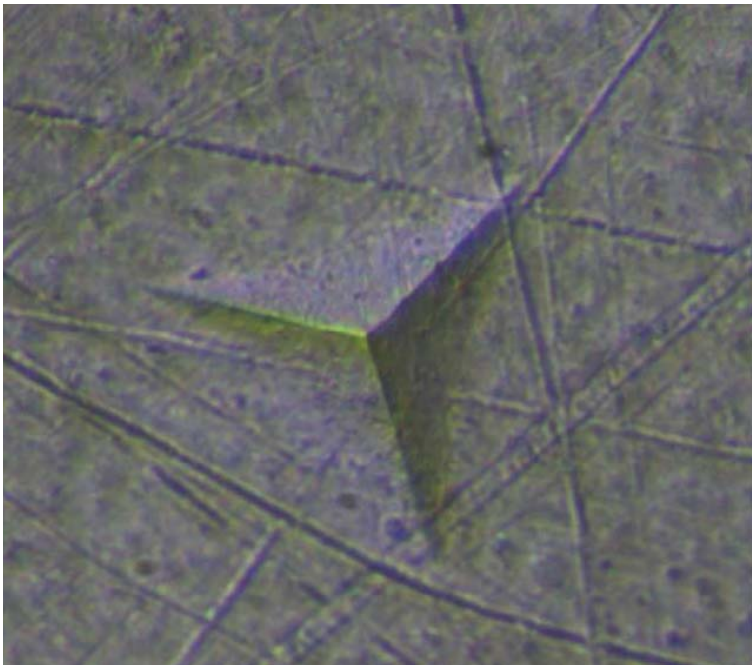

Figure 4.4a. Typical indent obtained from pure HDPE at a maximum load of 20mN.

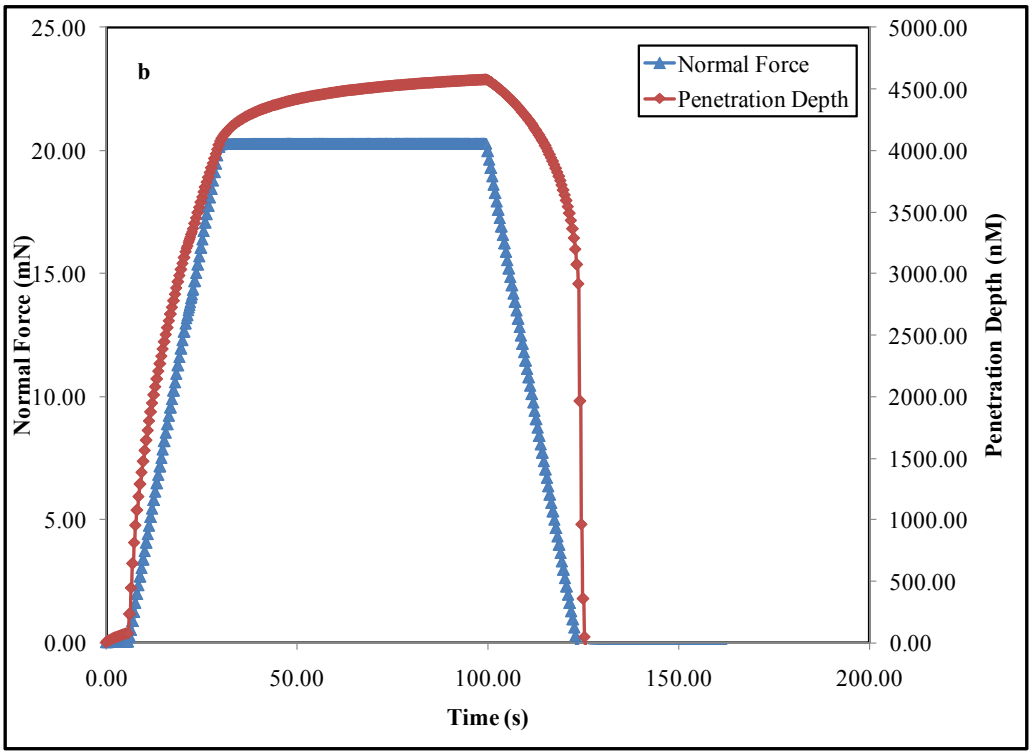

Figure 4.4b : Force-displacement curves obtained from nanoindentation of pure HDPE at a maximum load of 20 mN. (Normal force (mN) and penetration depth are plotted against time (s) of indentation)

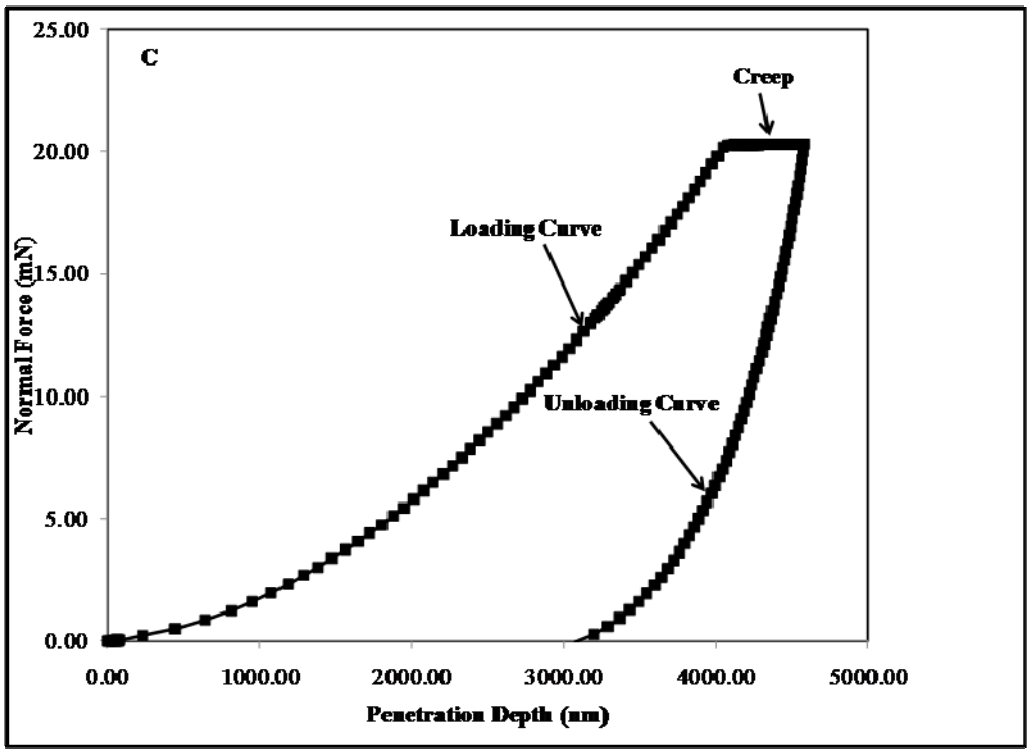

Figure 4.4c: Force-displacement curves obtained from nanoindentation of pure HDPE at a maximum load of 20 mN. (Normal force is plotted against depth of penetration). Flat region at the top of the curve indicates deformation at a constant force indicating creep. Modulus of elasticity is obtained from the slope of the unloading curve.

time-dependent recovery. The degree of recovery depends on the type of material, internal stress and temperature. Surface mechanical properties of HDPE composites studied here are shown in Table 4.6. It can be seen that all polymer and its composites show relatively low hardness and elastic modulus and high creep typical of viscoelastic materials. Hardness and creep characteristics are comparable for pure HDPE and HDPE/nanoclay samples. Addition of 1% C15A and 1% N1.44P to HDPE with compatibilizer reduces hardness and increases creep. However, additions of 2.5% and 5.0% C15A results in improved properties. Appreciable decrease in percentage creep is observed in samples with 5% C15A. Addition of 2.5% and 5% N1.44P increases hardness, elastic modulus and % creep compared to HDPE with compatibilizer. Highest creep was observed for sample with 2.5% N1.44 clay.

The results obtained from both the micro indentation and macro (DMA) testings are compared as shown in Figures 4.5, 4.6 and 4.7. In fact, Figure 4.5 shows that the macro creep and the indentation (micro) creep compare very well for HDPE/N1.44P nanocomposite at almost all the %loadings; the same trend is not visible for HDPE/C15A. For HDPE/C15A, the two creeps compared well up to about 1.2 %loading and some discrepancies began to set in immediately after that. Thus, higher %loading is related to decreasing micro creep and increasing macro creep for this nanocomposite. This phenomenon is due to the onset of aggregation of the C15A which in turn affect clay dispersion. In Figure 4.4, the indentation modulus and the Young modulus from mechanical testing are correlated. A better correlation is obtained for the two moduli. The trend of the two tests are similar up to about 2.5% clay loading for HDPE/C15A and the trend continues to be similar beyond 5% clay loading for HDPE/N1.44P nanocomposite.

Table 4.6 Surface mechanical properties obtained from different HDPE composite materials

Polymer type	**Nanoclay loading (wt%)**	**Instrumented Hardness, H_{IT} (MPa)**	**Vickers Hardness (VHN)**	**Modulus of Elasticity, E_{IT} (GPa)**	**Creep, C_{IT} (%)**
PURE HDPE	0	50.00	4.64	1.16	13.08
BHDPE	0	50.25	4.65	1.07	12.58
BHDPE+C15A	1	49.89	4.62	1.11	13.76
	2.5	65.24	6.04	1.19	12.34
	5	70.47	6.53	1.18	9.87
BHDPE+N1.44P	1	48.4	4.48	1.07	13.93
	2.5	56.9	5.27	1.06	17.92
	5	60.89	5.64	1.20	14.47

The change in indentation hardness with clay loading is presented for both nanocomposites in Figure 4.5. In this figure, similarity in the trend is also observed. Thus very good and consistent results were obtained for both nanocomposites and both tests.

The analyses of results from DMA and the nano indenter creep tests suggest that both tests can be accurately applied to investigate the properties of polyethylene nanocomposites. The low value of the Young modulus, in comparison with the indentation modulus from the nano indenter depends on the test used (Quadrini et al, 2010). It is evident that the tests are able to clearly identify the difference in the creep behavior between the two nanocomposites. In fact the results for HDPE/C15A have got comparable trend at lower %loading than the HDPE/N1.44P nanocomposite. On a general note, an interesting trend was discovered in the increase and decrease of both mechanical and thermal properties on HDPE/N1.44P nanocomposite. All properties first dropped when 1wt% of the clay was added. Then a gradual increase or decrease followed as the loading of the Nanomer was increased. This trend was observed for all properties except for the crystallization onset temperature.

4.7 Creep Compliance at End-Use Conditions

So far performances of both C15A and N1.44P have been excellent at 2.5wt% and 5wt%, respectively. In an attempt to select the best clay for producing the liner, creep resistance of the two clays at actual field temperature and pressure were measured. Each sample was subjected to a load of 7.5MPa at 50^{o}C for 300 seconds. The results obtained are shown in Figure 4.8. It can be observed that C15A nanocomposite has higher compliance than N1.44P. It was already established that addition of nanofillers into neat polymer can significantly improve the creep resistance of the matrix (Pegoretti, et al, 2007, and Zeng

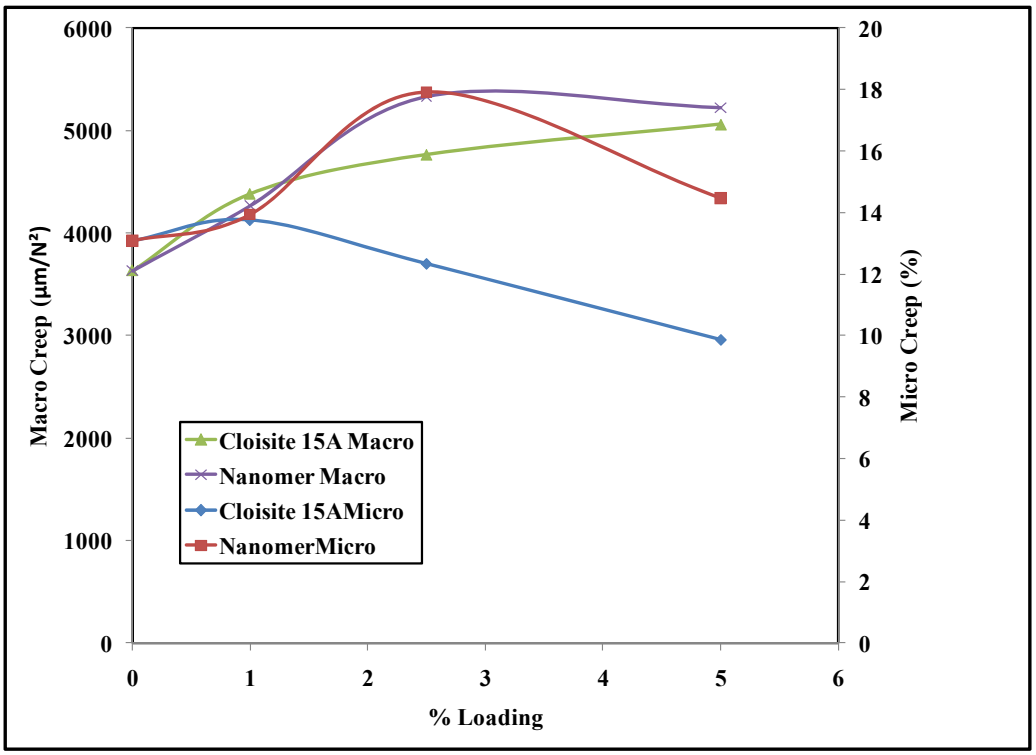

Figure 4.5: Comparison of Results of Micro and Macro Creep as a Function of %Loading

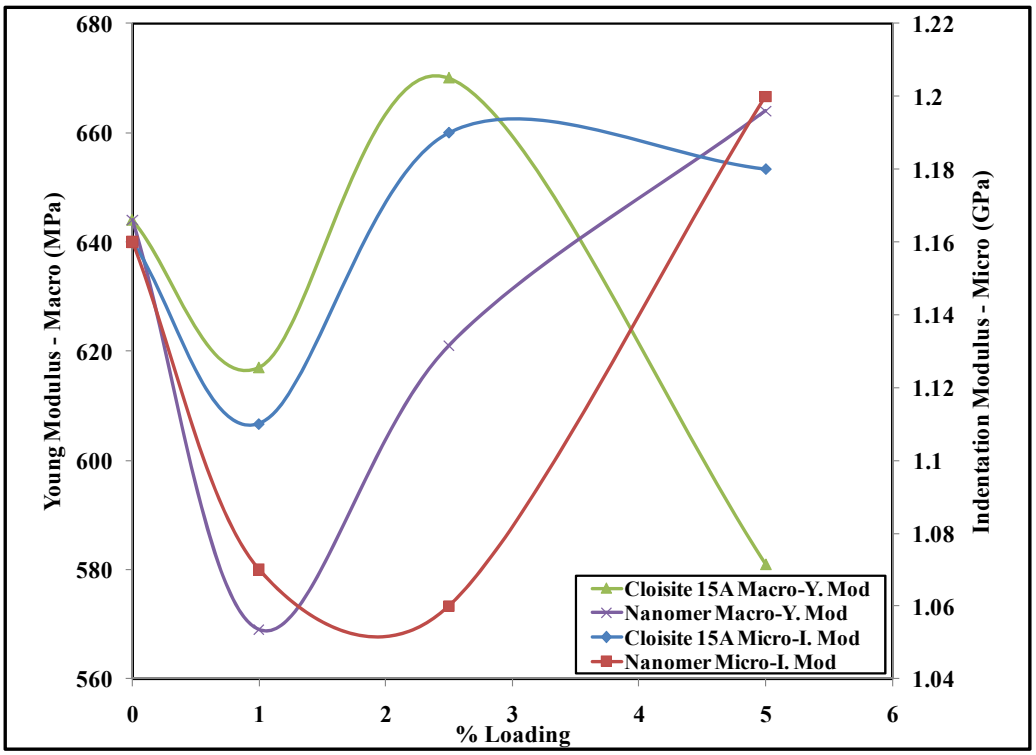

Figure 4.6: Comparison of Results of Micro and Macro Moduli

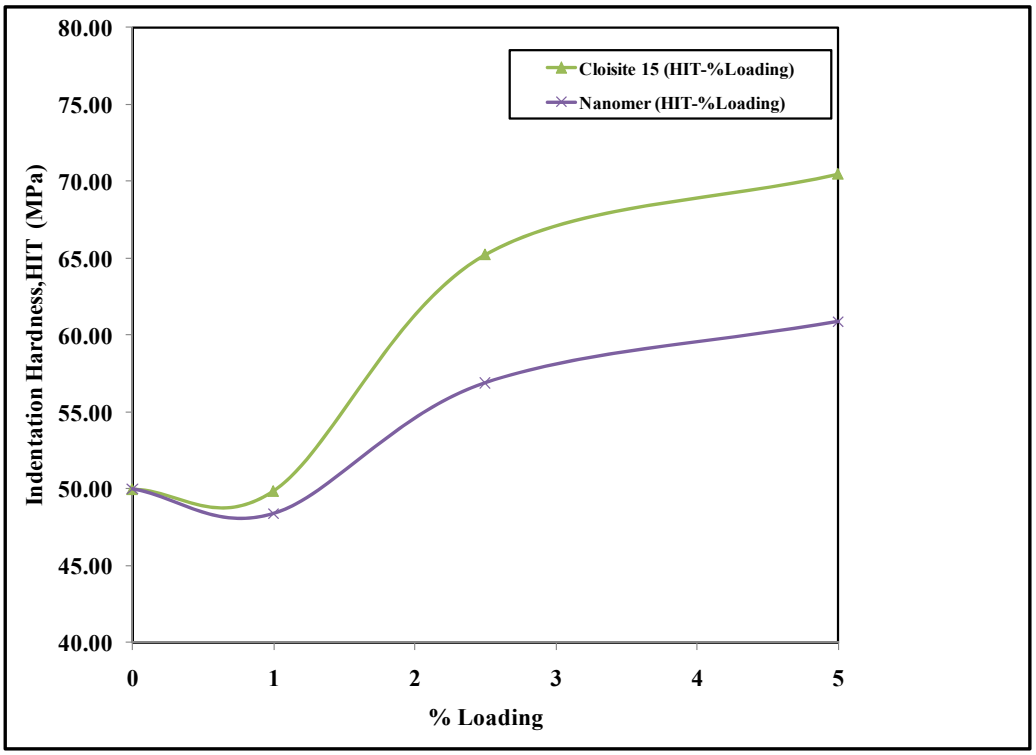

Figure 4.7: Variation of Indentation Hardness with %Loading of Nanoclay

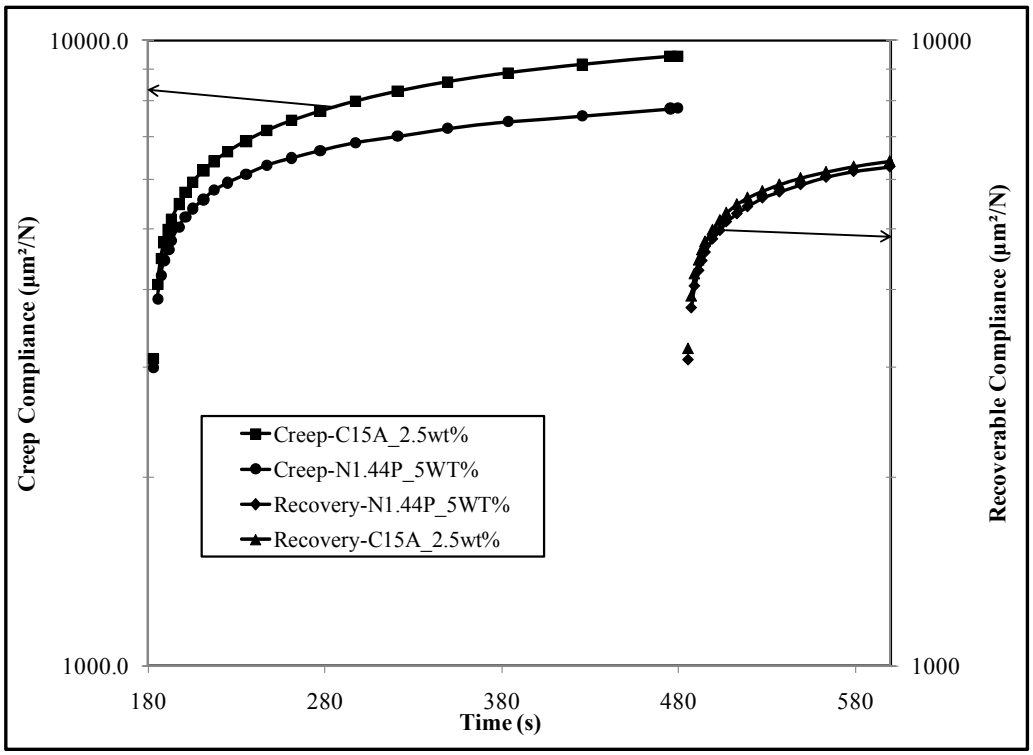

Figure 4.8: Creep Compliance measured at field conditions of 7.5MPa and 50^{o}C

and Yu 2010). The lower compliance exhibited by N1.44P nanocomposite can be associated with the quantity and type of clay contained in the sample. Also, the performance of N1.44P is always better at high loading. Within 100s, 78% strain recovery was recorded for C15A based nanocomposite while the recovery for N1.44P was 93%. This suggests that PE composites with N1.44P can recover from cyclic stresses in pipelines much better than C15A composites.

4.8 Permeability Measurement

This section is dedicated to the discussion of results of transport properties of CH_4, and CH_4/CO_2 mixture through high density polyethylene and its nanocomposites. The influence of various parameters such as temperature (30^oC - 70^oC), pressure (50bar - 100bar) and gas concentration were studied. The results of permeability coefficients are presented in Table 4.7 – 4.11.

4.8.1 Influence of temperature

A great number of literature data suggest that transport coefficient is dependent on temperature at a given pressure (Klopffer and Flaconnèche, 2001; Lin and Freeman, 2004; Raharjo et al, 2007; and Safari et al, 2009). Thus, the values of the measured permeability for pure HDPE were in agreement with what was reported in literature. For example, permeability coefficient of CH_4 in HDPE at 298 K was reported by Alamo and Mandelkern (2009) to be 0.3×10^{-8} cm^3(STP)/cm.s.bar while 0.58×10^{-8} cm^3(STP)/cm.s.bar was obtained in this work for the same gas at 304 K. The difference in the values is due to the fact that both measurements are taken at different temperatures. Moreover, temperature effect can be further compared with the results of Flaconnèche and

Klopffer (2001), where the permeability of CH_4 in HDPE is 5.1×10^{-8} cm^3(STP)/cm.s.bar at 350 K. In this work, permeability of 4.52×10^{-8} cm^3(STP)/cm.s.bar was obtained for pure HDPE at 345K as shown in Table 4.6. Thus, the latter permeability is lower because it was measured at lower temperature. So, these results for permeability are comparable with previous literature reports. In the range of temperature used, significant effects were noticed for all the samples. For example, increasing the temperature by 20^oC made the permeability to increase by about four times the initial value for pure HDPE as shown in Table 4.7. This result is expected since it is known that an increase in test temperature will increase the mobility of both the HDPE chain segments and the gas molecules (Flaconnèche and Klopffer, 2001). The increase is always represented using the Arrhenius equation.

$$P_e = P_o \exp\left(-\frac{E_P}{RT}\right) \tag{4.1}$$

where P_o is a constant, E_p is the apparent activation energy of permeation processs, T is absolute temperature and R is the universal gas constant (Stern et al, 1996).

Increase in permeability coefficient following an increase in temperature was observed for all the samples. However, the increments in each of the samples differ.

4.8.2 Influence of Pressure

The evolution of permeability with gas pressure has been reported to be dependent on the diffusing molecule type. Effect of pressure on transport coefficient of gases in polymer is not yet clear. This is because both increase and decrease in permeabilities have been

Table 4.7 Permeability Coefficients obtained for Pure HDPE Samples

Mole Fraction				
CH_4	CO_2	T(^oC)	P(bar)	($10^{-8}cm^3$(STP)/cm.s.bar)
1	0	30.9	105.7	0.573
1	0	50.8	104.6	1.94
1	0	69.5	101.8	4.52
0.8	0.2	31	105.2	1.01
0.8	0.2	50.1	100.8	3.03
0.8	0.2	69.8	102.1	5.84
0.8	0.2	70.2	54.6	6.55

reported. For instance, the effect of pressure on gas permeation through LDPE and PP was studied by Naito et al. (1991) at constant temperature of 25^{o}C and a pressure ranging 1-130atm. Their results showed that, at constant temperature, the permeability of highly soluble gases such as CH_4 and CO_2 increase slightly with increasing pressure. The outcome of these study was supported by Klopffer et al. (2001); and Koros and Madden (2003). Similar results were obtained by Lin and Freeman (2004). However, some of the results obtained by Flaconnèche et al. (2001) showed that between a pressure range of 40 to 100bar, pressure difference has no significant effect on gas permeability. Pressure increment from 40bar to 100bar at 80^{o}C resulted in only a very insignificant reduction in permeability from 29×10^{-8} cm^3(STP)/cm.s.bar to 28×10^{-8} cm^3(STP)/cm.s.bar. Also, same opposite behaviour was reported for both single and gas mixture Ghadimi et al. (2009) in LDPE and PDMS. In a study by Flaconnèche et al. (2001), permeability of CH_4 decreased from 4.3×10^{-8} cm^3(STP)/cm.s.bar to 3.7×10^{-8} cm^3(STP)/cm.s.bar by increasing the pressure from 40 to 100bar and then increased again when the pressure was reduced from 100 to 75bar at constant temperature of about 40^{o}C. The results obtained in the present work are in agreement with all the above previous studies. For instance, in the results shown in Table 4.7, when the temperature was increased by about 20^{o}C (from 50.1 to 70.2 ^{o}C) and the pressure decreased by about 50bar (from 100.8 to 54.6 bar), permeability increased by 62% despite the decrease in pressure. In this case it can be said that effect of pressure was overshadowed by that of temperature as observed in other similar results from literatures. The effect of pressure became obvious when at constant temperature of about 70^{o}C, the pressure was increased from 54.6bar to 102.1bar and this caused about 10.84% decrease in permeability. This is not surprising because pressure increase has two

opposing effect as explained by Klopffer and Flaconnèche, (2001). According to the authors, an increase in the pressure leads to an increase in polymer density via polymer compaction which consuquently reduces the free volume available for the penetrant molecule to permeate through and thus a decrease in permeability. A critical look at the change in permeability for BHDPE (Table 4.8) and its nanocomposites (Tables 4.9 – 4.11) showed that there was very little or practically no change in permeability when the pressure was increased by 50%. For example permeability changes of 0.71% (for BHDPE), 1.82% (for BHDPE+1wt% C15A), 0.28% (for BHDPE+2.5wt% C15A) and 0.46% (for BHDPE+5wt% N1.44P) were observed by changing the pressure by 50bar. The differences in the values of these increments are most likely due to the presence of nanoclay coupled with the fact that the changes in pressure are not exactly the same. Unfortunately, published permeability data are not available to compare these results for HDPE nanocomposites. However, these results were in agreement with previous studies when compared with other polymer nanocomposites. For example, the results of Merkel et al. (2003) on the pressure dependent of permeability of gases through poly (1-trimethylsilyl-1-propyne) showed that pressure dependent on permeability varies with nanoparticle contents. This phenomenon occurring in the nanocomposites can be explained by the second opposing effect. When pressure increase, there is also a corresponding increase in penetrant concentration and the diffusing molecule can plasticize the macromolecular chains, which results into increased free volume. Thus the opposite effect is suspected to have been responsible for keeping the permeability constant. It can also be inferred that these two opposing effects prevail in BHDPE, BHDPE+C15A and BHDPE+N1.44P samples while only the hydrostatic pressure effect prevail in pure HDPE.

Table 4.8 Permeability Coefficients obtained for BHDPE

Mole Fraction				
CH_4	CO_2	T(^oC)	P(bar)	($10^{-8}cm^3$(STP)/cm.s.bar)
1	0	50.6	103.1	2.16
1	0	70.0	104.8	5.28
0.8	0.2	50.47	104.5	3.13
0.8	0.2	69.9	101.9	6.98
0.8	0.2	70.1	52.0	7.03

Table 4.9 Permeability Coefficient obtained for BHDPE + 1wt% C15A

Mole Fraction				
CH_4	CO_2	T(^oC)	P(bar)	($10^{-8}cm^3$(STP)/cm.s.bar)
1	0	30.9	104.3	0.609
1	0	49.9	104.9	1.87
1	0	69.6	105.1	4.94
0.8	0.2	30.86	104.3	1.06
0.8	0.2	50.2	104.9	2.67
0.8	0.2	69.7	103.4	6.46
0.8	0.2	69.5	57.5	6.58

Table 4.10 Permeability Coefficient obtained for BHDPE + 2.5wt% C15A

Mole Fraction				
CH_4	CO_2	T(^oC)	P(bar)	($10^{-8}cm^3$(STP)/cm.s.bar)
1	0	50.3	105.2	1.95
1	0	69.7	102.9	5.19
0.8	0.2	50.5	104.5	2.91
0.8	0.2	69.8	101.5	7.13
0.8	0.2	69.7	53.5	7.11

Table 4.11 Permeability Coefficient obtained for BHDPE + 5wt% N1.44P

Mole Fraction				
CH_4	CO_2	T(^oC)	P(bar)	($10^{-8}cm^3$(STP)/cm.s.bar)
1	0	50.16	104.4	1.87
1	0	69.31	104.6	4.71
0.8	0.2	50	104.2	1.62
0.8	0.2	69.22	104.3	6.53
0.8	0.2	69.19	52.0	6.56

4.8.3 Influence of Compatibilizer

As explained earlier, sample BHDPE is a blend of HDPE and the PE –g-Maleic anhydride which was used as a compatibilizer. The presence of compatibilizer was observed to slightly increase the permeability at 50^{o}C and 100bar as well as at 70^{o}C and 100bar. These results are in agreement with what was reported by (Picard et al., 2008). Their results showed both increase and decrease in gas permeability.

4.8.4 Influence of Nanoclay

Table 4.7 – 4.11 and Figures 4.9(a-c) present pure CH_4 and mixed CH_4/CO_2 permeability coefficients in HDPE containing various amounts nanoclay loadings. The incorporation of nanoclays into polyethylene is found to substantially improve gas barrier property since the nanoclays are known to create tortuous path that retards the gas molecules movement through the polymer (Hu et al., 2008), however this is not always the case in nanoparticle filled polymers (Matteucci et al., 2008) as can be seen in the results of this study as shown in Figures 4.9 and Tables 4.7 – 4.11. Permeabilities of some samples increased, some decreased while others remained constant. For instance, permeability of pure CH_4 dropped by about 3.6% and that of mixture by 11.9% with the addition 1wt% of C15A in comparison with the pure HDPE as shown in Table 4.9 and Figure 4.9. Generally, with increasing clay content, the barrier properties are expected to improve as a result of the tortuous path created by nanoclay platelets. However, it was found that the permeability of pure gas were observed to be practically constant at low temperature but increased by 14.8% at high temperature on the addition of 2.5wt% C15A (Table 4.10). For gas mixture, the permeability decreased by 4% at low temperature and increased by about 8% at high

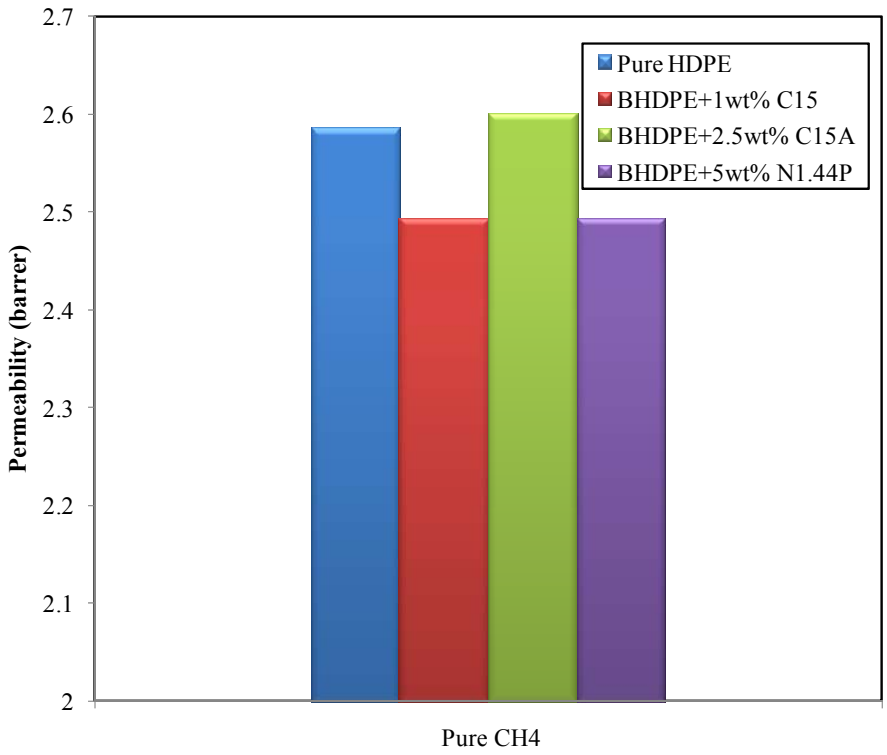

Figure 4.9a : Evolution of transport properties of Pure CH_4 as a function of nanoclay type and loadings 100bar

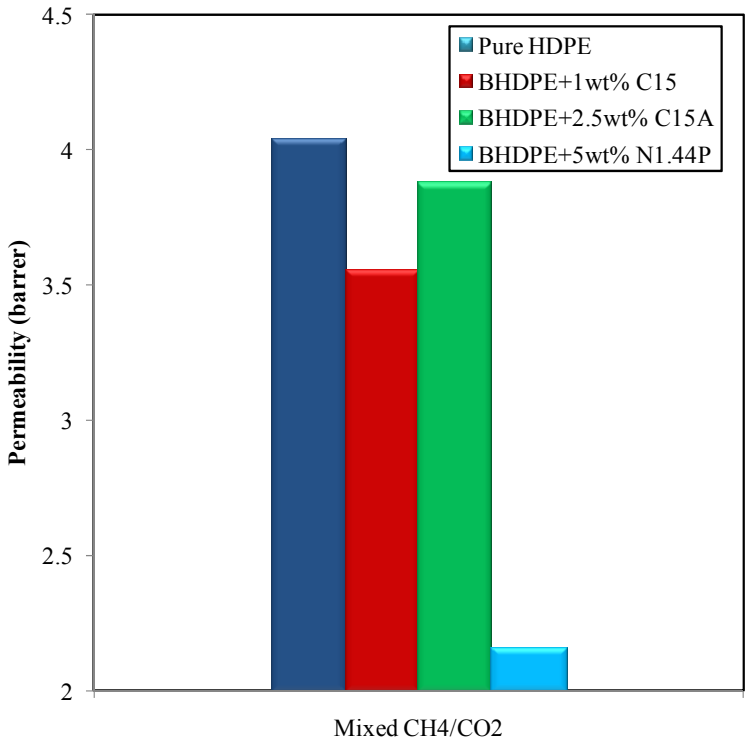

Figure 4.9b : Evolution of transport properties of mixed CH_4/CO_2 as a function of nanoclay type and loadings at 100bar

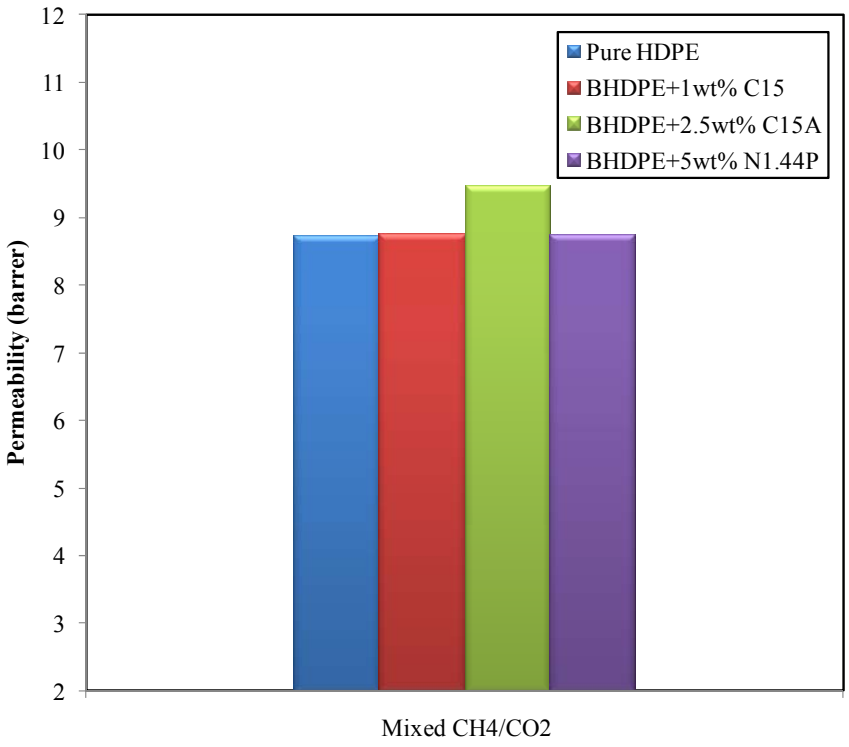

Figure 4.9c : Evolution of transport properties of mixed CH_4/CO_2 as a function of nanoclay type and loadings at 50bar

temperature. Consistently, the addition of 5wt% N1.44P was observed to improve the barrier property of HDPE. For example, the permeability of pure CH_4 was reduced by 3.6% at low temperature and increased by 4.2% at high temperature (Table 4.11). For natural gas, the barrier property improved by about 46.5% at low temperature and high pressure, and remained almost constant at high temperature and low pressure. At high temperature and pressure, permeability increased by 11.8% in comparison with neat HDPE. The results obtained are in agreement with the results reported from similar studies by Merkel et al. (2003), Lee et al., (2005), Matteucci et al. (2008), and Picard et al (2008) for polyethylene and other polymers.

Possible explanation for the increase in permeability was offered by Matteucci et al (2008) and Merkel et al. (2003). According to these authors, nanoparticles can inhibit the efficient seqmental chain packaging in polymers (especially glassy polymers) thereby increasing free volume in the polymer phase which consequently increase the permeability. Also in other heterogenous polymer systems such as rubbery polymer nanocomposites, voids at polymer – particle interface or between particle agrregates cause permeability to be greater in nanocomposites than in unfilled polymers.

4.8.5 Influence of Gas Concentration

Although constant gas concentration were used throughout the experiment, effect of concentration changes come into play when the effect of the presence of one gas on the permeability of the other is considered. Moreover, the increase in permeability of one penetrant in the presence the other has been reported previously by some authors. For example, Jordan and Koros have reported an increase in CH_4 and N_2 permeability in

PDMS in CO_2/CH_4 and CO_2/N_2 mixtures. This increase was explained (using the free volume analysis) by hypothesizing that highly sorbing CO_2 plasticized the polymer matrix and this resulted into an increase in light gas permeability. This is why in these results, at the same pressure and temperature (50^oC and 100bar), permeability of mixed gas is about twice that of pure gas in HDPE. At 70^oC and 100bar, permeability of gas mixture (CH_4/CO_2) is about 1.5 times that of pure CH_4 in BHDPE and 1.2 times in BHDPE+C15A.

CHAPTER 5

MATHEMATICAL MODELLING OF PERMEABILITY

5.1 Introduction

Selection of appropriate barrier polymer for replacement of traditional materials such as glass, metal and papers in engineering applications has been receiving great attention (Arora and Padua, 2010; Herrera-Alonso et al, 2009; Sorrentino et al, 2006; and Dhoot et al, 2003). There is a rapid increase in variety of challenges and opportunities facing practioners in the area of gas transport properties of polymeric membranes. Polymers with low permeability are sought after in industries such as packaging, oil production and the automotive industry (Flaconnèche et al, 2001). For example, for the packaging of carbonated soft drinks, the package should not allow the permeation of carbon dioxide, oxygen or water. In the packaging of products containing fats and oils like fried snacks and meat, protection against the effects of oxygen and light is required. For oil and gas applications, the main function of polymers is to ensure the leak-proof of pipes or liners for transporting crude oil or gas from wellheads to separation stations. Here, polymers are in contact with oil or gas at high temperature and high pressure.

In any of the above applications, specific barrier properties can be met in various ways. For example, polymers with variety of barrier properties can be produced by changing the operating conditions during manufacturing (Lotti et al, 2008 and Herrera-Alonso, 2009) and/or by addition of fillers (González-Vidal et al 2010; Muralidharana et al, 2008; Matteucci, 2008; Kumar, et al, 2008; and Picard et al , 2007). There are two types of

fillers – conventional fillers (such as kaolinite, talc, mica) and nano-fillers (such as nanoclays). Today, nanocomposites are of interest due to their long-term stability (Abdullah, et al 2006), improved mechanical, thermal, flame resistance properties (Herrera-Alonso et al, 2009; Pavlidou and Papaspyrides, 2008; and Zhang and Wilkie, 2003) as well as gas barrier properties (Herrera-Alonso et al, 2009; and Liu and Kee, 2005). These improved properties make nanocomposites an excellent alternative for use in many applications such as packaging, separation, and crude gas transport.

Offshore petroleum industries still use steel pipes as risers and flowlines for transporting crude oils and gases from well heads to separation stations. Such pipes are coated with internal polymeric (polyolefins) liner (sleeve) in order to avoid the corrosion of steel pipes by sour gas and ensure the integrity of the pipe network. Unfortuanately, these liners tend to allow gas to go through at high pressure and temperature. The natural gas is mainly methane but it can contain carbon dioxide. Permeated gases get collected within the annulus between the sleeve and the steel wall. Permeation of acidic gas such as CO_2 and H_2S can cause corrosion of steel pipes while permeation of CH_4 can cause pressure build up in the annulus to such a magnitude that can result in liner failure. Numerous techniques have been proposed to solve this problem. For example, one of the earliest work on barrier properties by Dale and Rogers in 1973 was done to investigate the effect of molding polystyrene at elevated pressures on the transport and mechanical properties of polymers. The authors concluded that properties of polymeric materials can be improved by the application of elevated pressures. Moreover, Benjelloun-Dabaghi (2002) proposed a model that represent an improvement in the design of the pipe.

In all the aforementioned cases and other applications, modeling of the permeation transport could be of crucial importance to obtain a better understanding of the process and even the design of new polymers with enhanced barrier properties. Considerable efforts have been used on correlating and predicting barrier properties of many polymeric composite materials reinforced with various types of fillers (Sun et al,2008 and Xu et al, 2006). Most of the previous works done on modeling of gas permeability through polymers has focused on glassy polymers at low pressure. This is probably due to the fact that previous work was directed towards low pressure applications such as food packaging (Arora and Padua, 2010). Moreover, many of these models were applied to pure (unfilled) polymers (Raharjo et al, 2007; Ghadimi et al, 2009; Safari et al, 2009; and Vopicka et al, 2010) and sometimes consist of parameters that are very hard to estimate. Although, the transformation of polymer matrix following the addition of nanometer scaled clay layers have been widely modeled, it was found that the available permeability models for polymer nanocomposites only considered the nanoparticles loadings and aspect ratios (Fredrickson and Bicerano, 1999; Bharadwaj, 2001; and Lu and Mai, 2007). Literature review showed that models which simultaneously take into account the effect of pressure, temperature, aspect ratio, crystallinity and nanoparticle loadings are yet to be developed. In this study, we combine for the first time the tortuosity based model of Nielsen with Naito model to evaluate the permeability of polymer clay nanocomposites to pure and mixed gases at high pressure (Bharadwaj, 2001 and Masaro and Zhu, 1999). The model was fitted against experimental data obtained for pure CH_4 and a mixture of CH_4 and CO_2. Efforts were concentrated on the significance of the model parameters and effects of temperature and pressure on permeability of gases through polymer nanocomposites.

5.2 Model Development

A mass balance around a binary system (solute/polymer sample) can be represented by simple transient continuity equation (Elabd and Barbari, 2002) given as:

$$\frac{\partial}{\partial t}(C_i) = \nabla \cdot J_i \tag{5.1}$$

It is widely accepted that the transport mechanism within the polymer matrix exhibits Fickian behavior (Choudalakis and Gohtist, 2009; and Dhoot et al, 2003). Based on Fick's first law, the diffusive flux (J_i) of specie *i* is proportional to the concentration gradient between the two sides of the material:

$$J_i = -D_i \nabla C_i \tag{5.2}$$

where D_i is diffusion coefficients of each gas species through the polymer and C_i is the concentration of each gas species at *x* at time *t*.

5.2.1 Diffusion Coefficient

Varieties of methods have been developed for estimating the diffusion coefficient (D_i). Models describing the estimation of D_i for gases, liquids and solids at low pressure can be found elsewhere (Welty et al, 2001 and Basmadjian, 2005). Other methods based on Fick's law including linear and nonlinear regression analysis are also presented in the literature (Vieth, 1991; Elabd and Barbari, 2002; Scheichl et al, 2005; and Cussler 2009). In addition to Fick's law method of determining the diffusion coefficient (regarded as steady state diffusion coefficient), Liu and Kee (2007) described other two methods – a graphical method from which the so called zero diffusion coefficient is estimated and a method for calculating the average diffusion coefficient. Physical models for estimating the diffusion coefficient for polymer solutions, gels and solids were reported by Masaro and

Zhu (1999). Diffusion coefficient models for polymer/clay nanocomposite were disscussed by Choudalakis and Gohtist (2009).

Three main factors have been identified to influence the mass transport mechanism of gasses through a nanoplatelet reinforced polymer. They include the volume fraction available for the penetrant molecule to traverse the polymer; the orientation of the nanoplatelets relative to the diffusion direction; and nanoplatelets aspect ratio (Choudalakis and Gotsis, 2009; Bharadwaj, 2001; Wilkinson, 2000; Fredrickson and Bicerano, 1999; and Bicerano, 1996). Based on this, the tortuosity based model of Nielsen was used to model the diffusivity of gases (D_n) through nanocomposite (with an assumption that the nanocomposite contains regular arrangement of parallel nanoplatelets) as:

$$\overline{D_n} = \frac{\overline{D_m}}{1 + \frac{L}{2W}\phi} \tag{5.3}$$

where $\overline{D_m}$ is the diffusion coefficient through the matrix, L and W are the length and the width of the nanoplatelets, respectively, and L/W is the aspect ratio. ϕ is the volume fraction of the nanoplatelets that are dispersed in the matrix (Lu and Mai, 2007; and Choudalakis and Gotsis, 2009). ϕ is calculated from the expression of Deepthi et al. (2010):

$$\phi = \frac{w_i / \rho_i}{\sum_{i=1}^{n} w_i / \rho_i} \tag{4}$$

where w_i and ρ_i are the weight and density of component *i*, respectively.

Now, D_m can be expressed as a function of gas pressure, p, and concentration, C, using the model of Naito (Klopffer and Flaconnèche, 2001):

$$\overline{D}_m(C, p) = \overline{D}(00)\exp(\beta_h p + \alpha C) \tag{5.5}$$

$\overline{D}(00)$ is the diffusion coefficient at the upstream side of the polymer sample and α is a constant. Equation (5.5) has been validated using diffusion of CO_2 in PVDF (Klopffer and Flaconnèche, 2001). β_h, is related to the activation volume V^* of the diffusion process by means of the relation:

$$V^* = -\beta_h RT \tag{5.6a}$$

In this work, we have proposed the modification of equation (5.6a) for high pressure application as follows:

$$\beta_h = -\frac{V^*}{ZRT} \tag{5.6b}$$

where Z is the compressibility factor.

Likewise, the C in equation (5.5) can be written in term of pressure and temperature for non-ideal gases:

$$C = \frac{p}{ZRT} \tag{5.7}$$

Equation (5.7) has been successfully used (in its ideal gas form for Z=1) by Matteucci et al. (2008) to model gas transport properties in MgO filled poly (1-trimethysilyl – 1- propyne) nanocoposite. It should be noted that the deviation from the ideal-gas behavior at a given temperature and pressure has been accounted for by the introduction of the Compressibility Factor, Z (Cengel and Boles, 2010).

Substituting equations (5.6b) and (5.7) into (5.5) gives:

$$\overline{D}_m = \overline{D}_o \exp\left(\beta \frac{p}{ZRT}\right) \tag{5.8a}$$

where $\beta = \alpha - V^*$

Similar expression for diffusion coefficient has been reported by Vieth (1991) and was also proposed in 1975 by Peterlin; and Raucher and Sefcik in 1983 (Klopffer and Flaconnèche, 2001). Substituting (5.8a) into (5.3), the diffusion coefficient in the nanocomposite can be written as:

$$\overline{D}_n = \psi \overline{D}_o \exp\left(\beta \frac{p}{ZRT}\right) \tag{5.9a}$$

where

$$\psi = \frac{1}{1 + \frac{L}{2W}\phi} \tag{5.9b}$$

5.2.2 Solubility Coefficient

Solubility, *S*, is the amount of gas dissolved in the polymer matrix at equilibrium and at a partial pressure *p*. It is defined through:

$$\frac{V_A}{V_P} = S(p)p \tag{5.10}$$

Here, V_A is the volume of gas at STP (that is at standard temperature, 298K and pressure, 0.1013MPa, conditions) dissolved into the polymer per unit volume of solution, and V_P is the volume of polymer per unit volume of solution (Baird and Collias, 1995). Thus, the unit of *S* is $cm^3(STP)/cm^3.Pa$

For a semi-crystalline polymer, the solubility depends on the degree of crystallinity of the polymer. With the assumption that diffusion occurs only in the amorphous phase, the solubility coefficient is expressed as:

$$\bar{S} = \bar{S}_o(1-\phi_c) \tag{5.11a}$$

where $\bar{S}_o$ is the solubility coefficient of the amorphous phase and ϕ_c is the degree of crystallinity of the polymer matrix (Baird and Collias, 1995; and Dhoot et al, 2003). In this work, the crystalinity was correlated with temperature using the expression below:

$$\phi_c = \frac{a}{T} + b \tag{5..11b}$$

where a and b are constants that can be obtained from DSC experiment and T is in Kelvin

5.2.3 Permeability Coefficient

Mathematically, gas permeability coefficient of a polymer is defined as:

$$P_e = \frac{J\,l}{f_2 - f_1} \tag{5.12a}$$

where P_e is the gas permeability coefficient in [cm^3(STP)cm/(cm^2.s.cmHg)], J is the steady state penetrant flux through the membrane [cm^3(STP)/cm^2s], l is the membrane thickness (cm), f_2 is the upstream fugacity (cmHg) and f_1 is the downstream fugacity (cmHg) (Raharjo et al, 2007).

Also, as demonstrated earlier, penetrant transport can be modeled using Fick's law. Substituting for flux from equation (5.2), then, in its simplest form (unidirectional transport of one penetrant), the law can be represented as:

$$P_e = \frac{-D\,l}{f_2 - f_1}\frac{dC}{dx} \tag{5.12b}$$

Where C is the penetrant concentration, x is the spatial coordinate and D is the effective diffusion coefficient in the polymer. Integrating (5.12b):

$$P_e = \frac{1}{f_2 - f_1}\int_{C_1}^{C_2} DdC \tag{5.12c}$$

where C_1 and C_2 are the penetrant concentrations at upstream and downstream pressures, respectively. Equation (5.12c) can be written as:

$$\overline{P_e} = \overline{D}\frac{C_2 - C_1}{f_2 - f_1} \tag{13}$$

where $\overline{D}$ is the concentration average diffusion coefficient defined as follows (Naito et al, 1993):

$$\overline{D} = \frac{1}{C_2 - C_1}\int_{C_1}^{C_2} DdC \tag{5.14}$$

when $C_2 >> C_1$ and $f_2 >> f_1$ (Benjelloun-Dabaghi, 2002; Belfiore, 2010; and Cengel and Ghajar, 2011). This is justified since in permeation experiments, one measures P_e by applying a downstream pressure close to zero (Flaconnèche et al, 2001). Thus (5.13) can be simplified as the product of $\overline{D}$ and $\overline{S}$ (Koros and Madden, 2003; and Choudalakis and Gotsis, 2009): That is:

$$\overline{P_e} = \overline{D}\,\overline{S} \tag{5.15}$$

where $\overline{S}$ is the solubility coefficient of the penetrant evaluated at the upstream face of the polymer as $\overline{S} = \frac{C_2}{f_2}$.

Substituting for $\overline{D}$ and $\overline{S}$ from equations (5.9a) and (5.11) then:

$$\overline{P_{en}} = \psi\kappa(1 - \phi_c)\exp\left(\beta\frac{p}{ZRT}\right) \tag{5.16}$$

where $\kappa = \overline{S}_o\overline{D}_o$.

5.2.4 Permeability of mixed gases

Equation (5.16) is a model for the permeation of single gas species. For a mixture of gases, the equation is modified and is written as:

$$\overline{P_{en}} = \psi\kappa(1-\phi_c)\exp\left(\beta\frac{p}{Z_m RT}\right) \tag{5.17}$$

where Z_m is the compressibility factor for the gas mixture. Z_m is calculated using the Virial equation (Smith et al, 2001):

$$Z_m = 1 + \frac{Bp}{RT} \tag{5.18a}$$

where B is the second Virial coefficient whose values are calculated from the following equations (Smith et al, 2001):

$$B = \sum_i \sum_j y_i y_j B_{ij} \tag{5.18b}$$

$$B_{ij} = \frac{RT_{cij}}{p_{cij}}\left(B^o + \omega_{ij} B^1\right) \tag{5.18c}$$

$$\omega_{ij} = \frac{\omega_i + \omega_j}{2} \tag{5.18d}$$

$$T_{cij} = \left(T_{ci}T_{cj}\right)^{1/2}\left(1-k_{ij}\right) \tag{5.18e}$$

$$p_{cij} = \frac{Z_{cij}RT_{cij}}{V_{cij}} \tag{5.18f}$$

$$Z_{cij} = \frac{Z_{ci} + Z_{cj}}{2} \tag{5.18g}$$

$$V_{cij} = \left(\frac{V_{ci}^{1/3} + V_{cj}^{1/3}}{2}\right)^3 \tag{5.18h}$$

where k_{ij} is an empirical interaction parameter specific to an $i-j$ molecular pair and it is usually set to zero (Smith et al, 2001). Gases behave differently at a given temperature and pressure, but they behave very much the same at their reduced temperratures and pressures:

$$p_r = \frac{p}{P_c} \text{ and } T_r = \frac{T}{T_c} \tag{5.19}$$

where p_r is the reduced pressure and T_r is the reduced temperature. The approach that the Z factor for all gases is approximately the same at the same reduced pressure and temperature is called the principle of corresponding states (Smith et al, 2001; and Cengel and Boles, 2010). If $i=j$, Eq. (5.18) results in the compressibility factor for pure gas species i.

5.3 Results and Discussion: Permeability Modeling

The variables and constants used for calculating the inputs of the model (Eqs. 5.16 and 5.17) are presented in Table 5.1. ϕ was calculated using Eq. (5.4) while Z was obtained from Virial equation using Eqs. (5.18 a - h). ϕ_c was calculated from Eq. (5.11b) using the data obtained from Differential Scanning Calorimetry. The calculation was done based on 293 J/g for 100 % crystalline polyethylene (Adewole et al, 2011 and Blaine, 2010).

Permeability of CH_4 and CH_4/CO_2 mixture in polyethylene and its nanocomposite were measured as functions of pressure and temperature and results obtained were presented in Tables 5.2 and 5.3 for pure HDPE and 1wt% Cloisite 15A, respectively. In the temperature range of 30^o-70^oC, significant effects were noticed for all the samples. For instance, increasing the temperature from 31^oC to 51 ^{o}C increases the permeability by about three times for pure HDPE as shown in Table 5.2. This result makes sense since the increase in

Table 5.1 Characteristics of the permeation experiment

Parameter	Value	Unit	Source
Temperature range	30.86 – 70.25	^{o}C	Permeation experiment
Pressure range	101.6 – 105.67	bar	Permeation experiment
Compressibility factor	0.716 – 0.885		Calculated
Aspect Ratio(α)	110		the manufacturer
Fractional Volume (ϕ)	0 - 0.0058		Calculated
Degree of Crystallinity (ϕ_c)	0.6356 – 0.6532		DSC experiment

Table 5.2 Permeability of Pure HDPE Samples

Mole Fraction					
CH_4	CO_2	T(^oC)	P(bar)	Crystalinity (ϕ_c), %	Permeability (P_e)* 10^8 (cm^3(STP)/cm.s.bar)
1	0	31	105.7	88.14	0.573
1	0	50	104.6	76.07	1.94
1	0	70	101.8	65.11	4.52
0.8	0.2	31	105.2	88.14	1.01
0.8	0.2	50	100.8	76.07	3.03
0.8	0.2	70	102.1	65.11	5.84

test temperature will increase the mobility of both HDPE chain segments and the gas molecules and enhances the permeation process (Raharjo et al, 2007; Safari et al, 2009; Naito et al, 1991; and Lin and Freeman, 2004).

Also, it can be observed that as the crystallinity increases the permeability was found to decrease. This is due to the fact that diffusion of gases in polymeric materials takes an effect within the amorphous region (Dhoot, 2003). So, an increase in the degree of crystallinity means a decrease in the amorphous domain and consequently a decrease in permeability (Choudalakis and Gotsis, 2009; and Klopffer and Flaconnèche, 2001). The decrease in permeability with temperature was also observed for all samples irrespective of the type of gaseous penetrants. Since crystallinity is a property of the polymer matrix, an increase in temperature increases the degree of mobility of segmental chains of the polymer and this leads to gradual reduction of the crystalline domain. The values of the measured permeability for pure HDPE as reported in this work are in agreement with previous literature reports. For example, the permeability coefficient of CH_4 in HDPE at 25^{o}C was reported by Alamo and Mandelkern (2009) to be 0.3×10^{-8} cm^3(STP)/cm.s.bar while 0.58×10^{-8} cm^3(STP)/cm.s.bar was obtained in this work for the same gas at 31^{o}C. The two values are of the same order of magnitude and the difference is due to fact that the measurements are taken at different temperature and crystallinity. Moreover, the permeability of CH_4 in HDPE with 63% crystalinity was measured by Flaconnèche et al (2001) and found to be 5.1×10^{-8} cm^3(STP)/cm.s.bar at 77^{o}C. In this work, a permeability of 4.52×10^{-8} cm^3(STP)/cm.s.bar was obtained for pure HDPE of 65% crystallinity at 70 ^{o}C. Again the results are of the same order of magnitude and our permeability is lower since it was measured at slightly lower temperature. So, our results for permeability are

comparable with the published literature. The effect of nanoclay dispersion in polyethylene matrix on permeability of pure CH_4 and the permeability of CH_4/CO_2 mixture is shown in Table 5.3. The incorporation of nanoclays into polyethylene is known to substantially improve gas barrier property since the nanoclays create tortuous path that retards the gas molecules movement through the polymer (Arora and Padua, 2010; Herrera-Alonso et al, 2009; and Picard, 2007). However, this is not sometimes the case in nanoparticle filled polymers (Matteucci, 2008). Permeabilities of some samples increased, some decreased while others remained practically constant. For instance, at 50^{o}C the permeability of pure CH_4 in the presence of 1wt% C15A dropped by about 3.6% and that of the mixture by 11.9% in comparison with pure HDPE as shown in Table 5.3. This suggests that the presence of CO2 has increased the permeability of the gas mixture for both pure HDPE and HDPE-C15A. At a higher temperature of about 70^{o}C, permeability of both pure and mixed gases increased by about 10% in the presence of 1wt% C15A. Possible explanation for the increase in permeability was offered by Matteucci et al (2008). The nanoparticles can inhibit the efficient seqmental chain packing in polymers thereby increasing free volume in the polymer phase which consequently increase the permeability. Also, in other heterogenous polymer systems such as rubbery polymer nanocomposites, voids at polymer – particle interface or between particle agrregates cause permeability to be greater in nanocomposites than in unfilled polymers. On the other hand, the presence of 20% CO_2 in the gas mixture has increased the permeability by 30-75% depending on temperature. The solubility of CH_4 is suggested to decrease in the presence of CO_2. So, CH_4 would likely be displaced from the fixed volume sites by CO_2 leading to a faster diffusion through the polymer matrix (Dhingra and Marand, 1998). Interestengly, the higher increases was

Table 5.3 Permeability of HDPE/1wt% C15A nanocomposite

Mole Fraction						
CH_4	CO_2	T(^oC)	P(bar)	Crystalinity (ϕ_c), %	Permeability (P_e)* 10^8 (cm^3(STP)/cm.s.bar)	% Difference From pure HDPE
1	0	31	104.3	86.82	0.609	+ 6.3
1	0	50	104.9	72.76	1.87	- 3.6
1	0	70	105.1	59.82	4.94	+ 9.3
0.8	0.2	31	104.3	86.82	1.06	+ 5.0
0.8	0.2	50	104.9	72.76	2.67	-11.9
0.8	0.2	70	103.4	59.82	6.46	+ 10.6

observed at the lowest temperature. This increase was almost the same for both pure HDPE and HDPE with 1% clay which suggests that the permeation was not influenced by the presence of samll amount of clay. This suggests that the temperature dependency of the combined diffusion and solubility of the two gases is quite different. It is clear that the coupling between diffusion and sorption of the two gases is the main reason for the observed behavior. However, in this study we can not distinguish between the contribution of each factor.

Figures 5.1-5.4 represent the experimental data along with the fits of the proposed model. In these Figures, the values obtained by linearising Eqs. (5.16) and (5.17) were plotted against $\frac{P}{ZRT}$. As can be seen from these Figures, there exists a good fit for the proposed model and the experimental data with correlation coefficient greater than 0.91. Values of β and κ are obtained from the slope and the intercept of the plots in 5.1-5.4 and results are presented in Table 5.4. The values of β can be used to account for the activation energy of permeation while κ is a characteristic measure of the pre – exponential factor in the popular Van't Hoff-Arrhenius equation for permeability behavior in polymers (Sun et al, 2008; Mrkic,2007; Koros and Madden, 2003; and Peacock, 2000). The negative sign of β is an indication that permeability decreases with increasing $\left(\frac{p}{ZRT}\right)$. Thus, permeability of the gas mixture (CH_4/CO_2) is higher than that of pure CH_4 in all the samples as shown in Tables 5.2 and 5.3. Conversely, the absolute values of β are higher for pure CH_4 gas than for CH_4/CO_2 mixture as reported in Table 5.4. This is due to the fact that the permeability of pure CH_4 in HDPE is low thus more energy is needed to move CH_4

Table 5.4 Model parameters

Gas Composition		Polymer	β	$\kappa \times 10^6$	R^2	Figure #
CH4	CO2					
1.0	0.0	PURE HDPE	-1379.5	34.692	0.98	5.1
0.8	0.2	PURE HDPE	-499.55	1.505	0.97	5.2
1.0	0.0	HDPE+1%C15A	-1383.1	55.496	0.96	5.3
0.8	0.2	HDPE+1%C15A	-516.92	1.965	0.92	5.4

molecules hence higher absolute value of β. On the other hand, the permeability of the mixed gas is higher and consequently less energy is needed to move the molecules through the polymer and so the value of β is lower. The drastic drop in $-\beta$ for mixed gases is suggested to be due to the high permeability of CO_2 as compared to CH_4, as well as, the synergistic effect that often results from the presence of other gas components (Ghadimi, 2009; Dhingra and Marand, 1998; and Costello and W. J. Koros, 1993).

This enhancement is suggested to be an activated state process (Baird and Collias, 1995; Flaconnèche, 2001; and Krevelen, 1990). Hence, Arrhenius equation is used to predict the permeability at different temperature:

$$P_e = P_{eo} \exp\left(-\frac{E_P}{RT}\right) \tag{5.20}$$

where P_{eo} is a pre-exponential factor, E_p is the apparent activation energy of the permeation processs. Increase in permeability following an increase in temperature was observed for all samples covered in this study as shown in Tables 5.2 and 5.3.

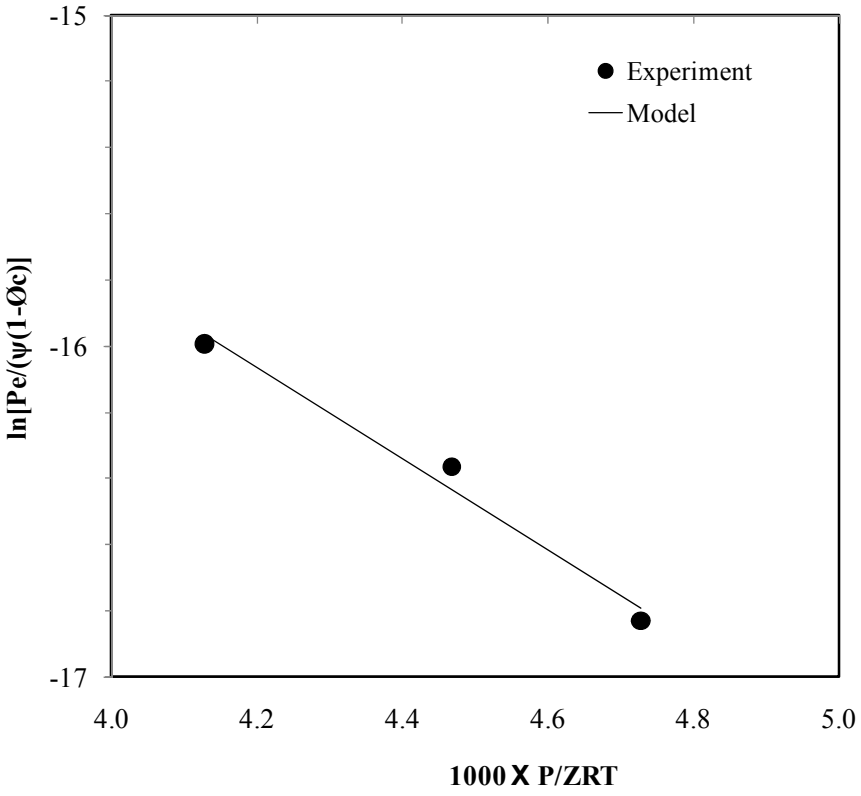

Figure 5.1 : Experimental permeability data and fit using eq. (16) for pure CH4 in Pure HDPE

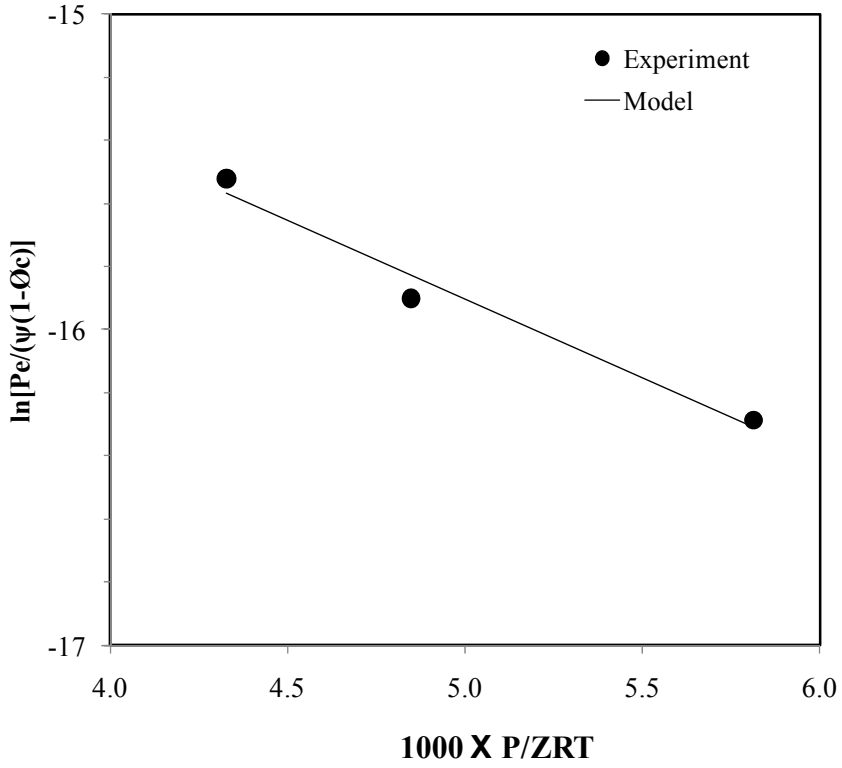

Figure 5.2 : Experimental permeability data and fit using eq. (17) for mixed gas in Pure HDPE

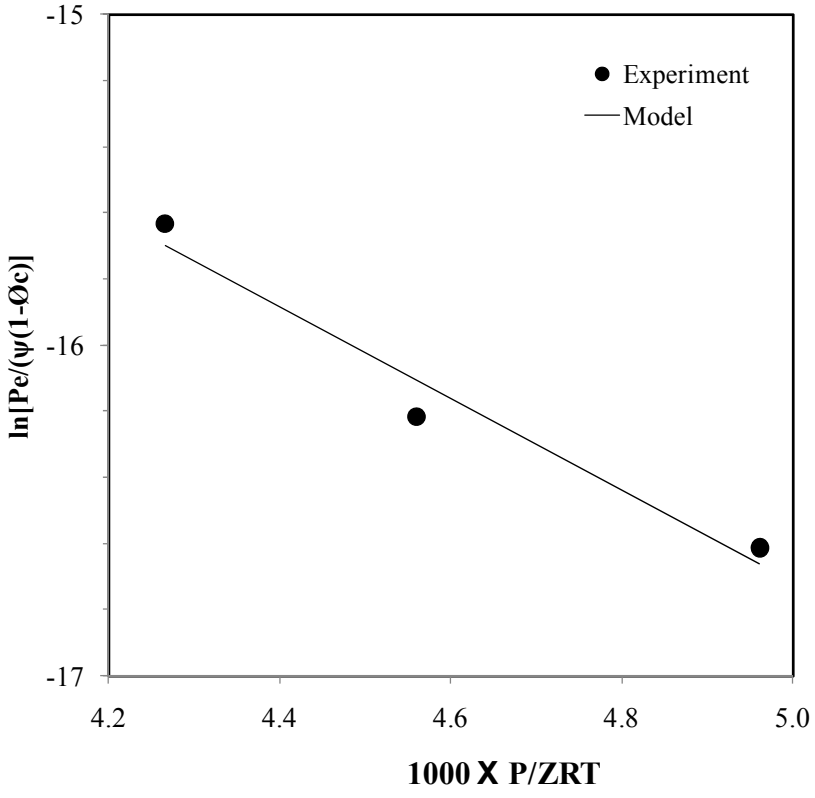

Figure 5.3 : Experimental permeability data and fit using eq. (16) for pure CH4 in HDPE/clay nanocomposite (1wt% Cloisite 15A)

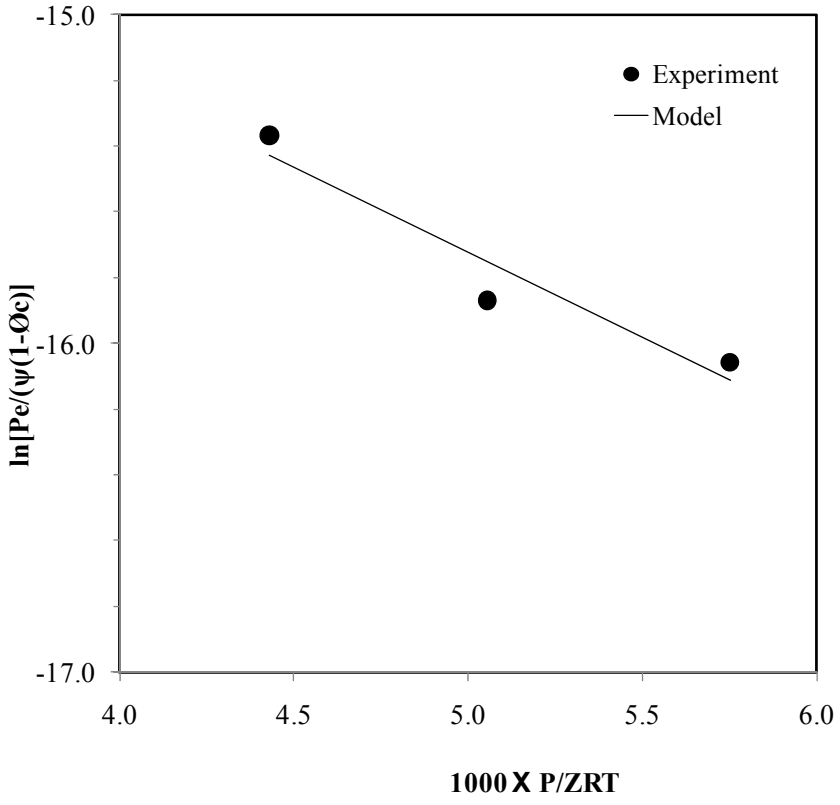

Figure 5.4 : Experimental permeability data and fit using eq. (17) for mixed gas in HDPE/clay nanocomposite (1wt% Cloisite 15A)

The activation energy of permeation and the pre-exponential factor were obtanied from the permeability data plots using Eq. (5.20). In this work, the presence of CO_2 was found to decrease the activation energy by about 5% as shown in Table 5.5. However, the addition of 1% clay to pure HDPE has reduced the activation energy by ~9% while no influence was observed in the case of the CH_4/CO_2 mixture. This suggests that the interaction of the clay with the two gases is different; howver, more work needs to be done to undersatnd the mechanism of permeation in the presence of the clay. This is an indication of an increase in permeability as explained earlier. In addition, it was observed that as the activation energy decreased, κ also decreased. This is in agreement with the relationship provided by Krevelen (1990); and Baird and Collias (1995). For comparison, the activation energy for pure CH_4 reported by Flaconnèche et al. [58] was in the range 40 – 47 kJ/mol. This is quite in agreement with values of activation energy reported here. There were no published data to compare the activation energies of pure CH_4 in polyethylene/nanoclay composite as well as mixed gases in both pure polyethylene and its nanoclay composites. It should be noted that only three data points were used in Figures 5.1-5.2 due to the long time involved in acquiring each of these data points especially at low temperatures. Each data point presented in Figures 5.1-5.2 takes about 10 days to be acquired.

The present model can be used for predicting permeability of gases in polymers and polymer nanocomposites and the results can be used as a guide for understanding the transport behaviour of gases in polymer nanocomposites prior to laboratory investigations. The presence of 1% clay in pure HDPE has increased the activation energy, E_p, by ~ 9% which is likely due to the increase in the tortuous path; hence more energy is needed to activate the process. However, the presence of CO_2 in the gas mixture has reduced E_p;

hence increased P_e. This increase in the permeability of CH_4 in the presence of CO_2 is likely due to the reasons discussed above. The same trend was observed in the case of HDPE+1%C15A with even more drop in E_p and P_{eo}. Overall, a model that predicts the permeation of gases through polymer nanocomposites at high temperature and pressure was developed. The model takes into consideration the compressibility of the gas or gas mixtures. However, more work should be carried out to understand and resolve the coupling between the diffusion and sorption in nanocomposites.

Table 5.5 Activation energy of permeation, E_p, and pre-exponential factor, P_{eo}, of penetrant in polyethylene and its nanocomposites

Gas Composition		Polymer	E_p (kJ/mol)	P_{eo}
CH4	CO2			
1.0	0.0	PURE HDPE	42.90	0.1360
0.8	0.2	PURE HDPE	40.94	0.1134
1.0	0.0	HDPE+1%C15A	46.84	0.6925
0.8	0.2	HDPE+1%C15A	40.26	0.0876

CHAPTER 6

6.0 CONCLUSION AND RECOMMENDATIONS FOR FUTURE WORK

6.1 Conclusions

Material selection for liner application in oil and gas pipelines remains one of the challenges faced by engineers in the industries. Liners that are presently in use usually fail to isolate the sour gas from steel pipes and eventually this leads to failure of the pipeline. It is essential to understand the reasons behind this failure. Possible reasons could be pure mechanical due to stress cycles and creep of polymers or the gas may diffuse in the liner due to high pressure or a combination of these two factors. The use of clay additives was suggested to improve the mechanical properties of the liner with special focus on creep. Also, the use of clay additives is expected to limit the diffusion of natural gas in the liner.

In this research, the influence of variuos nanoclays on morphological, transport, thermal, bulk and surface mechanical properties of PE-nanocomposite was investigated. Moreover, special emphasis was given to creep both at the micro and the macro levels. HDPE/ clay nanocomposites were prepared by melt blending of HDPE with organically modified clays (Cloisite 10A, Cloisite 15A, Cloisite 30B and Nanomer 1.44P), and a compatibilizer (polyethylene grafted maleic anhydride) using a masterbatch technique. The organoclay concentrations used were 1, 2.5 and 5wt%. Effect of clay on the morphology of the samples was investigated using Scanning Electron Microscopy (SEM) and X-Ray Diffraction (XRD) methods. A high pressure 2-D permeation cell was employed for the permeation test while Differential Scanning Calorimetry was used to measure the thermal properties. Moreover, the bulk mechanical properties were measured using the Instron

Mechanical testing instruments and the Dynamic Mechanical Analysis (DMA) machine. The surface mechanical properties were investigated using a nanoindenter. The conclusions of this study are summarized as follows:

Morphology

The results from the XRD and SEM indicated that:

- The organoclays were well dispersed in the sample of PE nanocomposites.
- Relative intercalation of 81.08% was achieved for C15A while 42.53% was realized for N1.44P compare to the neat organoclay.

Permeability

Results obtained from the permeation experiment revealed that:

- Permeation of gases through polyethylene nanocomposites can be improved by incorporation of nanoclay up to 5wt% loading.
- Barrier property of the nanocomposites to natural gas was improved by 46.5% due to the addition of 5wt% N1.44P.

Thermal

Results of thermal properties tests from the DSC analysis showed that:

- The crystallization and peak temperature increased while the onset temperature practically remained constant for HDPE with compatibilizer.
- The onset temperature of thermal decomposition decreased with increasing clay content.
- Degree of crystalinity depends on the efficiencies of the nanoparticles as nucleating agents.

- Incorporation of nanoclay into a polethylene matrix can bring about both nucleation as well disruption of attainable spherulite size.
- Increase in crystallinity was more pronounced at higher loadings of N1.44P.

Bulk Mechanical Properties

Analysis of the results obtained from tensile and DMA tests showed that:

- The mechanical properties were found to be better than that of the pure polymer at low loading (2.5wt %) for Cloisite 15A and at higher loading (5wt %) for Nanomer 1.44P.
- The ultimate strength and the toughness decreased slightly compared to the pure HDPE. This is due to stiffening and agglomerates effects of the clay which result in stress concentration sites.

Surface Mechanical Properties

From the results of the nanoindentation test, it can be concluded that:

- The nanoindentation measurements can be used to compare relative resistance to indentation as well as the creep behavior of various HDPE nanocomposites.
- Modulus of elasticity and creep data acquired from nanoindentation measurements of two types of HDPE nanocomposites with a range of loadings followed a similar pattern observed for corresponding bulk properties of the material.

Mathematical Modeling

The model developed in this study utilizes gas pressure and temperature, nanoparticle volume fraction and degree of crystallinity of polymer matrix as inputs. Experimental data obtained from the permeation experiments were fitted using the proposed model to get two parameters, β and κ. Moreover, the permeability data were also used to estimate the activation energy of permeation. From the mathematical modeling results of the fits, it can be concluded that:

- Plots obtained from the fits showed excellent agreement with the experimental data.
- The parameters obtained from the model can be used to account for the activation energy of permeation and the pre-exponential factors at high pressure.
- The activation energy obtained from experimental permeation data compared very well with published values.
- The developed model can be used for the prediction of gas permeability in polymer nanocomposite systems at high pressure and temperature.

Concluding Remarks

The addition of Cloisite 15A improved the properties of the nanocomposite at low loading while the nanocomposite obtained by addition of Nanomer 1.44P possessed better properties at higher clay loading. Accordingly, Nanomer 1.44P is suggested to be the best clay, among the clays covered in this study, for use in liner applications. Nanocomposite prepared from 5wt% of this clay possesses markedly better properties than pure HDPE. Specifically, the storage modulus of the Nanomer N1.44P (5wt%) nanocomposite increased by 93%, recoverable creep 93%, resistance to indentation by 22%, and 22%

increase in hardness. Also, barrier property of the nanocomposite to natural gas was found to improve by 46.5%. Although, C15A is also very good clay especially based on the tests performed at laboratory conditions and the quantity of clay required for bringing about marked property improvement, N1.44P was chosen based on its creep compliance behavior at field conditions. Furthermore, the methodologies employed in this study are useful tools for developing new formulations for production of nanocomposite for liner application. It can be concluded, therefore, that the objectives outlined for this work have been successfully achieved.

6.2 Recommendations for Future Work

As summarized above, present study was focused on selection of proper nanoclay additive for production of liner used in the oil and gas industries. Although this work has extensively covered many of the most essential properties of polyethylene as liner application, however, much still need to be done to cover areas which have not been studied in this work. Thus, the following recommendations are made for future work:

- The use of the methodologies employed in this work for the production of liners.
- Investigation of other transport properties such as solubility and diffusivity of the samples produced using our methodologies.
- Investigation of the effects of CO_2 concentration on the transport properties of the nanocomposites.
- Further study on the use of the two-step preparation approach using these methodologies. That is, in situ polymerization to produce a master batch then

followed by blending the masterbatch with PE to yield nanocomposite with desired wt%

- Extensive study on possible scale up and commercialization procedure in order to bring this liner to the open market.
- A study on the generation of more data points for temperature, pressure and gas concentration to investigate the versatility of the developed model.

Reference

Abbasi, S.H., M. A. Parvez and I. A. Hussein, “Nonisothermal Crystallization Kinetics Study of LDPE/MWCNT Nanocomposites: Effect of Aspect Ratio and Surface Modification,” J. Appl. Polym. Sci., 119, 290-299 (2011).

Abdullah, M., Khairurrijal, F. Iskandar, and K. Okuyama, "Semiconductor Nanoparticle - Polymer Composites," in "Nanocrystalline Materials Their Synthesis - Structure - Property Relationship and Applications," Tjong S. C., Ed., ELSEVIER, Amsterdam, (2006), pp. 275 – 310

Adewole J. K., U. A. Al-Mubaiyedh, A. Ul-Hamid, A. A. Al-Juhani and I. A. Hussein, Bulk and surface mechanical properties of clay modified HDPE used in liner applications, Can. J. Chem. Eng. (2011) (Accepted) .

Alamo, R. G. and L. Mandelkern “Polyethylene, Linear High Density,” in “Polymer Data Handbook,” Mark J. E., Ed., Oxford University Press, Oxford, (2009), pp. 634 - 650

Alexandre, M. and P. Dubois, "Polymer-layered silicate nanocomposites: preparation, properties and uses of a new class of materials," Mater. Sci. Eng. 28, 1–63 (2000).

Arora, A. and G. W. Padua, “Review: Nanocomposites in Food Packaging,” J. Food Sci., 75, 43 – 49 (2010).

Baird, D. G. and D. I. Collias, “Diffusion and Mass Transfer,” in “Polymer Processing Principle and Design,” Butterworth – Heinemann, Newton, (1995), pp. 63-94.

Balta-Calleja, F. J.,Ll. Giri, I. M. Ward and D. L. M. Cansfield, “Microstructure of bulk crystallized linear polyethylene: correlation of microhardness and yield stress,” J. Mater. Sci. 30, 1139 – 1143 (1995).

Barick, A. K. and D. K. Tripathy, "Thermal and dynamic mechanical characterization of thermoplastic polyurethane/organoclay nanocomposites prepared by melt blending," Mater. Sci. Eng. A 527, 812 – 823 (2010).

Basmadjian D., “Mass Transfer Priniciples and applications,” CRC Press, London, (2005) pp. 91-117.

Belfiore L. A., “Diffusion in Amorphous Polymers Near the Glass Transition Temperature,” in “Physical Properties of Macromolecules,” John Wiley & Sons, Inc., Hoboken, NJ, (2010), pp. 49-69.

Benjelloun-Dabaghi, Z., J. C. de Hemptinne, J. Jarrin, J. M. Leroy, J. C. Aubry, J. N. Saas and C. Travel-Condat, "MOLDI™: A Fluid Permeation Model to Calculate the Annulus Composition in Flexible Pipes," Oil & Gas Science and Technology, 57, 177-192 (2002).

Bharadwaj R. K., “Modeling the Barrier Properties of Polymer-Layered Silicate Nanocomposites,” Macromol, 34, 9189-9192 (2001).

Bicerano J., “Transport of Small Penetrant Molecules,” in “Prediction of Polymer Properties,” Marcel Dekker, Inc., New York, (1996) pp. 403-419.

Blaine, R. L., "Determination of Polymer Crystallinity by DSC," TA123, TA Instrument Publication, 1 – 3 (2010).

Cengel, Y. A. and M. A. Boles, **"**Gas Mixtures," in "Thermodynamics An Engineering Approach," McGraw Hill, New York, (2010).

Cengel, Y. A. and A. J. Ghajar, "Mass Transfer," in **"**Heat and Mass Transfer Fundamentals and Applications," McGraw Hill, New York, (2011), pp. 773 - 828.

Choudalakis G. and A. Gotsis, "Permeability of polymer/clay nanocomposites: A review," Eur. Polym. J., 45, 967–984 (2009).

Costello L. M. and W. J. Koros, "Comparison of Pure and Mixed Gas CO_2 and CH_4 Permeabilities in Polycarbonate: Effect of Temperature," Ind. Eng. Chem. Res., 32, 2277 – 2280 (1993).

Cui, L., Ma, X. and D. R. Paul, "Morphology and properties of nanocomposites formed from ethylene -vinyl acetate copolymers and organoclays," Polymer, 48, 6325 – 6339 (2007).

Cui, Y. H. and J. Tao, "DSC Analysis and Mechanical Properties of Wood - Plastic Composites," J. Reinf. Plast. Compos. 29, 278 – 289 (2010).

Cussler E. L., Diffusion Mass Transfer in Fluid Systems, Cambridge University Press, New York, 2009.

Deepthi M. V., M. Sharma, R. Sailaja, P. Anantha, P. Sampathkumaran, and S. Seetharamu, "Mechanical and thermal characteristics of hingh density polyethylene - fly ash Cenospheres composites," Materials and Design, 31, 2051 – 2060 (2010).

Dhingra, S. S., and E. Marand, “Mixed gas transport study through polymeric membranes,” J. Membr. Sci., 141, 45 – 63 (1998).

Dhoot, S. N., B. D. Freeman and M. E. Stewart, “Barrier Polymers,” in “Encyclopedia of polymer science and technology,” H. F. Mark, Ed., Wiley-Interscience, New Jersey, (2003), pp. 200-263.

Dominkovics, Z. and J. M. Pukanszky, “Sructure and properties of layered silicate PP nanocomposites: Expectations and reality,” in “Proc. 3rd Inl. Conf. High performace Fillers,” Hamburg, Germany, March 14 -15, 2007, Smithers Rapra Ltd., Shawbury (2007), pp. 92

Elabd, Y. A. and T. A. Barbari, “Multicomponent Diffusion of Hydrogen-Bonding Solutes in a Polymer,” AIChE J., 48, 1610-1620 (2002).

Finnigan, B., D. Martin, P. Halley, R. Truss and K. Campell, "Morphology and properties of thermoplastic polyurethane nanocomposites incorporating hydrophilic layered silicates," Polymer 45, 2249– 60 (2004).

Flaconnèche, B., J. Martin and M. H. Klopffer, “Permeability, Diffusion and Solubility of Gases in Polyethylene, Polyamide 11 and Poly(Vinylidene fluoride)”, Oil & Gas Science and Technology, 56, 261-278 (2001).

Flaconnèche, B., J. Martin and M. Klopffer, “Transport Properties of Gases in Polymers: Experimental Methods,” Oil & Gas Science and Technology, 56, 245-259 (2001).

Flores, A., F.J. Balta - Calleja, G.E. Attenburrow and D.C. Bassett, “Microhardness studies of chain-extended PE: III. Correlation with yield stress and elastic modulus,” Polymer 41, 5431 -5435 (2000).

Fornes, T.D., P.J. Yoon, H. Keskkula and D.R. Paul, "Nylon 6 nanocomposites: The effect of matrix molecular weight," Polymer 42, 9929– 40 (2001).

Fredrickson, G. H. and J. Bicerano, “Barrier properties of oriented disk composites,” J. Chem. Phys., 110, 2181–2188 (1999).

Fujiyama, M., "Morphology Development in Polyolefin Nanocomposites," in “Optimization of Polymer Nanocomposite Properties,” Mittal V., Ed., WILEY - VCH Verlag GmbH & Co KGaA, Weinhein, (2010), pp 67 - 92.

Ghadimi, A., M. Sadrzadeh, K. Shahidi, and T. Mohammadi, “Ternary gas permeation through a synthesized PDMS membrane: Experimental and modeling,” J. Membr. Sc., 344 , 225–236 (2009).

Giannelis, E. P., "Polymer layered silicate nanocomposites," Adv. Mater. 8, 29–35 (1996).

Goettler, L.A., "Overview of property development in layered silicate polymer nanocomposites," in “Ann. Tech. Confr. Soc. Plast. Eng.,” K. Winker, Ed., Boston, May 2 – 4, 2005, Society of Plastics Engineers, Newtown, CT, USA (2005), pp 1980–1982.

González-Vidal, N., S. Muñoz-Guerra, A. M. de Ilarduya, S. Benali, S. Peeterbroeck and P. Dubois, "Poly(hexamethylene terephthalate) – layered silicate nanocomposites," Eur. Polym. J. 46, 156 – 164 (2010).

Gopakumar, T., J. Lee, M. Kontopoulou and J. Parent, “Influence of clay exfoliation on the physical properties of montmorillonite/polyethylene composites,” Polymer, 43, 5483–5491 (2002).

Herrera-Alonso, J. M., E. Marand, J. C. Little, and S. S. Cox, “Transport properties in polyurethane/clay nanocomposites as barrier materials,” J. Membr Sci, 337, 208–214 (2009).

Hocine, N. A., "Mechanical Property Enhancement of Polymer Nanocmposites," in “Optimization of Polymer Nanocomposite Properties,” Mittal, V., Ed., WILEY - VCH, Weinheim, (2010), pp 123 - 138.

Hotta, S. and D. R. Paul, "Nanocomposites formed from linear low density polyethylene and Organoclays," Polymer 45, 7639–7654 (2004).

Hussein, I. A., H. I. Al-Abdul Wahhab and M. H. Iqbal, "Influence of Polymer Type and Structure on Polymer Modified Asphalt Concrete Mix," The Can. J. Chem. Eng. 84, 480 – 487 (2006).

Hwang, T. Y., S. M. Lee, Y. Ahn and J. W. Lee, "Development of polypropylene-clay nanocomposite with supercritical CO_2 assisted twin screw extrusion," Korea-Australia Rheol J. 20, 235-243 (2008).

Innocentini-Mei, L. H., "Thermomechanical Properties of Nanocomposite," in “Optimization of Polymer Nanocomposite Properties,” Mittal, V., Ed., WILEY - VCH, Weinheim, (2010), pp 351 - 68.

Jacquelot, E., E. Espuche, J. F. Gerard, J. Duchet and P. Mazabraudp, "Morphology and Gas Barrier Properties of Polyethylene-Based Nanocomposites," J. Polym. Sci., Part B: Polym. Phys., 44, 431– 440 (2006).

Jaffrin, Y. M. and C. Legallais, Biomedical Membrane Extracorporeal Devices, in: E. Drioli, L. Giorno (Eds.), Membrane Operations Innovative Separations and Transformations, WILLEY-VCH Verlag GmbH & Co. KGaA, Weinheim, pp. 411 – 431(2009).

Joshi, M., B. S. Butola and G. S. Kukaleva, "Rheological and Viscoelastic Behavior of HDPE/Octamethyl-POSS Nanocomposites," Macromolecules, 39, 1839 – 1849 (2006).

Kannan, M., and S. S. Bhagawan, "Mechanical Properties and Morphology of Nanoclay Filled Different TPU/PP Blend Nanocomposites: Structure Property Relations," J. Compos. Mater., 43, 1915 – 1925 (2009).

Khumalo, V. M., J. Karger-Kocsis and R. Thomann, "Polyethylene/synthetic boehmite alumina nanocomposites: Structure, thermal and rheological properties. eXPRESS Polym. Lett., 4, 264–274 (2010).

Klopffer, M. and B. Flaconnèche, "Transport Properties of Gases in Polymers: Bibliographic Review," Oil & Gas Science and Technology, 56, 223-244 (2001).

Koros, W. J. and C. W. Madden, "Transport Properties," in "Encyclopedia of polymer science and technology," H. F. Mark, Ed., Wiley-Interscience, New Jersey, (2003), pp. 291-381.

Krevelen, D. W., “Properties Determining Mass Transfer in Polymeric Systems,” in “Properties of Polymers Their Correlation with Chemical Structure; Their Numerical Estimation and Prediction from Additive Group Contribution,” ELSEVIER, New York ,(1990), pp. 535-583

Kumar, S. N., H. Yuelong, D. Yumei, Y. Le, M. G. Kmaran, and S. Thomas, “Gas transport Through Nano Poly (ethylene-co-vinyl acetate) Composite Membranes,” Ind. Eng. Chem. Res., 47, 4898 – 4904 (2008).

Lee, J., D. Jung, C. Hong, K. Y. Rhee and S. G. Advani, "Properties of polyethylene - layered silicate nanocomposites prepared by melt interc alation with a PP-g-MA compatibilizer," Compos Sci and Technol 65, 1996–2002 (2005).

Lim, S. T., Y. H. Hyun and H. J. Choi, "Synthetic Biodegradable Aliphatic Polyester/ Montmorillonite Nanocomposites," Chem. Mater. 4, 1839 – 1844 (2002).

Lin, H. and B. Freeman, “Gas solubility, diffusivity and permeability in poly(ethylene oxide),” J. Membr. Sc., 239, 105–117 (2004).

Liu, Q. and D. D. Kee, “Modeling of diffusion through nanocomposite membranes,” J. Non-Newtonian Fluid Mech., 131, 32–43 (2005).

Liu, Q. and D. D. Kee, “Mass Transport Through PDMS/Clay Nanocomposite Membranes,” Can. J. Chem. Eng., 85, 36 – 44 (2007).

Lotti, C., S. C. Isaac, M. C. Branciforti, R. M. V. Alves, S. Liberman and R. E. S. Bretas, "Rheological, Mechanical and Transport Properties of Blown Films of High Density Polyethylene Nanocomposites," Eur. Polym. J. 44, 1346 – 1357 (2008).

Lu, C. and Y-W. Mai, "Influence of Aspect Ratio on Barrier Properties of Polymer-Clay Nanocomposites," Phys Rev Lett., 95, 1- 4 (2005).

Lu, C. and Y-W. Mai, "Permeability modelling of polymer-layered silicate nanocomposites," Compos. Sci. Technol., 67, 2895 – 2902 (2007).

Madbouly, S. A., J. U. Otaigbe and A. K. Wicks, "Rheological Behavior of POSS/Polyurethane-Urea Nanocomposite Films Prepared by Homogeneous Solution Polymerization in Aqueous Dispersions," Macromolecules, 40, 4982-4991 (2007).

Masaro, L. and X. Zhu, "Physical models of diffusion for polymer solutions, gels and solids," Prog. Polym. Sci., 24, 731–775 (1999).

Matteucci, S., R. D. Raharjo, V. A. Kusuma, S. Swinnea and B. D. Freeman, "Gas Permeability, Solubility, and Diffusion Coefficients in 1,2-Polybutadiene Containing Magnesium Oxide," Macromol, 41, 2144-2156 (2008).

Mittal, V., "Polymer Nanocomposite: Synthesis, Microstructure and Properties," in "Optimization of Polymer Nanocomposite Properties," Mittal, V., Ed., WILEY - VCH, Weinheim, (2010), pp 1 – 19.

Mrkic, S., K. Galic, and M. Ivankovic, Effect of tempearture and mechanical stress on barrier polymeric films used for food packaging, J. Plast Film Sheeting 23 (2007) 239 - 256.

Muralidharana, M., S. A. Kumarb and S. Thomas, “Morphology and transport characteristics of poly (ethylene-co-vinyl acetate)/clay nanocomposites,” J. Membr. Sc., 315, 147–154 (2008).

Naito, Y., D. Bourbon, K. Terada, and Y. Kamiya, “Permeation of High-Pressure Gases in Poly(ethylene-co-vinyl acetate),” J. Polym. Sci. Part B: Polym. Phys., 31, 693-697 (1993).

Naito, Y., K. Mizoguchi, K. Terada, and Y. Kamiya, “The Effect of Pressure on Gas Permeation through Semicrystalline Polymers above the Glass Transition Temperature,” J. Polym. Sci. Part B: Polym. Phys., 29, 457-462 (1991).

Nguyen, Q. T. and D. G. Baird, "Preparation of Polymer–Clay Nanocomposites and Their Properties," Adv. Polym. Tech. 25, 270 – 285 (2006).

Paul, D.R. and L.M. Robeson, "Polymer nanotechnology: Nanocomposites," Polymer 49, 3187– 3204 (2008).

Paul, M. A., M. Alexandre, P. Degee, C. Henrist, A. Rulmont and P. Dubois, "New nanocomposite materials based on plasticized poly(L-lactide) and organo-modified montmorillonites: thermal and morphological study," Polymer 44, 443–50 (2003).

Pavlidou, S. and C. D. Papaspyrides, "A Review on polymer - layered silicate nanocomposites," Prog. Polym. Sci. 33, 1119 – 1198 (2008).

Peacock, A. J., “Properties of Polyethylene ,” in “Handbook of Polyethylene Structures, Properties and Applications,” D. E. Hudgin, Ed., Marcel Dekker Inc, New York, (2000), pp 123 - 241.

Pegoretti, A., A. Dorigato and A. Penati, "Tensile mechanical response of polyethylene – clay Nanocomposites," eXPRESS Polymer Letters, 1, 123–131 (2007).

Peppas, A. N., K. M. Wood and J. B. Thomas, Membranes in Controlled Release, in: K. Peinemann, S. P. Nunes, Membranes for the Life Sciences, Vol. 1, WILLEY-VCH Verlag GmbH & Co. KGaA, Weinheim (2008) pp. 175 - 190.

Phang, I. Y., T. Liu, A. Mohamed, K.P. Pramoda, L. Chen and L. Shen. "Morphology,thermal and mechanical properties of nylon12/organoclay nanocomposites prepared by melt compounding," Polym. Int. 54, 456–64 (2005).

Picard, E., A. Vermogen, J. F. G´erard, and E. Espuche, “Barrier properties of nylon 6-montmorillonite nanocomposite membranes prepared by melt blending: Influence of the clay content and dispersion state Consequences on modelling,” J. Membr. Sc., 292, 133–144 (2007).

Qi, R., X. Jin and C. Zhou, "Preparation and Properties of Polyethylene–Clay Nanocomposites by an In Situ Graft Method," J. Appl. Polym. Sci. 102, 4921–4927 (2006).

Quadrini, F, E. A. Squeo and A. Guglielmotti, "Indentation Creep of Polymers. I. Experimental," Polym. Sci. Eng., 50, 2431–2439, (2010).

Raharjo, R. D., B. D. Freeman, D. R. Paul, G. C. Sarti, and E. S. Sanders, “Pure and mixed gas CH_4 and n-C_4H_{10} Permeability and Diffusivity in Poly(dimethysiloxane),” J. Membr. Sc., 306, 75–92 (2007).

Ray, S. S. and M. Okamoto, "Polymer/layered silicate nanocomposites: a review from preparation to processing," Prog. Polym. Sci. 28, 1539–1641 (2003).

Safari, M., A. Ghanizadeh and M. M. Montazer-Rahmati, “Optimization of membrane-based CO2-removal from natural gas using simple models considering both pressure and temperature effects,” Int. J. Greenhouse Gas Control, 3, 3 – 10 (2009).

Samak, S. K., S. K. Nayak, and S. Mohanty. J., “Polypropylene Nanocomposites: Effect of Organo-modified Layered Silicates on Mechanical, Thermal & Morphological Performance,” J. Thermoplast. Compos. Mater. 21, 243 - 263 (2008).

Scheichl, R., M. Klopffer, Z. Benjelloun-Dabaghi and B. Flaconn`eche, Permeation of gases in polymers: parameter identification and nonlinear regression analysis, J. Membr. Sc. 254 (2005) 275–293.

Smith, J. M., H. C. Van Ness and M. M. Abbott, **“**Solution Thermodynamics: Theory**,”** in “Introduction to Chemical Engineering Thermodynamics,” McGraw Hill, New York, (2001), pp. 352-399.

Sorrentino, A., M. Tortora and V. Vittoria, “Diffusion behavior in polymer–clay nanocomposites,” J. Polym. Sci. Part B: Polym Phys. 44, 265–74 (2006).

Sperling, L. H., “Glass and Rubber Transition Behavior” in “Introduction to Physical Polymer Science,” Wiley Interscience, New Jersey (2006), pp 374.

Sun, L, W.-J. Boo, A. Clearfield, H.-J. Sue, and H. Q. Pham, Barrier properties of model epoxy nanocomposites, *J. Membr. Sc. 318* (2008) 129-136.

Suwanprateeb, J., “Calcium carbonate filled polyethylene: correlation of hardness and yield stress,” Composites: Part A 31, 353 – 359 (2000).

Suwanprateeb, J., “Rate-Dependent function in the correlation between hardness and yield stress of polyethylene composites,” Polym. Comp. 21, 238 - 244 (2000).

Suwanprateeb, J., “Rapid examination of annealing conditions for HDPE using indentation microhardness test,” Polymer Testing 23, 157–161 (2004).

Tjong, S. C., "Synthesis and Structure - Property Characteristics of Clay - Polymer Nanocomposites," in “Nanocrystalline Materials Their Synthesis - Structure - Property Relationships and Applications,” S. C. Tjong, Ed., ELSEVIER, Amsterdam, (2006), pp 311 – 348.

Usuki, A., N. Hasegawa and M. Kato, "Polymer-ClayNanocomposites," Adv. Polym. Sci. 179, 135–195 (2005).

Vieth, W. R., “Theory,” in “Diffusion In and Through Polymers,” Hanser Publishers, New York, (1991), pp. 15-47.

Vopicka, O., V. Hynek and V. Rabová, Measuring the transient diffusion of vapor mixtures through dense membranes, J. Membr Sc. 350 (2010) 217–225.

Watanabe, K., Y. Taka and O. Fujiwara, "Cole-Cole Measurement of Dispersion Properties for Quality Evaluation of Red Wine," Meas. Sci. Rev., 9, 113 – 116 (2009).

Welty, J. R., C. E. Wiers, R. F. Wilson, and G. Rorrer, "Fundamentals of Mass Transfer," in "Fundamentals of Momentum, Heat and Mass Transfer," John Willey & Sons, Inc, New Jersey, (2001), pp.398-432.

Wiese, F., "Membranes for Artificial Lungs", in: K. Peinemann, S. P. Nunes, Membranes for the Life Sciences (Eds.), Vol. 1, WILLEY-VCH Verlag GmbH & Co. KGaA, Weinheim, 2008, pp. 49 - 68.

Xu, B., Q. Zheng, Y. Song, and Y. Shangguan, Calculating barrier properties of polymer/clay nanocomposites: Effects of clay layers, *Polymer, 47*(2006) 2904-2910.

Zeng, Q. and A. Yu, "Prediction of the Mechanical Properties of Nanocomposites." In "Optimization of Polymer Nanocomposite Properties," Mittal, V., Ed., WILEY - VCH, Weinheim, (2010), pp 301 – 331.

Zhai, H., W. Xu, H. Guo, Z Zhou, S. Shen and Q Song, "Preparation and characterization of PE and PE-g-MAH /montmorillonite nanocomposites," Eur. Polym. J. 40, 2539–2545 (2004).

Zhang, J. and C. A. Wilkie, "Preparation and flammability properties of polyethylene–clay Nanocomposites," Polym. Degrad. Stabil. 80, 163–9 (2003).

Zhao, C., H. Qin, F. Gong, M. Feng, S. Zhang and M., Yang. "Mechanical, thermal and flammability properties of polyethylene/clay nanocomposite," Polym. Degrad. Stabil. 87, 183 – 189 (2005).

VITAE

Name : Jimoh Kayode ADEWOLE

Nationality : Nigerian

Present Address : Department of Chemical Engineering, King Fahd University of Petroleum & Minerals, P.O. Box 8608, Dhahran, 31261, Saudi Arabia.

Permanent Address : 30, Amilegbe, Ilorin, Kwara State, Nigeria

E- mail address : adekayojih@yahoo.com

Telephone Number : +966 552210035

Academic Background

M.Sc., Chemical Engineering, 2011
King Fahd University of Petroleum and Minerals, KFUPM.
Dhahran, Saudi Arabia

B.Sc., Chemical Engineering 2005
Obafemi Awolowo University, Ile Ife, Nigeria

Diploma in Computer Proficiency 2005
Ultra Brains Institute of Information Technology, Ile Ife

National Diploma Chemical Engineering 1998
Kaduna Polytechnic, Kaduna, Nigeria.